Universidade de Aveiro Departamento de Engenharia Cerâmica e do Vidro
2009

Amit Mahajan

Fabrication of Composite Thick Films of $BaLa_4Ti_4O_{15}$ and $Ba_4Nd_{9.33}Ti_{18}O_{54}$ by Electrophoretic Deposition

Produção de Filmes Espessos Compósitos de $BaLa_4Ti_4O_{15}$ e $Ba_4Nd_{9.33}Ti_{18}O_{54}$ por Deposição Electroforética

Universidade de Aveiro Departamento de Engenharia Cerâmica e do Vidro
2009

Amit Mahajan

Fabrication of Composite Thick Films of $BaLa_4Ti_4O_{15}$ and $Ba_4Nd_{9.33}Ti_{18}O_{54}$ by Electrophoretic Deposition

Produção de Filmes Espessos Compósitos de $BaLa_4Ti_4O_{15}$ e $Ba_4Nd_{9.33}Ti_{18}O_{54}$ por Deposição Electroforética

Dissertação apresentada à Universidade de Aveiro para cumprimento dos requisitos necessários à obtenção do grau de Mestre em Ciência e Engenharia dos Materiais (EMMS), realizada sob a orientação científica da Professora Dra. Paula Maria Vilarinho, Professora Associada do Departamento de Engenharia Cerâmica

A dissertation presented to the University of Aveiro to obtain the Master degree in Materials Science and Engineering (EMMS), under the scientific guidance of Professor Dr. Paula Maria Vilarinho, Associate Professor of the Department of Ceramics and Glass Engineering of the University of Aveiro, Portugal

The Board of Examiners

president

Prof. Dr. Maria Margarida Tavares Lopes de Almeida
Auxiliar professor from the University of Aveiro

Prof. Dr. Mário António Caixeiro Pereira
Auxiliar professor from the University of Minho

Prof. Dr. Paula Maria Lousada Silveirinha Vilarinho
Associate professor from the University of Aveiro

Acknowledgements

I oblige my deepest gratitude to supervisor Professor Paula M. Vilarinho for her invaluable guidance, support and encouragement through out the thesis. I thank her for critical supervision, powerful advisement and patient listening of my thoughts.

I would like to thank all the members of Department of Ceramics and Glass Engineering of the University of Aveiro, who shared scientific knowledge and made a friendly atmosphere during my stay. I am grateful to Dr. Surendran Peethambharan for his invaluable discussions on high frequency materials.

I would like to thank European Union for their financially support and all the co-ordinators of the European Master on Materials Science (EMMS) program. Especial thanks to Professor Margarida Almeida for her constant encouragement during my thesis. I would like to thank all my friends from EMMS, in particular Andreia, Asif, Liliana and Wenbin.

It is a pleasure to thank all my friends who made this period enjoyable and unforgettable, they are immense in number and the space provided is quite few so, I am not mentioning their names.

My thanks to God and my family for their blessings which help me to overcome the obstacles during my work.

Palavras-Chave

Filmes espessos, deposição electroforética, compósitos, BNT. BLT, elevado Q, microelectrónica, microondas.

Sumário

As comunicações sem fios experimentaram um crescimento excepcional nas últimas décadas e que se prevê que continue nos próximos anos (Capítulo 1, Referêcia 3) Com este crescimento há uma procura crescente de dispositivos de menores dimensões e mais versáteis, do que os actualmente existentes, que permitam maiores níveis de integração, possibilidade de operação a altas frequências e produção a custos reduzidos. Actualmente existe também a necessidade de desenvolver materiais com permitividade dieléctrica relativa (ε_r) entre 40 - 80, baixas perdas dieléctricas e coeficiente de temperatura da frequência de ressonância (t_f) próximo de zero. Actividades de investigação e desenvolvimento para explorar a utilização de tecnologias de fabrico de filmes finos e espessos para substituir os materiais cerâmicos em uso corrente, estão actualmente em curso.

Neste contexto, foi explorada no presente trabalho a fabricação de filmes espessos por deposição electroforética (EPD) do composto $BaLa_4Ti_4O_{15}$ (BLT), cuja selecção se relaciona com as óptimas propriedades que apresenta para aplicação às frequências das microondas. Foi igualmente tentada a preparação de filmes espessos compósitos de $BaLa_4Ti_4O_{15}$ (BLT) - $Ba_4Nd_{9.33}Ti_{18}O_{54}$ (BNT) para preenchimento do intervalo existente em termos de materiais com permitividades dieléctricas 40-80. A escolha da deposição electroforética de entre os vários processos de fabricação de filmes espessos prende-se com as características únicas desta técnica, nomedamente, elevada flexibilidade e simplicidade para aplicação a vários materiais e combinação de materiais, possibilidade de aplicação a uma gama variada de formas e estruturas tridimensionais complexas, densas e porosas e a capacidade de ser utilizada à escala industrial a baixos custos.

Neste trabalho foi seguida uma aproximação sistemática para a fabricação dos filmes espessos compósitos pr EPD. Primeiramente procedeu-se à síntese de pós monofásicos de BLT e BNT pelo processo convencional de reacção no estado sólido e a sua pureza foi confirmada por análises de Difracção de Raios X. O tamanho e distribuição de tamanho e a morfologia dos pós de BLT e BNT foram caracterizados por recurso a técnicas de determinação de tamanho de partícula e microscopia electrónica de varrimento. De seguida foram preparadas suspensões dos pós de BNT e BLT em diferentes meios suspensores, como água, etanol e trietanolamina. Ao mesmo tempo, foi estudada a estabilidade das suspensões por análises de tamanho de partícula e

medidas de transmitância de luz UV. As suspensões com estabilidade optimizada foram utilizadas para deposição de filmes espessos, em meio básico e meio ácido e foram estudadas as variáveis de processamento, como espessura, massa do depósito, corrente eléctrica em função do tempo e voltagem. Foi também discutido o efeito do passo de prensagem isostática, após deposição, na morfologia e densidade dos filmes e também na sua resposta dieléctrica.

Filmes de BLT de 10 mm de espessura depositados sobre folhas de platina e sinterizados a 1600ºC/1h exibem ε_r = 58, TCε_r +30ppm/ºC e perda dieléctrica de 0.002 a 1 MHz. Como termo de comparação foram preparados cerâmicos de BLT. Foi feita a caracterização estrutural, microestrutural e dieléctrica de filmes e cerâmicos de BLT, sinterizados entre 1400ºC e 1600ºC.

Filmes espessos compósitos de BNT/BLT e BLT/BNT foram preparados com sucesso por EPD. Através da combinação de camadas de BLT e BNT foram preparados filmes espessos compósitos de 30 μm com ε_r ~71, TCε_r ~-16ppm/ºC e perda dieléctrica de a 1 MHz. Estes resultados são de particular relevância visto que combinam a possibilidade de preparar filmes espessos com propriedades desenhadas para aplicações a frequências elevadas e das microondas com a capacidade de diminuir o tamanho do dispositivo. Embora preliminares estes resultados abrem novas oportunidades tecnológicas, que deverão ser mais exploradas.

keywords

Microwave Material, Electrophoretic Deposition, Composites, BLT, BNT, High Q, Microelectronics, Microwave Material

abstract

Wireless communications have experienced an exceptional growth in the last decades and similar growth is expected for next coming years, according to the ABI analysis [Chapter 1, Reference 3]. With this growth there is an increase demand for the production of devices of smaller dimensions and more flexible than the current in use ones, with increased integration, possibility of operation at high frequencies and produced with reduced costs. There is also a present demand to develop materials with relative permittivity (ε_r) between 40 - 80, low loss and near zero temperature coefficient of resonant frequency (t_f). Research activities to exploit thin and thick film technologies to replace the bulk ceramics are currently underway.

Within this context, in this work, the fabrication of thick films by electrophoretic deposition of the tertiary compound $BaLa_4Ti_4O_{15}$ (BLT) was exploited, because of the optimal properties for microwave applications of BLT. Simultaneously, the preparation of $BaLa_4Ti_4O_{15}$ (BLT) - $Ba_4Nd_{9.33}Ti_{18}O_{54}$ (BNT) composite thick films was attempted to fill the permittivity gap of 40-80 as describe above. The choice of electrophoretic deposition (EPD) technique over other thick film processing techniques is obvious because of its unique features, such as the high flexibility and simplicity for application with various materials and combinations of materials, and on a wide range of shapes and 3D complex and porous structures, and its ability to be scaled-up to the fabrication of large product volumes and sizes at low costs.

A systematic approach was used to fabricate the composite thick films. Firstly, BLT and BNT powders were prepared by solid state reaction synthesis and the phase purity of the powders was confirmed by XRD. The size and morphology of the powders were assessed by particle size analysis and scanning electron microscopy. BNT and BLT suspensions were prepared in different suspension media such as water, ethanol and acetone. The pH of the suspension was varied by dilute nitric acid and triethanolamine. Concomitantly the stability of the suspensions was characterised by particle size analysis and UV transmittance measurements. Stable suspensions were used for the deposition of particles in acidic and basic conditions, and the processing parameters such as thickness, deposit weight, current as a function of time and voltage were studied. The effect of iso static pressing and film thickness on the properties and morphology was also discussed.

10 mm thick BLT films on platinum foils and sintered at 1600ºC/1h exhibit ε_r = 58, TCε_r +30ppm/ºC and loss tangent 0.002 at 1 MHz. As a comparison tool, BLT ceramics were prepared as well. Films and ceramics were sintered between 1400ºC to 1600ºC and their morphology and dielectric response assessed.

BNT/BLT and BLT/BNT composite thick films were successfully prepared by electrophoretic deposition. By the combination of BLT and BNT layers a 30 µm composite thick film with ε_r ~71, TCε_r ~-16ppm/ºC and loss tangent of 0.002 at 1 MHz were prepared. These results are of particular relevance since they combine the possibility to prepare thick films with tailored properties for high frequency and microwave properties with the aptitude to decrease the device size. Although preliminary these results open further technological opportunities, that should be more explored

Table of Contents

List of Figures

List of Table

List of Symbols

List of Abbreviations

Table of Contents

List of Figures

List of Tables

List of Symbols

α_l – linear thermal expansion coefficient

E - dc bias electric field

f – frequency

k_B - Boltzmann constant (1.38066· × 10-23 J/K)

P - polarization

Pr - remnant polarization

Ps - spontaneous polarization

Qf - quality factor

T - temperature

Tanδ - loss tangent or dissipation factor

TCC – temperature coefficient of capacitance

$TC\varepsilon_r$ – temperature coefficient of relative permittivity

V – voltage

ε_r - relative permittivity or dielectric constant

ε_0 - dielectric constant of vacuum (8.854×10^{-12} F/m)

ε^* - complex dielectric permittivity

ε' - real part of dielectric permittivity

ε'' - imaginary part of dielectric permittivity

τ_f or t_f - temperature coefficient of resonant frequency

ω - angular frequency

Abbreviation

MW Microwave Frequency

(GPS) Global positioning system

MIC Microwave integrated circuit

MMIC Monolithic microwave integrated circuit

LAN Local area network

PCS Personal communication system

RF Radio frequency

IC Devices and integrated circuit

WLAN Wireless local area net

Chapter 1.
Introduction to Microwave Dielectrics

Abstract:

Microwave (MW) dielectrics are playing an important role in the wireless communication in the form of microwave devices such as resonator, filter and antennas. Microwave devices have application in terminals, base station, satellite and mobile phones. With the growth of telecommunication, demand is also increased for material with higher relative permittivity for miniaturization of the existing devices.

This chapter reviews the sequential evaluation of the dielectric ceramics and the properties to the corresponding materials. $BaO\text{-}R_2O_3\text{-}TiO_2$(BRT) (R = rare earth element) system belong to the family of high relative permittivity materials with low losses and show the potential to scaled down the existing microwave devices in thick film. From BRT family the two compounds selected for this studies are $Ba_4Nd_{9.33}Ti_{18}O_{54}$(BNT) and $BaLa_4Ti_4O_{15}$ (BLT). The literature review of these compounds are illustrated and chapter ends with the description of microwave material application

1.1 Introduction

The term microwave refers to electromagnetic energy having a frequency higher than 1 gigahertz (billions of cycles per second) and materials which shows resonance at this frequency are known as microwave resonators. Microwave signals propagate in straight lines and they are not or very little affected by troposphere, ionized regions in the upper atmosphere and barriers such as hills, mountains, and large human-made structures.

Most microwave systems operate in the 300 MHz to 30 GHz range of frequency in electromagnetic (EM) spectrum. For telecommunications, the most important markets are ultra-high frequency TV broadcasting (470 - 870MHz), satellite TV broadcasting (4 GHz) and the mobile phone network (900 MHz - 1800 MHz) [1]. In terms of devices, the microwave market is dominated by the bulky invar coaxial and cavity resonators which have 3 times lower cost then neodymium (Nd) and tantalum (Ta) based ceramics. Neodymium and tantalum based resonators are used where high quality factor (Qf) is

needed. In the last three decades, the discovery and development of the telecommunications and associated devices created a new era to ceramics and in particular to dielectric ceramics which have edge on the bulky metal resonators because of there low weight and possibility of miniaturisation. Today, dielectric ceramics are having key applications in resonators, filters and other components in microwave communication systems. Still there are various challenges for the new generation of microwave ceramics to be achieve, namely to reduce dielectric losses, to optimise the device design, to reduce the size (miniaturization) and to further lower the cost of ceramics resonators and filters.

The global market for the dielectric ceramics is of the order of $400 million; while the markets for the resulting devices and components, and for the end-user systems, are ~10 and ~100 times that size, respectively [2]. At the time of economic recession the only sector which is untouched by recession is telecommunication. A recent survey by ABI Research has predicted that mobile services revenues will continue to grow at nearly 1.2% through 2014 (Figure 1-1) [3].

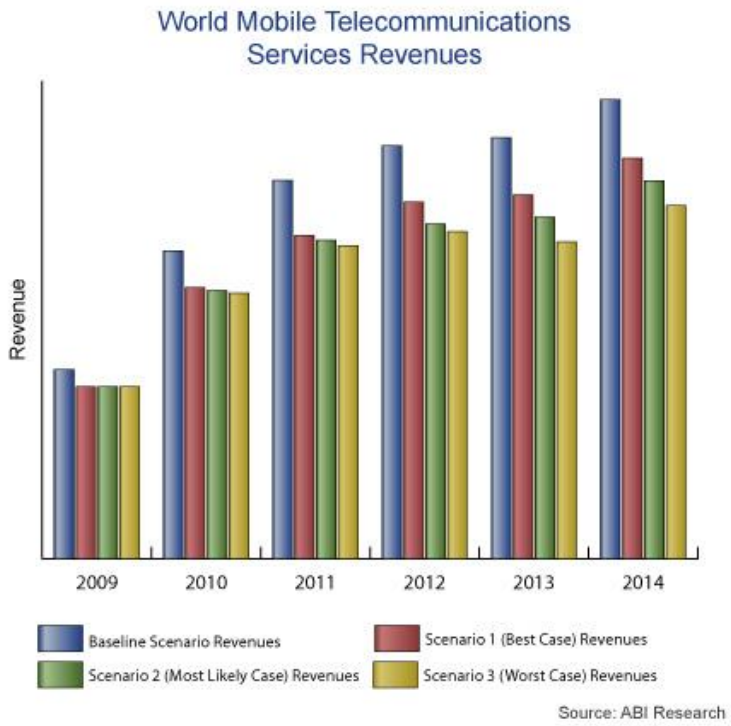

Figure 1-1: World mobile telecommunication revenue for next five years [3].

At the present, commercial microwave ceramics fall into two main categories: (i) ceramics with low dielectric permittivity, ε_r ($20 < \varepsilon_r < 45$) and quality factor (Qf) (100,000-20,000GHz) and (ii) ceramics with high ε_r (>80) and moderate quality factor (Qf) (10,000GHz) [1].

The three main prerequisites which make dielectric ceramic materials suitable for the microwave applications are:

- High Quality factor (Qf) or low dielectric loss (tan δ)
- High relative permittivity (ε_r)
- Near zero Temperature coefficient of thermal stability (t_f)

1.1.1 Relative Permittivity

Permittivity is a physical quantity that describes how an electric field affects, and is affected by a dielectric medium, and is determined by the ability of a material to polarize in response to the field, and thereby reduce the total electric field inside the material [4].

The overall net polarization experienced in a material, P, creates a dipole moment which augments the total displacement flux of dipoles, D. Thus,

$$D = \varepsilon_0 E + P \qquad (1\text{-}1)$$

where E stands for the applied field and ε_0 for the permittivity of free-space. And the net polarization can be written in terms of the susceptibility, χ,

$$P = \varepsilon_0 \chi E \qquad (1\text{-}2)$$

thus the relative permittivity can be defined in terms of the susceptibility that is directly related to the polarization mechanisms in a material:

$$D = \varepsilon_0 (1+\chi) E = \varepsilon_r \varepsilon_0 E \qquad (1\text{-}3)$$

where

$$\varepsilon_r = \frac{\varepsilon}{\varepsilon_0} = \text{relative permittivity} \qquad (1\text{-}4)$$

The relative permittivity, ε_r, is then the ratio of the natural permittivity of the material (ε) to the permittivity of free-space (ε_0). The permittivity, ε, is considered to be a

direct measure of the polarizability of a material and will govern both the phase variation and attenuation of an imposed field to the material. Thus, the permittivity, ε, is a complex quantity with both real and imaginary parts and can be written as,

$$\varepsilon = \varepsilon' + j\,\varepsilon'' \qquad (1\text{-}5)$$

the real part of the relative permittivity, ε', is termed the dielectric constant and is determined by the magnitude of P. It defines the amount of electrostatic energy stored per unit volume in a material for a given applied field, i.e. the amount of charge stored in a capacitor. The imaginary component of the permittivity, ε'', is called the loss factor and is governed by the lag in polarization upon application of the field and the energy dissipation associated with charge polarization. It represents the energy loss in a material; j is a complex number [5].

A high relative permittivity is desirable for circuit miniaturisation, because diameter of dielectric component is inversely proportional to the square root of its relative permittivity, so higher the permittivity smaller the size of microwave resonator.

$$d=\lambda_0 \cdot \frac{1}{\sqrt{\varepsilon_r}} \qquad (1\text{-}6)$$

where d stands for the diameter of the dielectric component, and λ_0 for the wavelength at the resonant frequency [6]. As a consequence, the size reduction of a dielectric component requires materials with a high relative permittivity.

1.1.2 Loss Tangent

The loss tangent, tanδ, relates to the electrical losses in the material and is given by:

$$\tan\delta = \frac{\varepsilon''}{\varepsilon'} \qquad (1\text{-}7)$$

where δ stands for loss angle, ε'' for the energy loss and ε' for the stored energy. In terms of an electrical circuit, tanδ represents the resistive part of the impedance and is directly proportional to the electrical conductivity [4].

The quality factor, Q is defined by:

$$Q = 1/\tan\,\delta \qquad (1\text{-}8)$$

and it is a measure of the efficiency or power-loss of a microwave system. This definition is not particularly useful for visualizalizing how Q relates to microwave communication. More succinctly, it is determined experimentally at the resonance frequency (f_o) divided by the bandwidth, (Δf_o), measured at 3dB below the maximum height at resonance [7]. Q is a measure of the selectivity of the resonator to a given frequency. Higher Q means a narrow peak which results in reduced risk of cross-talk within a given frequency range, which in turn gives high selectivity to a given frequency and therefore increase the density of channels in a given frequency band. Losses normally increase with increasing frequency; therefore Q is also frequency dependent. The relation between the two, Qf, where f is the measured frequency is always constant so, Qf values are quoted when comparing low loss (high Q) dielectric microwave ceramics [7].

1.1.3 Temperature Coefficient of Resonant Frequency (t_f)

The temperature coefficient of resonance frequency (t_f) is the parameter which characterises the thermal stability of the material. It measures the "drift" with respect to the temperature of the resonant frequency [4].

$$t_f = \frac{\Delta f}{f_0} \cdot \frac{1}{\Delta T} \qquad (1\text{-}9)$$

where f_0 stands for the resonant frequency at ambient temperature and Δf for the frequency variation among the temperature range ΔT. Conventionally, t_f specifies the resonant frequency change in parts per million per degrees centigrade (ppm/^{o}C). The poor temperature stability would cause the in and out drift of resonance of the carrier signal during hot and cold days. The practical requirement is that for a temperature ranging between -40^{o}C and 100^o, t_f should vary less then 10ppm/^{o}C [8].

Temperature coefficient of resonant frequency (t_f) is related with the temperature coefficient of the dielectric constant, $TC\varepsilon_r$, by the following relation:

$$t_f = -1/2\ TC\varepsilon_r - \alpha \qquad (1\text{-}10)$$

where α stands for the thermal expansion coefficient of the material [9]. $TC\varepsilon_r$ describes the maximum change in relative permittivity over a specified temperature range. t_f is

depending on the $TC\varepsilon_r$, which is typically reported between -2000 to 2000 ppm/ºC in dielectric materials [8]. This is the stringent restriction for the material with higher dielectric constant to be used for microwave systems. Wersing [6] related the $TC\varepsilon_r$ with polarizability and further with the structure to give a clear picture of the $TC\varepsilon_r$ variation in different structures and conditions. The large $TC\varepsilon_r$ of diatomic alkali halide is obviously caused by the strong increase of the ionic polarization with volume and by the large thermal expansion with the increase of the temperature. In materials with more complicated structures, $BaMg_{1/3}Ta_{2/3}O_3$, $BaZn_{1/3}Ta_{1/3}O_3$, the additional ionic polarizability not only raises permittivity but also shifts $TC\varepsilon_r$ to negative values. Both strong electronic and ionic polarizabilities also give rise to a softening of the lattice modes, thus the anharmonic contribution to $TC\varepsilon_r$ increases and makes $TC\varepsilon_r$ even more negative. This decrease of $TC\varepsilon_r$ with increasing permittivity is consistent with the behaviour of paraelectrics [6].

1.2 Important Groups of Microwave Ceramics

Microwave dielectric ceramics are characterized by high ε_r, low loss (high Q), and near zero t_f, making them attractive as electronic components in microwave applications, as mentioned previously. In the mid-1960s, Cohn and his co-workers performed the first extensive theoretical and experimental evaluation of the low loss dielectric resonators [10], based on rutile (TiO_2) ceramics. The poor temperature stability of rutile dielectrics prevented the development of practical components for commercial applications. A real breakthrough occurred in the earlies 1970s when $BaTi_4O_9$ based ceramics full filled the technical requirement, with ε_r ~38, t_f =15ppm/ºC. and Q=5000 at 2GHz [11]. Later, a modified $Ba_2Ti_9O_{20}$ with improved performance was reported by Bell Laboratories having ε_r ~40, t_f = 2 ppm/ºC and Q= 15000 at 2GHz [10]. The next major breakthrough came from Japan when the Murata Manufacturing Company produced $(Zr_{0.8}Sn_{0.2})TiO_4$ ceramics [12-13-14], which offers adjustable compositions so that the temperature coefficient could be varied between 10 to 12 ppm/°C. A list of important groups of dielectrics and their properties is tabulated in Table 1-1.

Table 1-1: Important groups of microwave ceramics [6].

Ceramics	Relative permittivity (ε_r)	t_f(ppm/°C)	Quality factor(Q) At 2 GHz	Quality factor(Q) At 20 GHz
$Ba_2Ti_9O_{20}$	40	2	15 000	2000
$Zr_{0.8}TiSn_{0.2}O_4$	38	10-12	15 000	3000
$BaTi_u[(Ni_xZn_{1-x})_{1/3}Ta_{2/3}]_{1-u}\ O_3$	30	-3-+3	26 000	5000
$Ba[Sn_x(Mg_{1/}3Ta_{2/3})_{1-x}]O_3$	25	~0	>40 000	10 000
Nd_2O_3-BaO-TiO_2.Bi_2O_3	~90	~0	3 000	-
$BiNdO_4$	~40	~30	4 000	-

The commercially available microwave ceramic compounds generally categories in to two groups; titanium based and tantalum based. Table 1-2 summarises the dielectric properties of commercial available microwave resonators for MW Ceramics with almost zero t_f. $CaTiO_3$-$NdAlO_3$ (CTNA) and $ZrTiO_4$-$ZnNd_2O_6$ (ZNZN)- based ceramics are dominating the base station market. $Ba(Co,Zn)_{1/3}Nd_{2/3}O3$(BCZN)-based ceramics are the most cheapest material for MW cavity resonators with high Qf of 90 000 [7]. Tantalum based compounds are used when there is the need of high Qf materials. $Ba(Mg_{1/3}\ Ta_{2/3})O_3$ (BMT) and $Ba(Zn_{1/3}\ Ta_{2/3})O_3$ are mainly used in satellites where selectivity to a given frequency is paramount. The presence of Ta makes this compound very costly for applications. The researchers are currently working on understanding the role of Ta, so that it could be replaced by low cost material. The ceramics based on Nd_2O_3 (or La_2O_3), BaO and TiO_2 were already quite common for capacitors with an almost temperature independent capacitance and now found importance in microwave application; they are known to be ´high ε_r´ microwave ceramics [6]. Within this family $Ba_4Nd_{9.33}Ti_{18}O_{54}$ (BNT) compound has a tungsten bronze structure with high permittivity of 80 and is commercially used as digital television receiver and could be used as dielectric resonator antennas and coaxial line resonator where Q is dominated by the metallization. Two decades ago, the $Ba_nLa_4Ti_{3+n}O_{12+3n}$ (BLT) homologous series was found near the $Ba_{6-3x}.R_{8+2x}Ti_{18}O_{54}$(R= rare Earth). In this series the compound $BaLa_4Ti_4O_{15}$ (BLT, n=1) has high relative permittivity ~44, with high Qf 47 000 GHz and t_f near to zero (-2ppm/°C). This material has optimal properties to be used as in telecommunication base stations.

In this work, the fabrication and properties of BNT and BLT dielectric thick films and thick film composite were exploited and it was verified that thick films present optimal

properties to be used as antennas, filters and other microwave application, in which miniaturization is required.

Table 1-2: Commercial available dielectric ceramics for cavity resonator for MW application with almost zero temperature coefficients of resonant frequency tf [7].

Material	Abbreviation	ε_r	Qf (GHz)
$BaMg_{1/3}Ta_{2/3}O_3$	BMT	24	250 000
$BaZn_{1/3}Ta_{2/3}O_3$	BZT	29	150 000
$Ba(Co,Zn)_{1/3}Nd_{2/3}O_3$	BCZN	34	90 000
$SrTiO_3$-$LaAlO_3$	STLA	39	60 000
$CaTiO_3$-$NdAlO_3$	CTNA	45	48 000
$ZrTiO_4$-$ZnNd_2O_6$	ZTZN	44	48 000
$Ba_4Nd_{9.33}Ti_{18}O_{54}$	BNT	80	10 000

1.3 BaO-Nd_2O_3-TiO_2 (BNT)

Interest has spread quickly to rare earth elements, BaO-R_2O_3-TiO_2 systems (R = rare earth, such as La, Sm, Nd, Pr), due to their high permittivity which makes possible for the size reduction. At the present the only commercially available group of high relative permittivity microwave materials were ceramics based on BRT solid solutions with relative permittivity ranging from 80 to 90. BaO-Nd_2O_3-TiO_2 (BNT) system stands out and has attracted the interest of researchers and industrialists due to its high relative permittivity. The earliest works on these systems are credited to Bolton [15] and Kolar *et al.* [16-17].

Kolar *et al.* [17] estimated the ternary compound $BaO.R_2O_3.4TiO_2$ as $BaO.R_2O_3.5TiO_2$. Later, Takahashi *et al*. [18-19] used the more precise co-precipitation method to synthesise the tertiary compound and based on X-ray, TEM and Raman spectroscopy analysis the authors proposed a corrected composition as $BaO.R_2O_3.4TiO_2$ (R = La, Nd, Sm and Pr) which confirmed the earlier results of Razagon *et al.* [20,21] and Matveeva *et al*. [22].

Later, Ohsato *et al*. [23] reported the structure of this compound, is a new pervoskite like column which has 2X2 unit cell of pervoskite. The crystal structure of BNT compounds essentially consists of a three-dimensional framework of corner-sharing pervoskite-like octahedra joined together according to a pattern similar to that of the tetragonal tungsten bronzes. The structure is typified by oxygen octahedra linked at the corners in a complex way to yield three types of channels: large pentagonal sites; diamond sites; and tiny triangular sites (Figure 1-2). The rare earth cations, i.e. Nd^{3+}, occupy the rhombic channels (diamond sites), Ba^{2+} cations fill the pentagonal channels [23]. The triangular channels are empty. The crystallography of BRT solid-solutions has been reported by different authors. Gens *et al*.[24] suggested Pba2 (No. 32) or Pbam (No. 55) as possible space groups for the solid solution with the lattice parameters calculated for the Nd-analogue are a = 12.30 Å, b = 22.21 Å, c = 3.84 Å. Later, Ubic *et al.* [25] found that more correct assignment of space group is $Pb2_1m$.

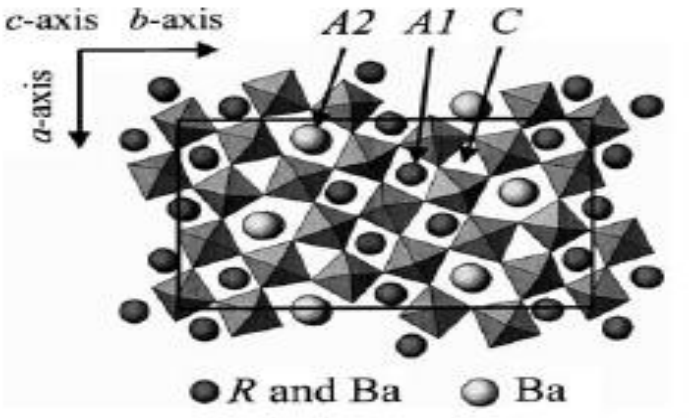

Figure 1-2: Tungsten-bronze type like crystal structure of the $Ba_{6-3x}R_{8+2x}Ti_{18}O_{54}$ solid solutions, in which R-rare earth [23].

Without any further ambiguity about the structure of the compound, the solubility limit and the formula for BRT (R=Nd and Sr) was studied by Ohsato *et al.*[26] on the tie line x= 0 to 1, depicted in Figure 1-3. Along the tie line, between $BaTiO_3$ and $BaO.R_2O_3.4TiO_2$ compound the ratio between Ti:O(1:3) remain fixed. Such solid solutions have different valence cations with large size: divalent Ba^{2+} and smaller trivalent rare earth

R^{3+}. To maintain electrostatic stability, three Ba^{2+} ions should be replaced with two R^{3+} ions and a vacancy. So the substitution formula along the tie line is as follows.

$$3Ba^{2+} \text{ «==» } 2R^{3+} + V_{Al}$$

where V_{Al} is the valence of A1 site. The derived chemical formula for the solid solution is $Ba_{6-3x}.R_{8+2x}Ti_{18}O_{54}$. The authors reported the formation of solid solution of the tertiary compound $Ba_{6-3x}.R_{8+2x}Ti_{18}O_{54}$ (R = Nd) for x ranges from $0.0 \leq x \leq 0.75$.

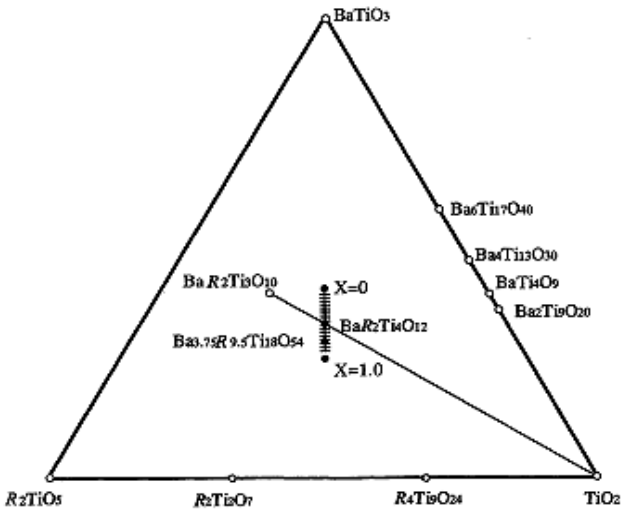

Figure 1-3: Ternary phase diagram of BaO-R_2O_3-TiO_2 system [26].

In later studies, Ohsato *et al*. [23] found that the tertiary component for x = 2/3 exhibit a high Qf factor of 10,000 and ε_r 80-85 because of higher ordering of Ba and Nd in A2 and A1 sites at this composition; another possible reason might be the lower internal strain compared with other compositions, which was obtained for the $\beta = 2\eta\tan\theta$ equation using Full Widths at Half Maximum (FWHM) of powder XRD, as illustrated in Figure 1-4.

The further solubility limit $0.7 \leq x \leq 1$ was studied by L Zang *et al*. [27] in which the authors reported good dielectric properties for composition x= 0.8, 0.9 and 1 with some secondary phases of TiO2 and $Nd_4Ti_9O_{24}$.

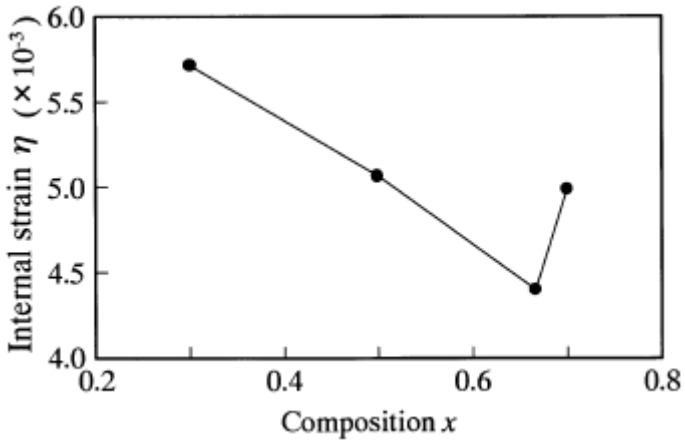

Figure 1-4: Internal strain versus composition(x) of Nd in $Ba_{6-3x}.R_{8+2x}Ti_{18}O_{54}$ [23].

BNT (1:1:4) have high Qf and permittivity but the t_f (+59ppm/ºC) does not match the application requirements. To make this material more useful in terms of practical applications it has been reported that t_f can be tuned by the following approaches (i) by the use of additives; (ii) proper variation of the Nd : Ba ratio, and (iii) or combination of different rare earth elements. For example, Yong Jun [28] substituted Ba with some fraction of Bi to get t_f near zero but simultaneously observed that large amounts of Bi reduce markedly Qf. By substituting Ba by Pb in BNT(114), Wakino *et al*. [29] achieved a high ε_r of 85-88, a t_f near zero and Qf = 6000GHz. Later, Nishigaki [30] achieved better microwave properties by substituting some Ba by Sr. Yong *et al*. [31] substituted Bi for Nd in $Ba_{6-3x}.R_{8+2x}Ti_{18}O_{54}$ and achieved excellent dielectric properties of ε_r = 99.1, t_f = -5.5ppm/ºC and Qf = 5890GHz. The substitution of Nd and Ti in $BaNd_2Ti_4O_{12}$ by Bi and Zr originated an increase of the permittivity from 80 to 125 but quality factor decreasees from 3000 to 600 and 4GHz, as reported by Nenasheva *et al* [32]. Kim *et al* [21] studied the effect of additional quantities of Nd and Ti on BNT ceramics. With the increase of Nd the sintering temperature increases and the quality factor decrease and vice versa for titanium excess. The authors concluded that, the deviation from BaO/Nd_2O_3 = 1, the properties decrease because of the formation of secondary phases.

In addition, as a result of the anisometric crystal structure (lattice parameter b(22.15)>a(12.13)>c(3.819)), BRT series tend to show anisotropic development of elongated grains in the microstructure at particular processing conditions. Therefore the

dielectric properties of BRT ceramics display significant anisotropy as reported by Negas [33], and Hoffmann and Waser [34].

In particular for BNT (1:1:4, x=2/3, discussed above), Wade *et al*. [35] confirm the anisotropic behaviour for ceramics prepared with and without template, and found that in perpendicular direction to the (0 0 1)-textured $Ba_4Nd_{9.33}Ti_{18}O_{54}$ (BNdT) t_f decreased from 59.2 ppm/ºC to 35 ppm/ºC and with template it goes to zero.

An anisotropic behaviour was also reported very recently for thick film of BNT(1:1:5) prepared by electrophoretic deposition [36]. It was reported that with increasing sintering temperature there is an increase in the aspect ratio of the ceramic grains and $TC\varepsilon_r$ changes from -114 to +12ppm/ºC. These results are of particular importance since it demonstrates that by controlling the processing parameters one may tailor the $TC\varepsilon_r$ of thick films and at the same time to miniaturise the device size.

Summary of important findings in the BNT system is given in Table 1-3.

Table 1-3: Important properties reported for BaO_2-Nd_2O_3-TiO_2 (1:1:4) system.

$Ba_{6-3x}.R_{8+2x}Ti_{18}O_{54}$	Relative permittivity	t_f or $TC\varepsilon_r$(ppm/ºC)	Qf (GHz)	Group
BNT(1:1:4) substitute Ba with Pb	85-88	0	6000	Wakino (1984)
$BaNd_2Ti_4O_{12}$ substitute Nd and Ti with Bi and Zr	125	--	600	Nenasheva (2001)
BNT(x=2/3) (Perpendicular)	65.4	+35.3	8900	Ohsato (2006)
BNT (x=2/3) (parallel)	71.8	+109.2	9400	Ohsato (2006)
BNT (x=2/3) + Template (perpendicular)	79.8	0	9500	Ohsato (2006)
BNT (x=2/3)	83	59.2	9300	Ohsato(2001)
Ba6−3*x*(Nd0.85,Bi0.15)8+2*x*Ti18O54	99.1	-5.5	5290	Y. J. Wu (2001)

1.4 $BaLa_4Ti_4O_{15}$ (BLT)

The large majority of microwave dielectric ceramics have the perovskite type structure or a related one. Perovskites have the general formula ABO_3. The classic prototype (high-temperature) symmetry is a primitive cubic cell, but perovskites may

undergo many types of phase transitions on cooling and the symmetry is rarely cubic at room temperature so as tertiary compound of $BaO–La_2O_3–TiO_2$ system.

In the $BaO–La_2O_3–TiO_2$ system, Saltykova *et al*. [37] found the $Ba_nLa_4Ti_{3+n}O_{12+3n}$ homologous series exists with three kinds of compounds on the $La_4Ti_3O_{12}–BaTiO_3$ tie line near the tungstenbronze-type like $Ba_{6-3x}R_{8+2x}$ $Ti_{18}O_{54}$ (R = rare earth) represented in the phase diagram of the $BaTiO_3–La_4Ti_3O_{12}$ binary system of (Figure 1-5): n = 1, $BaLa_4Ti_4O_{15}$; n = 2, $Ba_2La_4Ti_5O_{18}$; and n = 4, $Ba_4La_4Ti_7O_{24}$. Different R&D groups have written the compound formula in different ways the Fritz group in France represent it as $(Ba,La)_nTi_{n-1}O_{3n}$, where n = 5, $BaLa_4Ti_4O_{15}$ [38-39-41].

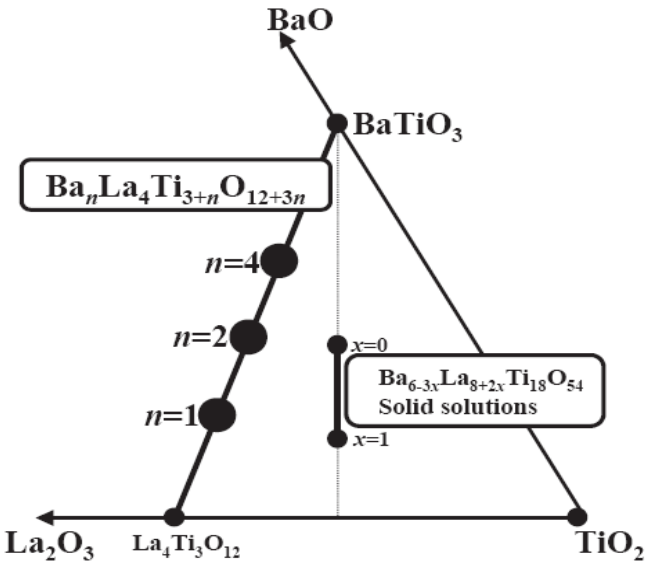

Figure 1-5: Phase diagram of the $BaTiO_3$-$La_4Ti_3O_{12}$ binary system [41].

The crystallographic system of $BaLa_4Ti_4O_{15}$ compound is an hexagonal perovskite like layer structure as proposed by Saltykova *et al*. [37]. Harre *et al*. [38] further analyzed the crystal structure of $BaLa_4Ti_4O_{15}$ without distinguish Ba/la sites by using X-Ray diffraction. This structure stacking with $(Ba, La)O_3$ close-packed layer consists of one perovskite slab with cubic closed packing and another junction slab with an hexagonal closed packing type.

Later, the crystal structure as a function of the Ba/La ordering was analyzed using Rietveld refinement of neutron powder diffraction by Teneze *et al*. [39] and distinguishes the Ba and La sites in the crystal structure of $BaLa_4Ti_4O_{15}$ compound. Ohsato *et al.* [40] have also successfully distinguished the sites of Ba^{2+} and La^{3+} in $BaLa_4Ti_4O_{15}$ compound by the X-ray analysis of single crystal regardless of similarity for atomic scattering factors. G. Trolliard *et al.* [41] study the microphases in the $La_4Ti_3O_{12}$-$BaTiO_3$ system by using HRTEM to investigate the coherent intergrowth occurrence in this system.

It has been reported that the structure of BLT corresponds to a close packing of AO_3 (where A = Ba, La) mixed layers [41]. Within the layers, the A and O atoms are ordered (Figure 1-6(a)). Each A atom is surrounded by six oxygen atoms, whereas each oxygen atom has two linearly coordinated A atoms among its six nearest neighbours. To avoid any direct A–A connection, successive layers are shifted from each other by a $1/3(0\ 1\ -1\ 0)_H$ vector, so that the A atom positions in one layer project into the centre of a triangle formed by the A atoms in the adjacent layers (position 1 or 2 in Figure 1-6(a)). One quarter of the octahedral interstices between two such layers are surrounded exclusively by oxygen atoms and are occupied by Ti atoms (the small open circles in Figures 1-6 (b)–(d)). All oxygen octahedra located within the cubic-close-packed (ccp) part of the sequence are corner shared and occupied by Ti atoms. In each triplet of face-sharing octahedra, characteristic of the hexagonal-close-packed (hcp) part of the sequence, the central octahedra are vacant. The lattice parameter *a* is determined by the hexagonal sublattice of A atoms and remains nearly constant at ~5.6 A°. The *c* parameter depends on the stacking sequence of AO_3 layers (the thickness of each octahedral sheet is ~2.2 A°). In the case of BLT, n = 5, and a cooperative tilting of TiO_6 octahedra within the perovskite blocks leads to doubling of the c-axis. As a consequence, BLT is ascribed as a trigonal structure with the space group P.3c1, and the lattice parameters derived from x-ray diffraction data are a = 5.5720 A° and c = 22.500 A° (≈10 × 2.2 A°), respectively, in the hexagonal setting [14].

Reaney *et al*. [42] further investigated the structure of BLT ceramics because of the existing asymmetric peak in X-Ray diffraction studies. Based on energy-dispersive x-ray analysis and raman spectroscopy it was concluded that there is a heterogeneous distribution

of the constituent cations, may induce asymmetry which cause the presence of two hexagonal phases of slightly different lattice parameter.

The dielectric properties of $BaLa_4Ti_4O_{15}$ ceramics were reported by Vineis *et al.*[43] to be $\varepsilon_r = 43$, Qf = 11583GHz and $t_f = -17$ppm/ºC. La was substituted with various cations as Al, Y, Sm, Nd and Gd for composition n=1 in order to obtain t_f near zero and best results were achieved for Al with $t_f = +1.3$ ppm/ºC, $\varepsilon_r = 44$ and Qf = 47000GHz.

The dielectric properties of $Ba_nLa_4Ti_{3+n}O_{12+3n}$ were investigated by Ohsato *et al.* [44] as well and it was found that properties for `n´ ranges from 0.8-2, ε_r stays constant around 45 and Qf varies between 30000GHz to 48000GHz and t_f from -21 to -12ppm/ºC. For n = 2 to 4, ε_r, t_f increases and Qf decreases because of the formation of secondary phases $Ba_5La_4Ti_8O_{27}$. It was then concluded that compounds ranging from n = 1 to 2 are the suitable materials for microwave applications in base stations of portable telephones with $\varepsilon_r = 44$, Qf = 47000GHz and $t_f = +1.3$ ppm/ºC.

On further investigation on dielectric properties and phase formation for ceramics of $Ba_xLa_4Ti_{3+x}O_{12+3x}$ where `x´ ranges from 0-1 Yamada *et al.* [45] found that for homologous compound $Ba_nLa_4Ti_{3+n}O_{12+3n}$, n = 0, the single phase exists for $Ba_xLa_4Ti_{3+x}O_{12+3x}$, x = 0.0-0.5 and for n = 1 and in the intermediate region the two phase co-exist.

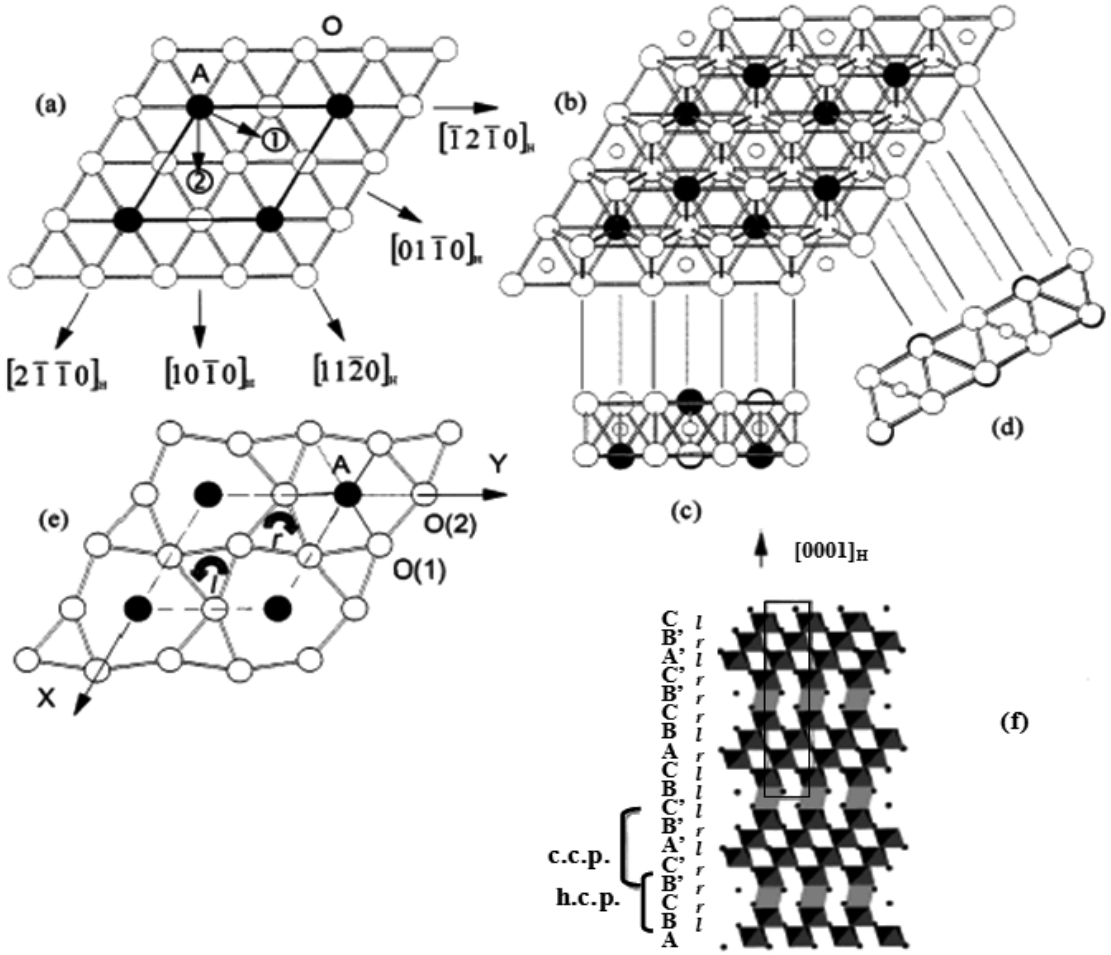

Figure 1-6: (a) Arrangement of A and O atoms in the AO_3 mixed layers; (b) stacking of two adjacent AO_3 layers, showing the TiO_6 octahedra; (c) view of this stacking along $[1\ 0\ -1\ 0]_H$; (d) view of this stacking along the $[1\ 1\ -2\ 0]_H$ direction; (e) the distorted AO_3 layers in BLT–r and l visualize the clockwise and counter clockwise rotations of corner-sharing octahedral respectively; (f) schematic representation of BLT as viewed along $[2\ -1\ -1\ 0]_H$, where the rotations of TiO_6 octahedra around the c-axis are represented by r (clockwise) and l (counter clockwise). ccp and hcp represent cubic close-packed and hexagonal close-packed, respectively[14].

Jawahar *el at*. [46] investigated the properties of $MO–La_2O_3–TiO_2$ where M is Ba, Sr and Ca. For $BaLa_4Ti_4O_{15}$ ceramics with relative density of 96.2% they found that ε_r = 49, Qf = 16222 GHz and t_f -13ppm/ºC, which are similar to the results to those reported by Ohsato *et al.* [2].

For improving the properties of BLT, Longtu Li *et al*. [47] substitute small amounts of Ba by Ca and Sr in $(Ba_{1-x}A_x)La_4Ti_4O_{15}$ (where A is Ca and Sr). It was reported that with Ca substitutions, the permittivity of the sample increases and t_f approaches from -3 to -10ppm/ºC, ε_r = 46, Qf 52800. In the case of Sr substitution the temperature of sintering is reduced to some extent and achieve high Qf up to 53,000 GHz, ε_r = 49 and t_f -3ppm/ºC.

Similar to BNT in BLT ceramics, the large anisotropy in the lattice parameters (a = 5.5720 A° versus c = 22.500 A°) promotes the growth of lath or plate-like particles. Such grains have been reported to align during powder pressing with the a, b plane normal to the pressing direction, and the final sintered body is therefore grain-oriented [42]. Anisotropy in the dielectric permittivity was absorbed by 20% in these ceramics, when measured in the parallel and perpendicular direction to the pressing one.

All the work mentioned above prepared the tertiary compound ($BaLa_4Ti_4O_{15}$) by the solid-state method. Y. Fukami *et al*. [48] in his studies use the molten salt synthesis method using NaCl, KCl and NaCl–KCl flux. Similarly the authors mixed the BLT templets (plate-like) during the synthesis and observed the anisotropic microstructure in the sintered ceramics. The samples prepared with templates shows higher properties then sample prepared without templates.

Hong Zheng *et al*. [49] used glass as a sintering aid material for the composites of BLT and BNT. The sintering temperature was reduced from 1400-1500ºC to 950-1140ºC respectively. The addition of glass did not introduce considerable changes in ε_r and t_f but the Qf (~2305GHz) was deteriorated. Table 1-4 represents the important properties reported for BaO_2-La_2O_3-TiO_2 (1:2:4) compound.

Table 1-4: Important properties reported for BaO_2-La_2O_3-TiO_2(1:2:4) system.

BaO_2-La_2O_3-TiO_2(1:2:4)	**Relative permittivity**	**t_f (ppm/^oC)**	**Q.f (GHz)**	**Group**
$BaLa_4Ti_4O_{15}$	43	-17	11 583	Vineis(1996)
$BaLa_4Ti_4O_{15}$, La substitute by Al	44	+1.3	47000	Vineis(1996)
$Ba_nLa_4Ti_{3+n}O_{12+3n}$ for n= 0.8 to 2	~45	-21 - -12	30000 – 48000	Ohsato(2002)
$BaLa_4Ti_4O_{15}$	49	-13	16222	Jawahar (2002)
$(Ba_{1-x}A_x)La_4Ti_4O_{15}$, A = Ca -Sr	46 - 49	-10 - -3	52800 - 53000	Li (2008)
$BaLa_4Ti_4O_{15}$	45	-2	43 589	Reaney (2006)
$BaLa_4Ti_4O_{15}$ (perpendicular to pressing direction)	52	-	-	Reaney (2006)
$BaLa_4Ti_4O_{15}$ (parallel to pressing direction)	42	-	-	Reaney(2006)

1.5 Application of Microwave Ceramics

Microwave ceramics are used as a dielectric resonator. The term dielectric resonator is defined as a, cylinder with relative permittivity ε_r sufficiently high for a standing electromagnetic wave to be sustained within its volume because of reflection at the dielectric–air interface. Dielectric resonators generally consist of a "puck" of ceramic that has a large dielectric constant and a low dissipation factor. The resonance frequency is determined by the overall physical dimensions of the puck and the dielectric constant of the material.

There are many field modes possible within a resonant chamber. These modes are divided into four basic types, depending on their field components. A propagating electromagnetic wave can have both longitudinal and transverse components. If both the electrical and magnetic fields have only transverse components then the mode is called a transverse electric and magnetic mode or TEM mode. If the electric field´s longitudinal component is zero but the magnetic field is allowed a non zero longitudinal component, then the mode is called a transverse magnetic mode or TM mode. Conversely, if the magnetic field´s longitudinal component is zero but the electric field is allowed a non zero longitudinal component, then the mode is called transverse electric, or TE mode. If the both electric and magnetic field are allowed non zero longitudinal field components, then the mode is a hybrid field different modes.

TE and TM modes are generally written with subscripts, TE_{nmp}, to donate the geometry. The first script, n denotes the number of azimuthal or circumferential field variations in the resonator. The second subscript, m, denotes the number of radial field variations in the width of the resonator. The last subscript p denotes the number of axial variations of the field along the resonator's height. It can be express as the sum $p = l + \delta$, where δ is a non integer number smaller than unity and depends in a complicated way on propagation constant and geometry; and $l = 0,1,2,\ldots$.A diagram of all modes are represented in Figure 1-7.

$TE_{01\delta}$ mode resonator is suitable for the resonator with high Q such as channel filters for the base station. This mode resonator has the highest Q values in the resonator

type but the size is very large. However, TM_{010} modes have 65 % less Qf then $TE_{01\delta}$ mode resonator but size is only about 15 % of $TE_{01\delta}$ mode resonator. TEM is the most common coaxial type resonator; it is widely used as filters in mobile phone and many other radio communication equipment.

Dielectric resonators are increasingly being used at lower frequency, down to 1GHz in mobile telecommunications application frequently as filters. Dielectric resonators at this frequency are bulky but still smaller then cavity resonators. The dielectric ceramics with permittivity higher then 38 is acceptable for this application with high Qf. For further reducing the size, the researches are looking for materials which have high dielectric permittivity with high Q factor [50]. Figure 1-8 shows an example of a space qualified commercial dielectric resonator filter that has been designed for direct broad cast TV satellites operate at 12GHz.

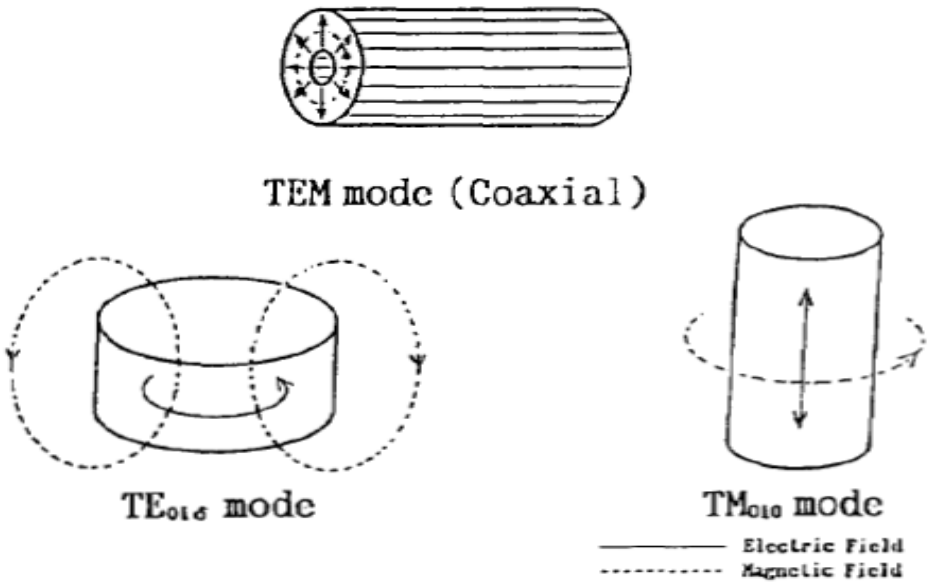

Figure 1-7: Various types of dielectric resonators. [51]

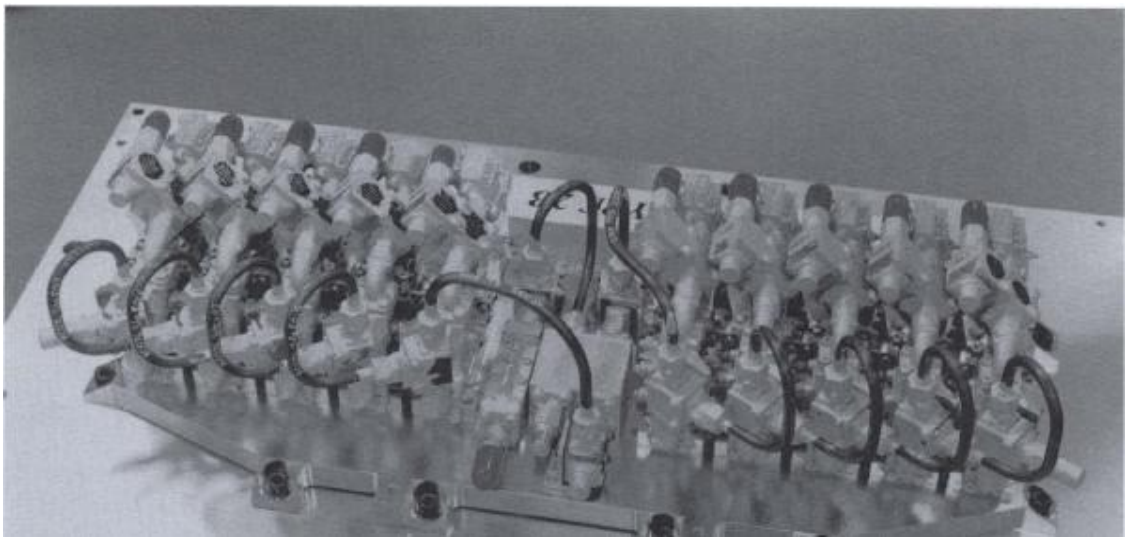

Figure 1-8: A Commercial dielectric resonator filter bank. courtesy of matra marconic space.(UK). Ltd. [50]

The integration of antenna technology and active devices to form transceiver modules and electronically scanned array has usually been accomplished in numerous configurations using microstrip patch antennas. However, open dielectric resonators offer attractive features as integrated antenna elements, which still need to explore. The advantage includes their small size, mechanical simplicity, high radiation efficiency, relative large width etc. [7]. The most successful fabricated components have been in the area of antennas, either surface-wave antennas or leaky-wave antennas. [52] Several types of miniature antennas are now in use.

As said above, application of dielectric materials in microwave components is very cost effective and lead to a significant miniaturization of the device, particularly when microwave integrated circuit (MIC) or monolithic microwave integrated circuit (MMIC) structures are used. Excellent performance in filters and oscillators are currently being achieved. Additional applications include radar, satellite, portable telephone, satellite broadcasting, ultra-high speed wireless local area network (LAN), intelligent transport system (ITS) comprising ladder for anti-collision, security systems detectors and so on [53]. Miniature dielectric-filled coaxial resonators are commonly used in wireless headsets (cellular and personal communication system (PCS) phones). Recently available very high-Q materials will extend commercial applications of DRs to much higher frequencies. Applications of as high as 100 GHz are being reported [52].

In spite of all of these recent development further progresses required for dielectric to be used at high frequency and MW in order to full fill the recent requirements demanded by the telecommunication industry, namely

1) Decrease the size, what implies the replacement of bulky dielectrics by thick and thin films dielectrics;
2) Decrease the dielectric losses, what implies the look at alternative engineering solutions, besides the control of the intrinsic properties of the material
3) Decrease of the fabrication costs, what implies the research for low cost based technologies and low sintering temperature materials.

1.6 References

[1] I M. Reaney and R Ubic, International Ceramics Issue1,2000, 48-52.

[2] A Terell Vanderah, Article in Science Compass, 8Nov2002, Vol. 298, 1182-1184.

[3] www.abiresearch.com/eblasts/archives/analystinsider_template.jsp?id=175" A weekly technology research update from ABI Research Wednesday – July 1, 2009.

[4] V Raghavan, " Material Science and Engineering" 4th Edition, publisher Prince-hall India, 1997.

[5] C Kittel "Introduction to Solid State Physics", 4th Edition, publisher John Wiley and Sons, Inc,, copyright 1971.

[6] W Wersing, Ceramics, Composites and Intergrowth, Cur. Opin. Sol. St. Mater. Sci., 1, 715–31 (1996).

[7] I M Reaney, D Iddles., J. Am. Ceramic Society, 2006, 89[7], 2006, 2063-2072.

[8] R J Cava, J Matter Chem., 2001, 11, 54-62.

[9] R Freer, Br. Ceram. Soc. Proc., 1995, 55, 171.

[10] S B Cohn, (1968) IEEE Trans. Microwave Theory Tech. MT16, 218.

[11] D J Masse, R A Purcel, D W Ready., Maguire EA, Hsrtwig CP: New low-loss high-K temperature-compensated dielectrics for microwave applications. In Proc IEEE 1971,1628-l 629.

[12] H M O´bryan, J Thomos. J K Plourde, J. Am. Ceramic Society, 57, 1974, 450.

[13] K Wakino, M Katsube, H Tamura, T Nishikawa and Y Ishikawa., (1977) IEEE. Four Joint Conv. Rec. 235.

[14] K Wakino, K Minai and H Tamura., (1984), J. Am. Ceram. Soc. 67, 278.

[15] D Kolar and D Suvorov., (1993) Journal of the European Ceramic Society 2, 229.

[16] R L Bolton, (1968) PhD Thesis, University of Illinois, USA.

[17] D Kolar, Z Stadler, S Gaberscek and S Suvorovr., Deutsch Keram. Ges. 55(1978) 346.

[18] J Takahashi, T Ikegami and K Kageyama., J.Am. Ceramic Society, 74, (1991) 1868.

[19] J Takahashi, T Ikegami and K Kageyama., J.Am. Ceramic Society, 74.(1991) 1873.

[20] E S Razgon, A M.Gens, M B Varfolomeev, S S Korovin and V S Kostomarov, Zh Neorg Kim, 25 (1980) 1701. Translation:Russ.J.Inorg. Chem.25 (1980) 945.

[21] E S Razgon, A M Gens, M B Varfolomeev, S S Korovin , V S Kostomarov,Zh Neorg. Kim., 25 (1980) 2298. Translation:Russ.J.Inorg. Chem.25 (1980) 1274.

[22] R G Matveeva, M B Varfolomeev, and L S llýushchenko, Z H N Kim., 29 (1984) 31. translation: Russ. J. Inorg. Chem. 29(1984) 17.

[23] H Ohsato., (2001) Journal of the European Ceramic Society 21, 2703-2711.

[24] A M Gens, M B Varfolomeev, V S Kostomarov, and S S Korovin., (1981) Russian J. Inorganic Chem. 26, 482.

[25] R Ubic, I M Reaney and William E. Lee., J. Am. Ceram. Soc., 82 [5] 1336–38 (1999).

[26] H Ohsato., Jap. J. Appl. Physics, Vol. 32, (1993), 4323-4326.

[27] L Zhang, X M Chen, N Qin, X Q Liu., Journal of the European Ceramic Society 27 (2007) 3011–3016.

[28] Y J Wu and X M Chen., Journal of the European Ceramic Society 19, 1123 (1999).

[29] K Wakino, K Minai and H Tamura, (1984) J. Am. Ceram. Soc. 67, 278.

[30] S Nishigaki, H Kato, S Yaho and R Kamimura: Ceram. Bull. 66(1987) 1405.

[31] Yong Jun Wu and Xiang Ming Chen, J. Mater. Res., Vol. 16, No. 6, Jun 2001.pp1734-38.

[32] E A Nenashevaa, N F Kartenko, Journal of the European Ceramic Society 21 (2001) 2697–2701.

[33] T Negas and P K. Dacies, (1995) Ceram.Trans. 53, 179.

[34] C Hoffmann and R Waser, (1997) Ferroelectrics, 201, 127.

[35] K Wada, Ken-ichi Kakimoto, H Ohsato Gokiso-cho, Showa-ku., Journal of the European Ceramic Society 26 (2006) 1899–1902.

[36] Fu Zhi, Paula M Vilarinho, Aiying Wu, and A I Kingon, Advance Functional Material 2009, 19, 1-11.

[37] V A Saltykova, O V Mel'nikova, N V Leonova and N F Fedorov: Russ. J. Inorg. Chem. 30 (1985) 105.

[38] N Harre, D Mercurio, G Trolliard and B Frit., Mater. Res. Bull., 1998, 33, 1537–1548.

[39] N Teneze, D Mercurio, G Trolliard and B Frit., Mater. Res. Bull., 2000, 35, 1603–1614.

[40] H Ohsato, Y Tohdo, K Kakimoto, T Okawa and H Okabe., Ceram. Eng. Sci. Proc., 2003, 24, 75–80.

[41] G Trolliard, I N Harre, D Mercurio, and B Frit, Journal of Solid State Chemistry (1999)145, 678-693.

[42] I M Reaney, H Zheng, D I Woodward, L Gillie., J. Phys. Condens. Matter 18 (2006) 7051–7062.

[43] C Vineis, P k Davies, T Negas and S Bell, Materials Research Bulletin, Vol. 31, No. 5, 1996, 431-437.

[44] Takashi Okawa, Katsumas Kiucchi, Hiraoki Okoki Okabe and Hitoshi Ohsato. Ferroelectrics, 2002, Vol 272, 345-250.

[45] H Yamada, T Okawa, Y Tohdo, H Ohsato., Journal of the European Ceramic Society 26 (2006) 2059–2062.

[46] Isuhak Naseemabeevi Jawahar, Narayana Iyer Santha, and Mailadil Thomas Sebastian, Pezholil Mohanan., J. Mater. Res., Dec 2002 Vol. 17, No. 12, 2084-89.

[47] L Li, Jing Pei, Zhenxing Yue, Fei Zhao, Zhilun Gui.Journal of Alloys and Compounds 459 (2008) 390–394.

[48] Y Fukami, K Wada, K Kakimoto, H Ohsato. Journal of the European Ceramic Society 26 (2006) 2055–205.

[49] H Zheng, I M Reaney, D Muir, T. Price, D. M. Iddles., Journal of the European Ceramic Society 27 (2007) 4479–4487.

[50] Hari Singh Nalwa ., "Handbook of Low and High Dielectric Constant Materials and their Applications. Volume 2: Phenomena, Properties and Applications", Publisher Academic Press on April 13, 1999.

[51] T Okawa, H Utaki, T Takada, Applications of Ferroelectrics, 1994.ISAF '94., Proceedings of the Ninth IEEE International Symposium on, 7 Aug 1994,1 367-371.

[52] A Hessel., (1969) General characteristics of traveling-wave antennas in Antenna Theory, New York: McGraw-Hill, 19, 151.

[53] S J Fiedziuszko, I C Hunter, T Itoh, Y Kobayashi, T Nishikawa, S N Stitzer and K Wakino., (2002) IEEE Trans. Microwave Theory Tech., 50, 706.

Chapter 2.
Electrophoretic Deposition Technique

Abstract:

With the evolution of microelectronics, the size of the devices is getting smaller and smaller with hybrid functionality. To make such devices, thick film technology is becoming more and more important in particular for electronic devices, namely for surface mounted devices, hybrid integrated circuits and sensors. A number of established techniques for thick films fabrication have been reported, such as screen printing, ink-jetting, tap casting and Electrophoretic deposition (EPD). Among all the above techniques, electrophoretic technique has gain considerable importance because of its high reliability, low cost and high performance products. In this chapter, a review on EPD technique is presented, which includes EPD mechanisms and kinetics, fabrication parameters (such as deposition and suspension variables), and applications.

2.1 Introduction

History of EPD

EPD is known since 1808, when a russian scientist Ruess saw that clay particles move in the presence of the electric field. The first practical use of EPD was reported in 1933 in a USA patent for the deposition of thoria particles on platinum substrates [1] The use of EPD for the fabrication of ceramics was first investigated by Hamaker [2] in 1940 and more recently in 1980´s it received a great deal of attention for the fabrication of advanced ceramics.

More recently, the number of applications has quickly developed, and as noted by Boccaccini [3], there has been a considerable increase in the areas of application of EPD in the last 10 years, denoted by the existence of more than a thousand articles and patents related to EPD. Figure 2-1 shows the extraordinary increase of the number of published scientific papers, identified in a Web of Science search. The keywords “electrophoretic deposition”, from only less than 100 papers before 1970s to more than 1800 papers published since 2000.

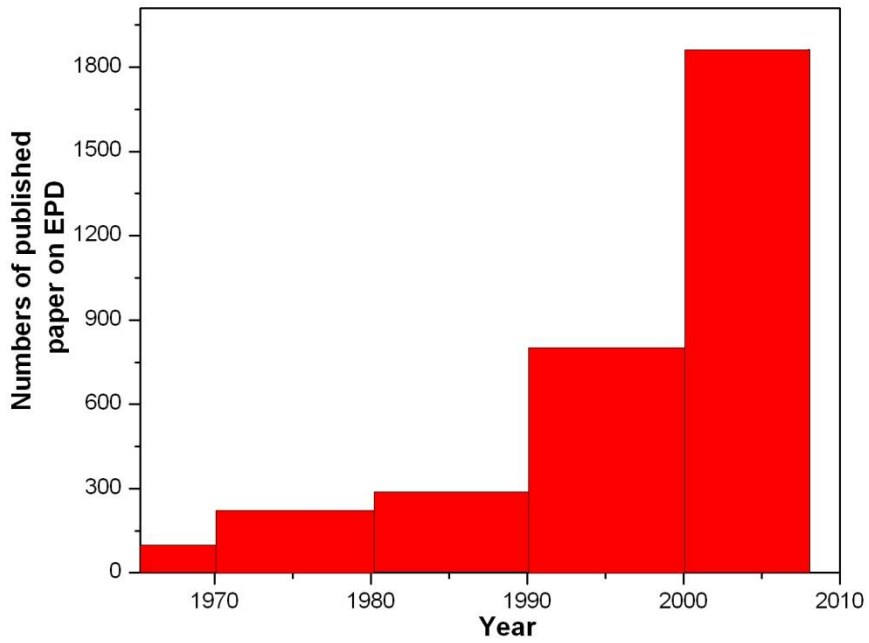

Figure 2-1: Number of published scientific papers on EPD from 1965 until 2008. The search was conducted by using the keyword "electrophoretic deposition" in Web-of-Science®

Definitions of EPD

Electrophoretic deposition (EPD) is a colloidal process, which is used for coatings and fabrication of films. It has gain considerable interest not only in academia but also in industries because of the versatility of its use with different materials and substrates and cost effectiveness. The other advantages of EPD include the possibility to be used to deposit coatings on complex shaped materials and despite being a wet process it offer easy control of over thickness and morphology of the deposited film by controlling the processing parameters like voltage and time.

The term "electro deposition" is somewhat ambiguous because it can refer to either electroplating or electrophoretic deposition, although it more often refers to the former. In the electroplating processes, a coating is produced by the diffusion and migration of individual ions in the solvent to the deposition electrode where they are electrochemically converted to an insoluble form, in which the reaction is the reduction of metal ions in solution to form the metal. In contrast, EPD uses charged particles that move under an external electric field to form consolidated films onto the opposite electrode (Table 2-1).

[4]. There are two types of EPD depending on which electrode the deposition happens. When the particles are positively charged, the deposition is formed on the cathode and the process is called cathodic EPD. On the contrary, the deposition formation on positive electrode (anode) is termed as anodic EPD (Figure 2-2). By suitable modification of the surface charge on the particles, both of the two modes of deposition are possible. [4]

Table 2-1: Characteristics of electrodeposition techniques. [5]

	Electroplating	Electrophoretic Deposition
Moving species	ions	solid particles
Charge transfer on deposition	ion reduction	none
Required conductance of liquid medium	high	low
Preferred solvent	water	organic
Deposition rate	small(~1 μm/min)	high(~10 μm/min)

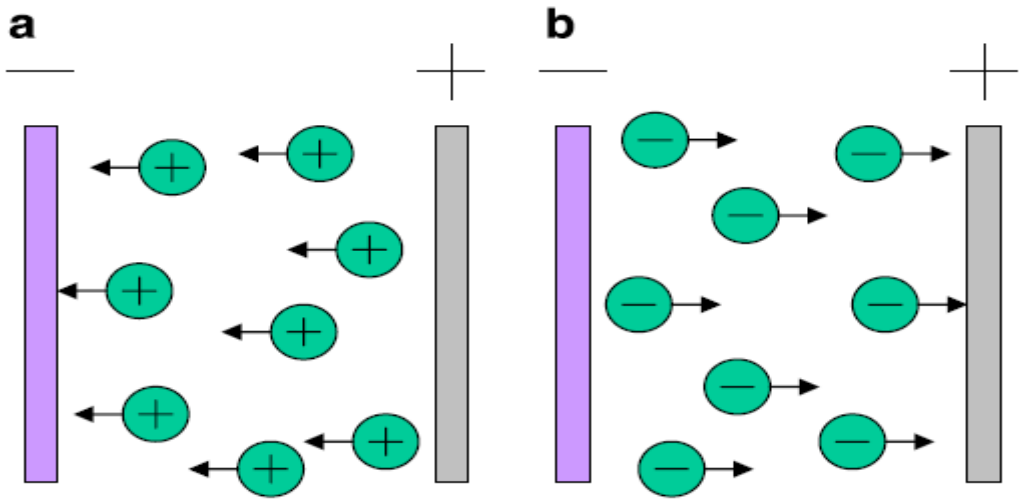

Figure 2-2: Schematic illustration of EPD process a) Cathodic EPD and b) Anodic EPD [6].

2.2 Charge Mechanisms on Particles

In terms of principle, during EPD the particles in the suspension move towards the electrode if they have enough charge on the surface. Four mechanisms have been identified by Omer van der Biest *et at*. [5] by which the powder particles get charged:

1) A selective adsorption of ions from the liquid onto the solid particle;
2) Dissociation of ions from the solid phase into the liquid;

3) Adsorption or orientation of dipolar molecules at the particles surface;
4) Electron transfer between the solid and liquid phase due to different work function.

In the case of ceramic particles, the last mechanism is not applicable but the first two invariably occur. The sign of the net charge on the particle will depend not only on whether the ions involved are positive or negative, but also on whether mechanism (a) or (b) is dominant. Also, a positively-charged particle may even behave like a negative one, which is attracted to a positive electrode, if an excess of negative ions are attracted to the vicinity of the particles. Consequently, it is difficult to predict whether a deposition will occur on positive or negative electrodes in an unknown system.

2.3 Electrical Double Layer Concept and Zeta Potential

The electric double layer concept is a very important one for the surface chemistry of materials in colloidal science field, i.e. in EPD. It describes the variation of the electric potential near a surface, and has a large bearing on the behaviour of colloids. Development of a net charge at the particle surface affects the distribution of ions in the surrounding interfacial region, resulting in an increased concentration of counter ions (ions with oppose charge to that of the particle) close to the surface. The liquid layer surrounding the particle consists of two parts: an inner region where the ions are strongly bounded and an outer (diffuse) region where they are less firmly associated. Within this diffuse layer is a boundary known as the slipping plane, within which the particle acts as a single entity. [7]

An assumed negative charge particle in a suspension is surrounded by ions with a positive charge in a concentration higher than the bulk concentration of these ions; this is the so-called electrical Double-Layer as illustrated in Figure 2-3 (a).The double layer thickness is of great importance in colloid stability and, for that matter, on flocculation, since it controls the range of the double layer interaction. The thickness is determined by the concentration and valence of the ions in suspension. A high concentration of ions (high ionic strength) in the medium generally results in a decrease in the double layer thickness and consequent decrease in the potential. [8] When an electric field is applied, the charged particles and surrounding ions will move in opposite directions. However, the ions are also attracted by the particle, and as a result, a fraction of the ions surrounding the particles will

not move in the opposite direction but will move along with the particles. Hence, there is a surface of shear between the particles and the surrounding ions. As shown in Figure 2-3 (a) the potential at the surface of slipping plane is termed the zeta-potential or electrokinetic potential [9].

The schematic curve of zeta potential versus pH value is depicted in Figure 2-3 (b). The zeta potential is affected by the pH environment and is usually positive for low pH values and negative at high pH.

Numerous physical and chemical factors can influence the magnitude and sign of the zeta potential. It may depend on the presence or absence of added electrolytes, or on the concentration of the suspension itself. In addition, zeta potential can be controlled by a variety of charging agents such as acids, bases and specifically adsorbed ions or polyelectrolytes, in the suspension [10]. Thus it is possible to use a variety of additives that affects the charge magnitude and its polarity in the suspension on EPD. Generally, the main criteria for selection of a charging agent are the preferred polarity and deposition rate of the particles.

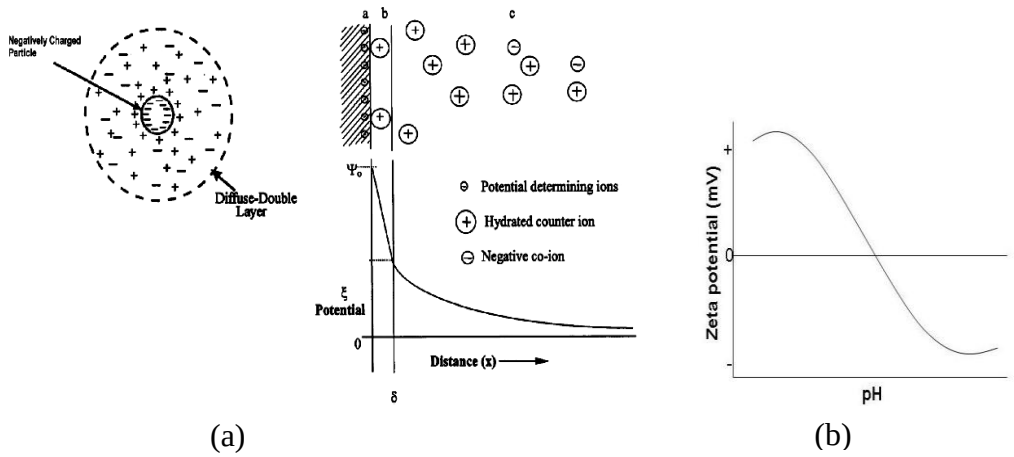

(a) (b)

Figure 2-3 (a) Schematic representation of the double layer surrounding a charged particle and evolution of the electric potential from the surface potential, [11], and (b) Zeta potential versus pH value.

The zeta potential is the main parameter determining the electrokinetic behavior of particles in suspension, and as a consequence is a key factor in the EPD process. It is imperative to achieve a high zeta potential and a uniform surface charge density on the surface of suspended particles for a successful EPD. Zeta potential plays a role in: (i) the stabilization of the suspension by determining the intensity of repulsive interactions between the particles, (ii) determining the direction and migration velocity of particles during EPD and (iii) determining the quality of the deposit. As zeta potential is closely related to the particle's double layer thickness, it provides also information on the agglomeration of the particles in the suspension. In general, the higher the absolute value of the measured zeta potential, the better is the dispersion of the particles in the suspension [9].

2.4 Mechanisms of Deposition

Although EPD is an old process still the exact mechanism of deposition is not entirely clear. However some theories discussed possible mechanisms.

Hamaker *et al*. [12] have suggested that EPD is a sedimentation process due to gravitation. The pressure by incoming particles enables the particles next to the deposition electrode to overcome the inter particle repulsion and sit on the electrode. Koelmans has calculated the ionic strength near the electrode and found that it is equal to the ionic strength required for the flocculation of a suspension [13]. Grillon has suggested that particle neutralizes upon contact with the deposition electrode or the deposit [14]. Sarkar and Nicholson [1] suggested the double layer of counter ions also move with the particle but the double layer is thinner ahead of the moving particle and thicker behind (illustrated in Figure 2-4), therefore the concentration of ions near the electrode is higher as compared to the solution. Thus, the counter ions recombine with their incoming co-ions to reform the original salt, which result in the thinning of the double layer of the particle in the deposit. As a result there is a decrease in the repulsion near the substrate because of the thin double layer what allows the particles to over come this repulsion barrier and attached to each by weak force such as van der Waal forces, allowing a deposit to be formed.

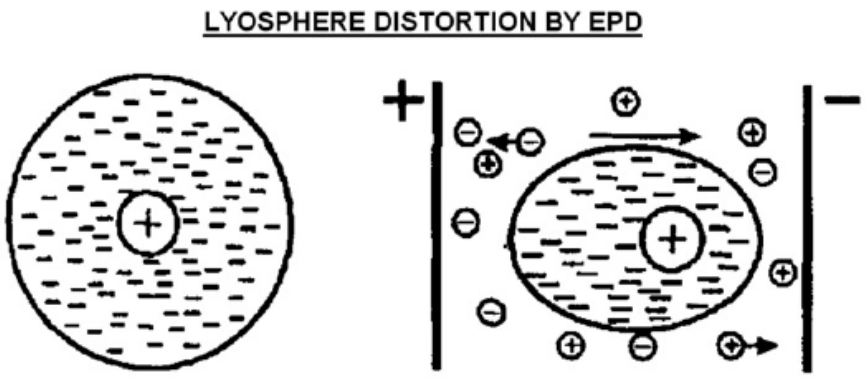

Figure 2-4: Mechanism of double layer thickness with application of voltage by Sarkar [1].

2.5 Kinetics of Electrophoretic Deposition

To make EPD process commercially more viable the knowledge of the kinetics of EPD process is necessary.

Hamaker [2] proposed that the amount of deposited film is proportional to the concentration of the suspension, time of deposition, surface area of deposit, and the electric field. This yield of deposition varies linearly with applied field according to Hamaker's equation

$$M = \int_0^t \alpha A C \mu E dt \qquad (2.1)$$

where M stands for the mass deposited in time t (s), C for the particle concentration in the suspension (kg/m^3), E for the electric field (V/m), A for the electrode area (m^2), μ for the electrophoretic mobility (m^2/V·s)), a stands for and α stands for a coefficient representing the fraction of particles deposited near the electrode.

In principle, EPD can be conducted under constant current or constant voltage with either constant or variable concentration against deposition time. Sarkar *et al*. [15] studied the kinetic aspects of EPD through schematic plots of deposit weight versus deposition time for four possible deposition conditions (Figure 2-5): curve A (constant current and constant suspension solid concentration), curve B (constant current but decreasing

suspension solid concentration), curve C (constant voltage and constant suspension solid concentration) and curve D (constant voltage but decreasing suspension solid concentration). The curve A shows that the rate of deposition is constant with time, differently, the rate of deposition decreases asymptotically against deposition time in either of the B, C, or D curves. Apparently, the deposition efficiency is highest in curve A, followed by curves B, C, and D, respectively in a certain deposition time. By comparison of the curves A, B, C and D, it clearly reveals that the highest efficiency is realized by constant current and constant suspension solid concentration in terms of the deposition weight or thickness. In addition, it is much easier to predict and to control accurately the deposited yield or thickness in constant current and constant suspension solid concentration.

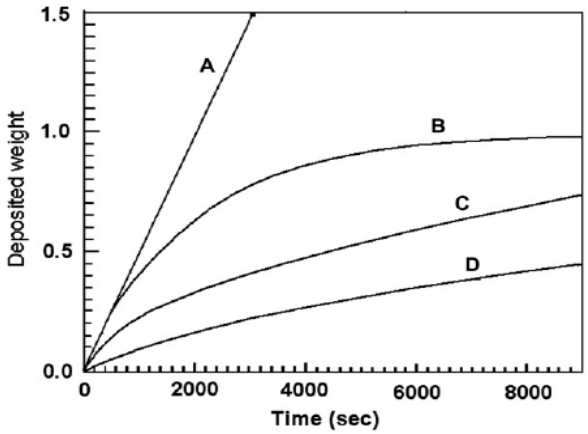

Figure 2-5: Deposited weight as a function of the deposition time [1].

2.6 Parameters Related with Suspension

The main suspension parameter is the medium.

In EPD, water based and organic based mediums are used for deposition. Generally the non aqueous medium is preferred over aqueous medium due to the reasons discussed ahead. In water based medium electrolysis takes place at lower voltages (~5V), which results in the formation of gas bubbles at the electrodes and formation of poor coatings or films. The density of the electric current is also higher in water suspensions which results in the heating of the suspension and sometimes loss of stability. The above stated reasons limit the use of aqueous medium at high voltages.

However, high voltages may be desirable in order to achieve high coating thicknesses or to increase the rate of deposition. In such applications, organic solvents are used as a medium. The organic solvents used are generally polar solvents such as alcohols and ketones. Ethanol, acetone, and methyl ethyl ketone are examples of solvents which have been reported as suitable candidates for electrophoretic deposition and their properties are summarised in Table 2-2.

Table 2-2: Physical properties of solvents [16].

Solvent	Viscosity(cP)	Relative dielectric constant
Methanol	0.557	32.63
Ethanol	1.0885	24.55
n-Propanol	1.9365	20.33
Iso-propanol	2.0439	19.92
n-Butanol	2.5875	17.51
Ethylene glycol	16.275	37.7
Acetone	0.3087	20.7
Acetylacetone	1.09	25.7

The other parameters besides the suspension medium that affect the quality of the suspension are:

1) Particle size and particle size distribution
2) Dielectric constant of the suspension
3) Conductivity of the suspension
4) Viscosity of the suspension
5) Zeta Potential
6) Stability of the suspension

Concerning the particle size and particle size distribution, it is advisable to have a particle size within the range of 1-20 micrometer [16]. The use of particles with bigger sizes results in sedimentation because of gravitational force originating poor film quality. In addition, a lower particle size and particle size distribution allows to avoid the formation of cracks in the films as Sato N *et al.* [17] observed in $YBa_2Cu_3O_7$ (YBCO).

The behaviour of the dielectric constant of the suspension media was studied by Powers *et al*. [18] in different suspensions with beta-alumina particle. The authors found that the deposition only take place for the solvent with dielectric constant in range of 12-25. For lower dielectric constant, the deposition fails because of the insufficient dissociative power of solvent and in the case of higher dielectric constant the high ionic concentration in the suspension reduces the thickness of the double layer and consequently the electrophoretic mobility.

In terms of conductivity of the suspension, based on the systematic studies of Ferrari and Moreno [19] on the effect of conductivity and the viscosity of the suspension, it was observed that if the conductivity of the suspension is very low, the particle charge electronically and suspension looses the stability; on the other hand if the conductivity is high the particle motion is very slow. However, applied current can increase the margin of the suitable conductivity region for EPD. It is generally accepted that the suitable regions of conductive are different for different systems.

As to the zeta potential it indicates the degree of repulsion between adjacent, similarly charged particles in dispersion. As mentioned previously, a high zeta potential will confer stability to the suspension i.e. the solution or dispersion will resist to agglomeration. So, colloids with high zeta potential (negative or positive) are electrically stable while colloids with low zeta potentials tend to coagulate or flocculate. Table 2-3 represent the stability behaviour of the colloids with zeta potential.

Zeta potential plays a major role in the: 1) stability of the suspension, 2) determination of the direction of the particle migration and 3) green density of the compact film [5]. A high particle charge is indeed required for a good stability of the suspension that will ensure also a high and homogeneous green density of the deposited film. If the particle charge is low, the particle tend to coagulate, the interspaces between the particles are high and lead to a poor green density of the compact. Higher surface charge particle during deposition keeps the particles apart from each other, avoids coagulation and leads to a high particle density. Therefore, it is essential to control the amount of suspension and additives.

The stability of the suspension is characterized by the settling rate and the tendency to undergo or to avoid flocculation. Stable suspensions show no tendency to flocculation, settle slowly and form dense and strongly adhering deposits at the bottom of the container. The stability is mostly referred by the value of the zeta potential of the system high the zeta potential value better is the stability of the suspension [5]. The stability of the suspension can be explain by the DLVO theory.

Table 2-3: The stability behaviour of colloids corresponds to zeta potential values [24].

Zeta Potential(mV)	Stability behaviour of the colloids
from 0 to ±5,	Rapid coagulation or flocculation
from ±10 to ±30	Incipient instability
from ±30 to ±40	Moderate stability
from ±40 to ±60	Good stability
more than ±61	Excellent stability

DLVO theory established by Derjaguin and Landau [20] and Verwey and Overbeek [21]. According to this theory, the stability of a colloidal system is determined by the total energy of interaction, determined by the sum of the electrical double layer repulsive forces (VR) and the van der Waals attractive forces (VA) which the particles experience as they approach each other. Increasing the ionic strength can significantly reduce the repulsive forces. The behaviour of particle separations depends critically upon the ionic strength and hence the electrolyte concentration of the suspension. At very low ionic strengths, the potential energy is high, make strong repulsive forces producing a totally dispersed system. At a slightly higher but still low enough ionic strengths, the role of electrolytes, such as, coagulants or flocculants, is either to reduce the electrostatic repulsion and hence making it easier for the particles aggregation, thereby destabilizing the suspension. But, re-dispersion is also possible by diluting the electrolyte solution to decrease the ionic strength. Finally, in a high ionic strength, the colloid particles experience no repulsive forces. Consequently, fast coagulation occurs and the system is completely unstable under such circumstances.

The original DLVO theory only considered the van der Waals and electrostatic interactions in the suspension. Recently, it was proposed that the stabilization of colloidal dispersions might also be affected by steric stabilization and structural forces. [22] These mechanisms become important when long chain macromolecules are adsorbed to the particles surface. When these particles with polymer chains protruding from their surfaces come close to each other, sharp repulsive steric interactions will happen. In this case the chain configuration of the polymer is a very important parameter in steric stabilization [23] and determines the quality of the dispersant. Caution must be paid in using sterically stabilized suspension for EPD. For example, in extreme cases, adsorbed polymers can reverse the sign of surface charge, so the deposition may fail or could occur on the counter electrode.

2.7 Parameters Related with Deposition Process

2.7.1 Effect of Deposition Time

Basu *et al.* [25] have observed that for constant applied voltage during initial time of deposition the thickness stay linear with time and deviates from the linearity for longer time of deposition. A similar finding was observed by Chen and Liu [26] for ZnO coatings on copper substrate as shown in Figure 2-6. In constant voltage deposition the electric field decrease with the deposition time because of the formation of an insulating layer of ceramic particle on the electrode [26].

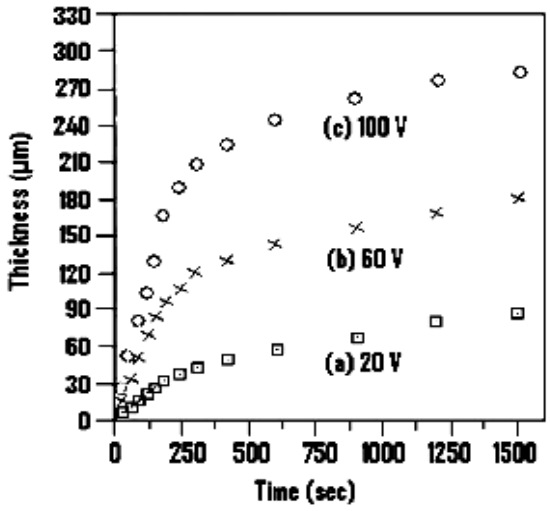

Figure 2-6: Thickness versus time at constant voltage for ZnO suspensions [26].

2.7.2 Effect of Applied Voltage

The deposition thickness increases linearly with the constant time and varying applied potential. Powders can be deposited more quickly under high applied fields, but the quality (morphology and density) of the deposit can be affected by applied high fields. Indeed Basu *at al* [25] found that the more uniform films are formed at moderate electric fields between 25-100 V/cm and the films deposited under higher fields have poor surface texture. Recently in the work of Fu Zhi *et al*.[27] on BNT thick films by EPD it was found that for high voltages the deposition thickness decrease drastically (shown in Figure 2-7) and the quality of the deposited films is non uniform. A high applied field may cause turbulence in the suspension and the coating may be disturbed by flows in the surrounding medium during its deposition. At the same time under high applied fields, particles move very fast so that they may not have enough time to sit in their best positions to form a close-packed structure.

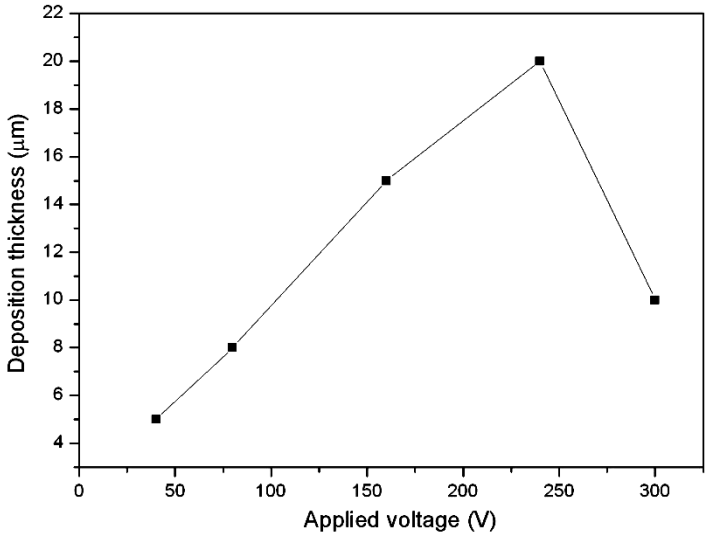

Figure 2-7: Deposition thickness versus applied voltage for constant time [27].

2.7.3 Conductivity of the Substrate

Conductivity of the substrate is an important parameter and it affects the quality of the green films deposited by EPD. Substrate of low conductivity such as $La_{0.9}Sr_{0.1}MnO_3$ (LSM) leads to a decrease of the deposition rate and non-uniform green films. [28].

2.8 Applications of EPD Technique

The EPD technique can be applied for any class of materials which are available in the form of fine powders, this includes ceramic, metal, polymer, and glasses. This process already gain success in various applications and can be used to produce coatings, for shape monolithic, laminated and graded free-standing objects, and for infiltration of porous materials and woven fibre preforms for composite production.

Coatings – EPD is already in used for coatings, being the automotive industry one of the examples. German car maker companies are coating 800 bodies per hour by EPD [29]. Other examples are the deposition of insulating glass for electronic applications [30] and superconductive coating [31-32]. Worthwhile to note is the possibility of coating almost any complex shaped object, such as metal cone with ceramic glaze [33] or Carbon Cathode Tube coated with phosphor [34].

Monoliths - For traditional ceramics, such as sanitary ware, the main advantage of EPD lies in its higher speed and in the low wear of the moulds compared with tape casting. Tiles, closed and open end tubes, hemispheres, tubes with changes in diameter, and conical sections are some of the shapes that have been made by EPD. Technical ceramics such as alumina [35-36], silicon carbide [31-35], and aluminium nitride [37-38] have been shaped by EPD and are commercially available in the market for a long time. A good example of the classical use of EPD is the fabrication of Beta-alumina tubes, used as electrolyte in sodium sulphur batteries [39-40].

Laminated materials - Laminated structures can be fabricate by EPD by depositing one layer over the other by moving from one suspension to another. Nicholson *et al.* [41] have produced ZrO_2/Al_2O_3 laminates with alumina layer as thick as 12µm and zirconia layer of 2µm from ethanol based suspension. Vandeperre and Van der Beist [42] deposited layers of SIC-based interlayers. You *et al*. [43] reported the fabrication of SiC/TiC laminated structures as illustrated in Figure 2.8.

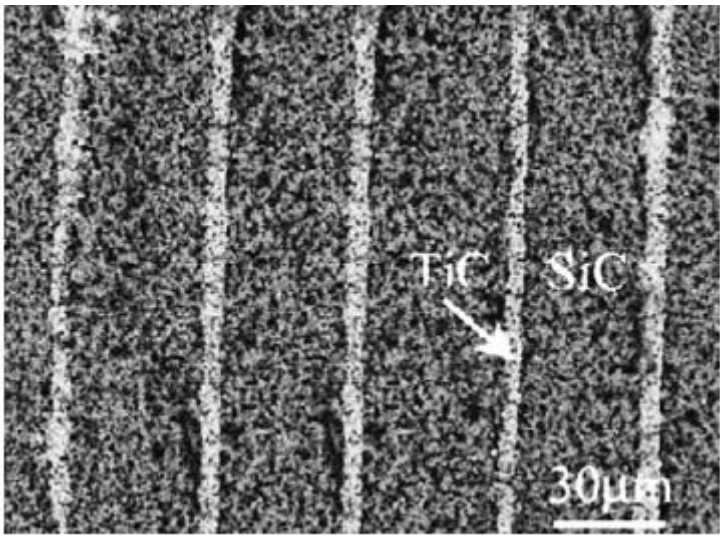

Figure 2-8: SiC/TiC laminated structure produced by constant-current EPD [43].

Fibre reinforced ceramic matrix composites - EPD is a simplest and cost effective method for fabrication of high-quality fibre reinforced ceramic matrix composites. Kaya *et al*. [44] used EPD to infiltrate performs with tight fibre weave architectures using different anodized ceramic particles, including silica and boehemite sols, as well as dual-component sols of mullite compositions. Figure 2-9 depicts the EPD infiltrated Ni-coated carbon fibres reinforced alumina matrix composites containing 30 vol% of fibre loading.

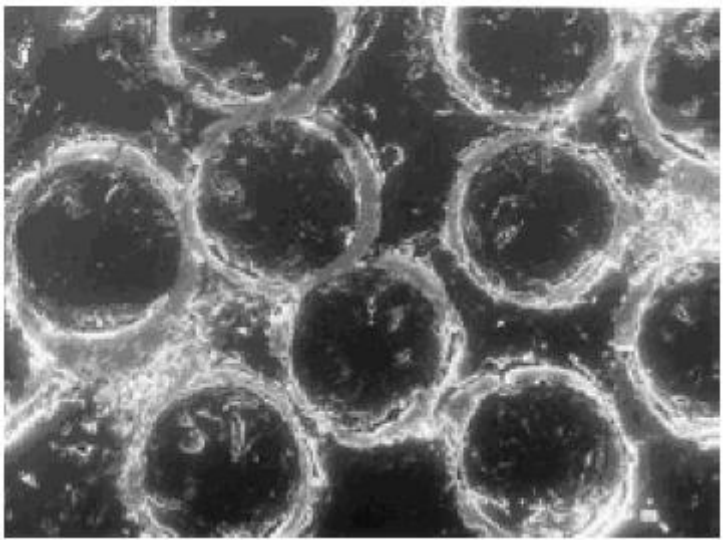

Figure 2-9: Ni-coated carbon fibre perform infiltrated with boehmite sol. [44]

Deposition of nano particles into nanostructures – The rising interest in the field of nanostructure is because often these structures exhibit new properties that are remarkably different from the bulk ones and because by controlling the size one can manipulate the properties. EPD of nanoparticles was first investigated by Giersig and Mulvaney [45, 46] to prepare ordered monolayers of gold nanoparticles. Tebellion and Clased [47] investigated the structured deposition of gold, silver and rare earth carbonate nanoparticles.

In the last few years the interest of the scientific community in carbon nanotubes (CNTs) has increased significantly as reflected by the huge number of papers published and patents [48-49]. To further expand the horizon for the application of CNTs researchers are using EPD for making thin films of CNTs. Jung et al. [50-51] deposited the thin film of Single wall carbon nanotube (SWCNT) in aqueous media and the deposited film showed good field emission properties. Hasabe et al. [52] deposited the SWCNT on SnO_2 electrode for solar cell application. Boccaccini *et al*. [53] have deposited MWCNTs onto highly porous bioactive glass scaffolds with the intention of imparting a monotopography to the pore wall surfaces (Figure 2-10). The scientist have also successfully synthesized the nanorods, nanowires and nanotubes of ZnO by EPD.[54].

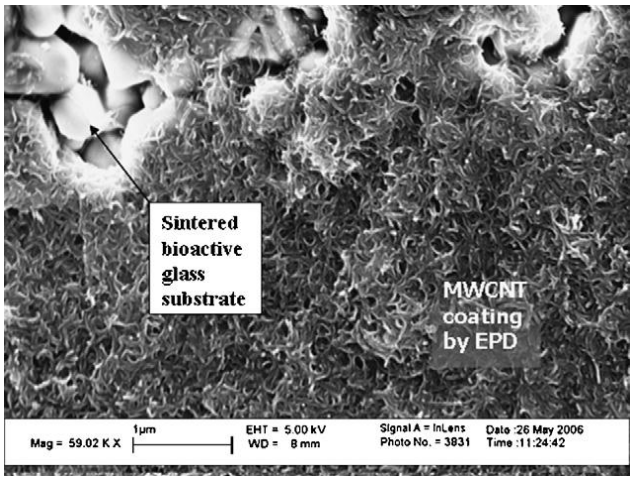

Figure 2-10: SEM micrograph of the electrophoretically deposited MWCNT coating on the surface of a bioactive glass foam [53]

2.9 References

[1] P Sarkar, P S Nicholson., 1996.J.Am. Ceram. Soc. 79(8):1987-2002.

[2] H C Hamaker., Trans Farad Soc 1940; 36:279-83.

[3] A R Boccaccini, F Chicatun, J Cho, O Bretcanu, Q Chen, J A Roether, S Novak, and Q Z Chen., (2007) Adv. Funct. Mater. 17, 2815

[4] I Zhitomirsky., (2002) Adv Colloid Interface Sci. 97, 279.

[5] Besra Laxmidar, Liu Meilin., Progress in Material Science 52 [2007] 1-61.

[6] O Omer, Vander Biest and J Luc Vandeperre, Annu. Rev Mater. Sci. 1999. 29: 327-352.

[7] O Z Stern., (1924) Electrochem 30, 508.

[8] P Sennet, J P Olivier., (1965), In: Ross S, editor. Chemistry and physics of interfaces, Washington (DC): Am Chem Soc., P73–93

[9] J Lyklema., (1977) J. Colloid Interface Sci. 58, 242.

[10] M Zarbov, I Schuster, L Gal-Or., (2002), the Electrochemical Society Inc, USA, Proc. 21, 39.

[11] N L Weise., editor. SME Mineral processing handbook, vol. 1. New York: Society of Mining Engineers; 1985. p. 5.42.

[12] H C Hamaker,E J W Verwey., 1940. Trans. Farad Soc. 36:180-85.

[13] H Koelmans., 1955. Philips Res. Rep. 10:161-93.

[14] F Grillon, D Fayeulle and M Jeandin. ,1992. J Mater. Sci. Lett 11 : 272-75.

[15] P Sarkar,D De and H Rho., (2004) J. Mater. Sci. 39, 819.

[16] N Heavens., In Binner GP, editorial , Advanced ceramics processing and technology, Vol. 1. Park ridge (NJ), USA: Noyes Publications 1990.p. 255-83.

[17] N Sato, M Kawachi, K Noto and N Yoshimoto., Physica C 2001; 357-360:1019-22.

[18] R W Powers., J. Electrochem Soc 1975;122:482–6.

[19] B Ferrari and R Moreno., Mater Letter 1996;28,353–5.

[20] B Derjaguin and L D Landau., (1941) Acta Physico chemica. URRS 14, 633.

[21] E J W Verwey and J T H G Overbeek., (1948), Elsevier, Amsterdam, the Netherlands.

[22] J A Lewis., (2000) J. Am. Ceram. Soc. 83, 2341.

[23] D F Evens and H Wennerstrom., "The Colloidal Domain" , Wiley-VCH, 2nd edition (1999).

[24] http://en.wikipedia.org/wiki/Zeta_potential

[25] R N Basu, C A Randall, M J Mayo., J Am Ceram Soc 2001;84(1):33–40.

[26] F Chen and M Liu., J Eur Ceram Soc 2001;21:127–34.

[27] Fu Zhi, "$BaNd_2Ti_5O_{14}$ Thick Films for Microelectronics Fabricated by Electrophoretic Deposition" PhD thesis, University of Aveiro(2008).

[28] Z Peng and M J Liu., J Am Ceram Soc 2001;84(2):283–8.

[29] J Eberhard. 1997., Galvano–Organo 66(678):621–23.

[30] A Sussman and T J Ward, 1981. RCA Rev.42(6):178–97.

[31] J Miziguchi, M Suzuki and H Yamato and M Mastsumura, J. Electrochem. Soc. 138(10), 1991, 2942–46.

[32] A D Sharma, A Sen and H S Maiti., 1993. Ceram.Int. 19:65–70.

[33] M Ortner., 1964. Plating (9):885–89.

[34] M J Shane, J B Talbot, B G Kinney, E Sluzky and K R Hesse., 1994. J. Colloid Int. Sci.165:334–40.

[35] J M Andrews, J Dracass, A H Collins, D C Cornish. 1969. Proc. Brit. Ceram. Soc. 12:211–29.

[36] J H Jean. 1995. Mater. Chem. Phys. 40: 285–90

[37] L J Vandeperre, O Van der Biest, F Bouyer, J Persello and A Foissy., 1997. J. Eur. Ceram.Soc. 17(2):373–76.

[38] L J Vandeperre, O Van der Biest, Bouyer F, A Foissy., 1998. Ceram. Bull. 77(1):53–58.

[39] J H Kennedy, A Foissy., 1975. J. Electrochem.Soc. 122(4):482–86

[40] R W Powers., 1986. Ceram. Bull. 65(9):1270–77

[41] P S Nicholson, P Sarkar., Proceedings of the international symposium on advanced ceramics for structural and tribological applications, Vancouver, BC, August 20–24, 1995. p. 475–81.

[42] L Vandeperre, O Van der Biest, W J Clegg., 1997. In Key Engineering Materials, 127:567–74.

[43] C H You, D L Jiang, S H Tan, Ceramic International, 2004, 30, 813-815.

[44] C Kaya, F Kaya, S Atiq, R Boccaccini., Br Ceram Trans 2003;102(3):99–102.

[45] M Giersig, P Mulvaney., J Phys Chem 1993;97:6334–6.

[46] M Giersig, P Mulvaney.,Langmuir 1993;9:3408–13.

[47] J Tabellion and R Clasen, J. Mater Science, 2004, 39, 803-811.

[48]A R Boccaccini, J Cho, J A Roether, B J C Thomas, E J Minay and M S P Shaffer, Carbon, 2006, 44, 3149–3160.

[49] T Belin and F Epron., A review. Mater. Sci. Eng. B, 2005, 119, 105–118.

[50] S J Jung, J Hahn,H J Jung and J S Suh, Nano Letters, 2006, 6, 1569–1573.

[51] J Hahn, S M Jung, H Y Jung, S B Heo, J H Shin and J S Suh,. Appl. Phys. Lett., 2006, 88 [Art. No. 113101].

[52] T Hasabe, S Fukuzumi and P V Kamat,. J. Phys. Chem. B, 2006, 110, 25477–25484.

[53] A R Boccaccini, F Chicatun, J Cho, O Bretcanu, Q Chen, J A Roether. Funct. Mater., 2007, Vol. 17,15, 2815–2822.

[54] C S Rout, S H Krishna, S R C Vivekchand, A Govindaraj and C N R Rao., Chem. Phys. Lett., 2006, 418, 586–590.

Chapter 3. Objective of this thesis

"On many levels, RF/microwave today compares to digital's (silicon based circuitry) level of integration a quarter century or so ago — essentially a lot of large (by current standards) components bunched together. Digital, however, has been on a seemingly unstoppable evolution toward ever-smaller, less-costly, and more- tightly integrated components, driven largely by the demands of consumer electronics such as cell phones, pocket-sized GPS devices, digital cameras, and even hearing aides. The same is not true for RF/microwave … " *in Military & Aerospace Electronics August, 2004, by J.R. Wilson* [1].

However as frequencies continue to move stealthily up because the density of available spectrum is increasing and as noise and couplings become more problematic for digital circuits, there is currently a market drive for the search of solutions intermediate between digital and RF/microwave circuits. Within this context, miniaturization (small and compact), integration and lowering costs are key words in the RF/microwave arena.

New advanced technology to build low loss, lower phase noise integrated circuits with low cost, high density, small size and lightweight are indeed required in this rapidly growing wireless industry. [2] One example is miniaturization of systems such as planar circuits, antennas, filters, couplers, baluns, etc. Because of this demand of smallness, thin and/or thick dielectric films are now being considered to replace dielectric components currently utilized in bulk ceramic form. This drives the use of thick film processing techniques, such as Electrophoretic Deposition (EPD), for the fabrication of dielectric thick films for RF and High Frequencies.

Although thin film technologies are being explored for the wireless circuit technology as well, they are expensive with limited suitability for commercial mass production [3]. Alternatively, thick films technology offers advantages such as low cost, reproducibility and feasibility to be large-scale continuous process. Thick films allow designers to combine microwave and digital functions on proper substrates and to incorporate components to the main structures, which offers increased potentials in terms

of reliability, miniaturization of circuits, circuit design capabilities, continuous flow in production processes, and hence a reduction in cost [4]. Besides, thick dielectric films have the capability of withstanding high voltages and high thermal conductivity, which led to applications in mobile phone RF power amplifiers where small physical size and high power handling is necessary; in addition, thick dielectric films can also be used as substrates in microelectronic devices to support mechanically other materials and to ensure their adhesion on it, which may be difficult to achieve with thin film materials [4].

As describe before, among low loss dielectrics, the $BaO\text{-}Re_2O_3\text{-}TiO_2$ (Re = La,Nd,Sm,Pr) system represents an important commercial family of microwave materials. Although BNT ceramics are currently being produced for resonators, antennas and substrates [7], as shown in Figure 3-1(a) and BLT has optimum properties for base station application, the high permittivity of BNT and BLT make them suitable candidates for the miniaturization in to thick films.

On the other hand the fabrication of dielectric films on metal foils is presently of interest for devices integrated into electronic packaging due to cost and space benefits. [13] For example, as shown in Figure 3-1 (b), the current microstrip patch antenna usually requires the metallization of a ground plane on one side of the dielectric materials by screen printing. However, this metallization process can be avoided by directly depositing the dielectric layer on a metallic substrate. In this case, for the reasons above described and in particular the possibility of being scaled up, EPD looks like very appealing for this purpose.

(a)

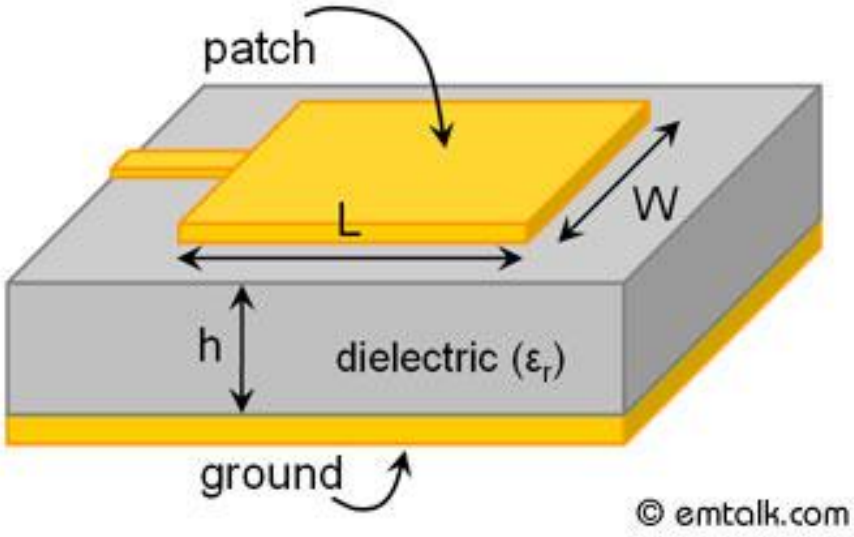

(b)

Figure 3-1: Photographs of commercially available microwave resonators and substrates (after Morgan Technical Ceramics Ltd) (a) and schematic representation of a microstrip patch antenna (b) (ww.emtalk.com)

Hence the general objective of this thesis is to contribute, from the materials science perspective, to the pool of scientific and engineering knowledge that will allow the development of next generation of small, integrated and low cost based RF/microwave devices.

As said before, for microwave dielectrics, there are three significant properties to be considered: (i) the relative permittivity, that determines the size of the electronic component; (ii) the loss tangent (or quality factor, Q) that determines the selectivity and performance of the device and (iii) the temperature coefficient of the resonant frequency that determines the frequency stability of the device [5]. And among the materials recognised to full fill these requirements tungsten bronzoids $BaO–Ln_2O_3–TiO_2$ (Ln = Nd, La, among others) with high ε_r (80- 90) and low losses (Q = 10,000) and low t_f (+ 59ppm/ºC) represent an important commercial family of microwave materials [6].

$BaO\text{-}Nd_2O_3\text{-}TiO_2$ ceramics are currently being produced for resonators, filters and substrates, among others applications [7], but the commercial use of BNT thick films has not yet been reported. However, the first results on the fabrication and characterization of BNT thick films that have been published very recently [8-9] are quite promising. It is demonstrated that 52 µm thick $BaNd_2Ti_5O_{14}$ films exhibit a dielectric constant and a loss tangent of 107 and 0.0006 (Q of 1600) at 1 MHz, respectively, $TC\varepsilon_r$ is below +58.5 ppm/°C and the losses are not significantly increased up to the gigahertz regime. Particularly relevant is the demonstration that with thick films besides facilitating scaling to small device sizes for high frequency operations, the control of substrate constraint and sintering conditions can be used to control grain anisotropy and thus microwave properties of BNT films, namely tuning $TC\varepsilon_r$ to zero.

Another member of the tungsten bronzoid family is $Ba_nLa_4Ti_{3+n}O_{12+3n}$ (BLT). BLT has hexagonal perovskite structure with ε_r~44, Q.f~47,000 GHz and t_f - 2ppm/ºC. Similarly to BNT, BLT dielectric characteristics may allow for further miniaturization of filters and oscillator components in systems ranging from cellular telephones to global positioning technologies [10]. Contrary to BNT, there are no reports on the fabrication and characteristics of BLT thick films.

In terms of Microwave Material, materials for resonators according to Ian M. Reaney [11] there is currently a lack of dielectric materials with dielectric permittivity between 45 and 80, together with low losses and low t_f as shown in Figure 3-2.

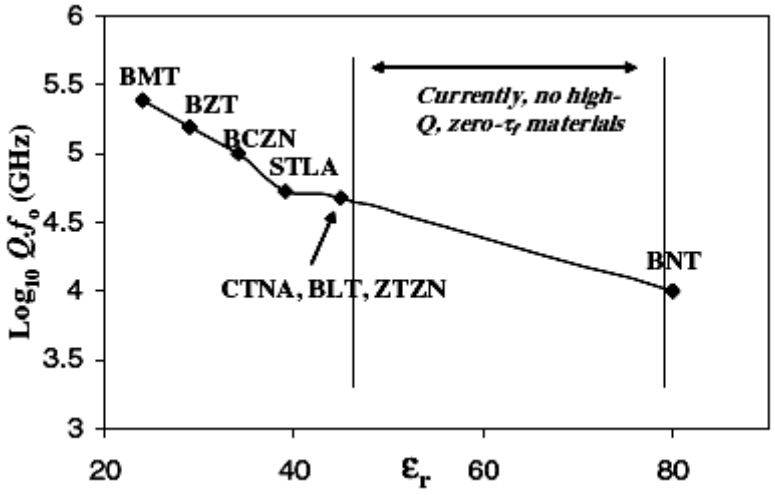

Figure 3-2: $\log_{10}$ Q.f_o versus ε_r for commercial or equivalent dielectric microwave dielectric ceramics [11].

One way of full filling this need is by engineering materials, for example by fabricating composite materials in which the properties will be tailored by mixing appropriate contents of end members that *per se* have opposite t_f. Composite MW ceramics of xBNT-(1-x)BLT system were synthesise and the best properties were obtained for the composition x = 0.55 and 0.75 with ε_r = 61, t_f < -21ppm/ºC and Qf > 10,000GHz [12]. Another approach to tailor the dielectric properties of MW materials, namely to achieve temperature stability, recently explored in the field of thin films, is the fabrication of layered structures.

However no such approaches have yet been considered for dielectric thick films.

Hence, the specific objective of this thesis is the proof of concept of electrophoretic deposition of structured, microwave composites, that includes: i) to develop a method of fabricating structured functional composites using electrophoretic deposition, ii) to fabricate planar $BaLa_4Ti_4O_{15}$ (BLT) and $Ba_4Nd_{9.33}Ti_{18}O_{54}$ (BNT) composites, iii) to fabricate and characterized $BaLa_4Ti_4O_{15}$ (BLT) thick films and iii) to characterize the structured composites using dielectric spectroscopy and analytical electron microscopy and XR diffraction.

For that BNT ($Ba_4Nd_{9.33}Ti_{18}O_{54}$) and BLT ($BaLa_4Ti_4O_{15}$) powders were synthesised, and suspension were prepared and optimised to ensure perfect electrophoretic deposition conditions, and BLT and BLT / BNT (and vice versa) composites were fabricated in this work. Due to the lack of information, BLT thick films were prepared by EPD for the first time and their properties evaluated. Simultaneously, and as a comparison tool, BLT ceramics were prepared from the same powders used to fabricate the thick films.

References

[1] J R Wilson, Article on "RF and microwave industry struggles to meet the high demands of the military" Aug 2 004 , link. http://mae.p ennnet.com/ar ticles/article_displa y.c f m?Section=ARCHI&C=Feat&ARTICLE_ID=209980.

[2] D.Stephens, P R Young, and I D. Robertson., (2005) IEEE Trans. On Microwave theory and Tech. **53**, 3832.

[3] P Barnwell and J Wood., (1998) Fabrication of low cost microwave circuits andstructures using an advanced thick film technology, IEMT/IMC Proceedings.

[4] K Abe, A Ikegami, N Sugishita, N Taguchi, T Isogai,I Tsubokawa and H Ohtsu., (1979) IEEE Trans. On Components Hybrids and Manufacturing Tech. **2**, 434.

[5] A W Scotta., (1993) Understanding Microwaves, New York: Wiley.

[6] K Wakino , K Minai and H Tamura., (1984) J. Am. Ceram. Soc. 67, 278.

[7] Wolfram Wersing., Ceramics, Composites and Intergrowth, Cur. Opin. Sol. St. Mater. Sci., **1**, 715–31 (1996).

[8] Zhi Fu, Aiying Wu and Paula M Vilarinho., Applied Physics Letters 90. (2007), 052912.

[9] Zhi Fu, Paula M Vilarinho, Aiying Wu, and Auhus I. Kingon., Adv. Functional Materials, 2009, 1-11

[10] I. N. Jawahar, N. I. Santha and M. T. Sebastian., Journal Mater. Res., Vol. 17, No.12, Dec 2002.

[11] I M Reaney, David Iddles., Journal Am. Ceram. Soc., 89 [7] 2063 – 2072 (2006).

[12] H Zheng, I M. Reaney, D Muir, T. Price, D. M. Iddles., *Jpn. J. Appl. Phys. Part 1*, 44, 5A, 3087-3090 (2005).

[13] W J Borland and S Ferguson, (2001) Embedded Passive Components in Printed Wiring Boards, a Technology Review, CircuiTree Magazine.

Chapter 4. Experimental Procedure

Abstract

In this chapter details of the experimental procedure used in this work are described which includes: i) the synthesis of $BaLa_4Ti_4O_{15}$ (1:2:4) (BLT) and $Ba_4Nd_{9.33}Ti_{18}O_{54}$ (1:1:4) (BNT) powders, ii) preparation of the suspensions for the electrophoretic deposition and the studies of the suspension stability, iii) fabrication of thick films by EPD, iv) preparation of ceramics and v) description of films and ceramics characterization.

4.1 Introduction

The steps followed for the synthesis and characterization of $Ba_4Nd_{9.33}Ti_{18}O_{54}$ (BNT), $BaLa_4Ti_4O_{15}$ (1:2:4) (BLT) thick films and thick composites films of BNT - BLT is presented in the flowchart of Figure 4-1.

As for the first step, $BaLa_4Ti_4O_{15}$ (1:2:4) (BLT) and $Ba_4Nd_{9.33}Ti_{18}O_{54}$ (BNT) powders were prepared by conventional solid state method. Both powders were characterized in terms of their structure, phase purity and morphology. In the following steps, suspensions of BNT and BLT powders were prepared under different conditions and characterized in terms of stability in order to optimise the film deposition process. BLT and BNT thick films were deposited on platinum foil substrates by EPD and the processing variables were modified to change the final morphology and physical characteristics of the films. The deposited films were dried in air followed by iso static pressing and sintered at different temperatures. Structure, phase content and microstructure of the films were assessed by X Ray Diffraction and Scanning Electron Microscopy (SEM). The electrical response of the films was characterized by impedance spectroscopy as a function of temperature and frequencies (within the radio frequency range) and under different applied voltage. BLT ceramics were prepared to compare with films electrical response.

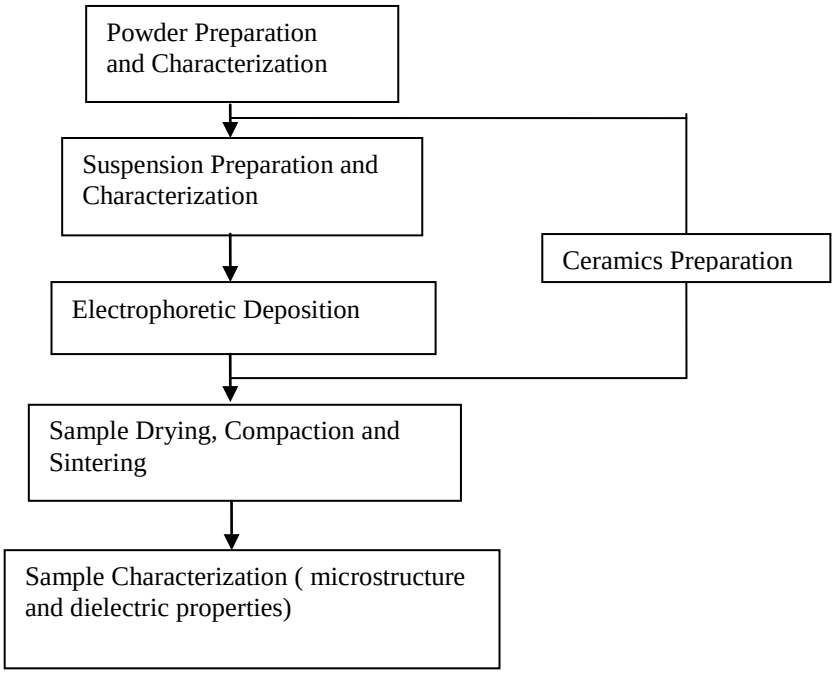

Figure 4-1: General flow chart of the experimental work conducted in this work.

4.2 Synthesis of BLT and BNT Powders

$BaLa_4Ti_4O_{15}$ (1:2:4) (BLT) and $Ba_4Nd_{9.33}Ti_{18}O_{54}$ (1:1:4) (BNT) powders were synthesised by solid state reaction. The starting precursors, $BaCO_3$ (Aldrich, Product No.: 513-77-9, purity>99.9%), Nd_2O_3 (Aldrich, Product No.:1313-97-9, purity >99.9%), La_2O_3 (Aldrich, purity>99.9%),) and TiO_2 (Aldrich, Product No.:1317-80-2, purity >99.9%), were weighted and mixed according to the correct stoichiometry. La_2O_3 and Nd_2O_3 are very hydroscopic in nature so, both the powders were heated at 850ºC for 3h, cooled down in desiccators and weighted immediately before mixing with the rest of the reagents. The mixed powders were ball milled in ethanol media, with zirconia balls for 24h followed by drying in oven at 100ºC for 12h. The dried powders were then taken out of the crucibles and grounded by using mortar and pestle.

The grounded powder was calcined in a programmable furnace equipped with an automatic temperature controller. The temperature for calcination was chosen according to the results from Differential Thermal Analysis (DTA) / Themogravimetry (TG), obtained with a heating rate of 5 ºC/min. The phase purity of the calcined powders was examined by using X-Ray Diffraction (equipped with EDS).

After calcination and phase purity examination, the powders were ball milled for 24h at 180rpm to get small particle size, which is crucial for a good stability of the suspension and an improved green density of the film. The particle size distribution was determined by a Particle Size Analyzer (Coulter LS 230). The specific surface area of milled BLT and BNT powders was determined by BET(Gemini 2370 V5.00). The calcined milled powders were dried at 100ºC for 24h and kept inside the desiccators to avoid any reaction with air which could lead to the aging of the powders. The powders morphology was observed with a scanning electron microscope (SEM) (Hitachi, S-4000 SEM / ED)

4.3 Suspension Preparation and Suspension Medium

Suspensions were prepared in different media such as water, acetone (>99.9%, Merck) and ethanol (>99.9%, Merck). For varying the pH of the media diluted HNO_3 (≥99.8%, Aldrich) and triethanolamine (>99%, Merck) were used.

Suspension prepared in glass beaker with 1g of BLT or BNT powders were mixed in 100 ml of each of the suspension medium. The powders were slowly added into the suspension media under constant stirring by ultrasonication, to promote the dispersion of powders in the suspension. A further dispersion of the suspension was conducted by using magnetic stirring for approximately 1 to 2h.

In order to increase the charge of the particles and to achieve high zeta potential values for the prepared suspensions, several additives such as dilute nitric acid and triethanolamine were analysed.

EPD Apparatus

The EPD set up used in this work is presented in Figure 4-2. It is composed of the EPD cell, the ultrasonic bath and the power source. The home made EPD cell consists of three main parts: the base, the mask and the metal pole for conductive connection. Platinum foils of 11 ×11 × 0.025 mm (99.95%, Good fellow, UK) were used as substrate for the film deposition and as counter electrode (cathode) as well. The substrates were placed between the each mask chambers and screwed from the back with the back lid. The

two equal masks were mounted on the base, and the two steel poles provided the electrical connection to the external power source. As represented in Figure 4-2 on the left side of the EPD cell is the ultrasonic bath (Branson, USA) and on right side the DC power source (EPS, Stromversorgung Gmbh, Germany); the EPD cell is located at the top of the magnetic stirrer.

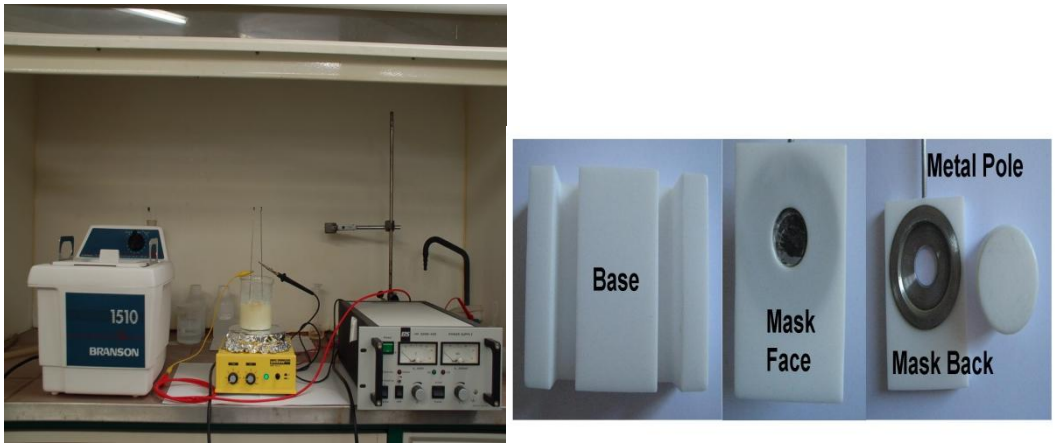

Figure 4-2: EPD setup in the left side and the EPD mask on the right side.

4.4 Deposition of Films

For film deposition, the EPD cell was immersed in the suspension in a 250 ml of glass beaker. The platinum foil as working electrode (cathode) was separated by 2 cm from the Pt counter electrode (anode) in the EPD cell.

Prior to each EPD cycle the suspensions were ultrasonically dispersed and magnetically stirred (Yellowline, IKA Werke GmbH & Co. KG Germany) for 2 to 5 min, followed by settling for 1-2 min in order to settle down of coarse particles.

Constant voltage and constant time mode was used in the current work to deposit BLT and BNT films on Platinum foil. The electric current through the EPD cell was monitored by a digital multimeter (MY-64, MASTECH, Hong Kong) located in series with the EPD circuit, during the EPD process.

BNT/BLT and BLT/BNT composites films were fabricated on platinum substrate by electrophoretic deposition, as well. The deposition was carried out in acetone based suspension with triethanolamine as an additive for both systems. Composite films were deposited layer by layer, namely a BLT layer followed by a BNT layer and the other way around, a BNT layer followed by a BLT one. After each deposition and prior to the second deposition films were dried for at least one day in desiccators so that acetone evaporates slowly and minimise the formation of pores. A systematic diagram of the composite preparation is presented in Figure. 4-3. Isostatic pressing was not performed on the composite thick films because in many cases it leads to the peal off of the films.

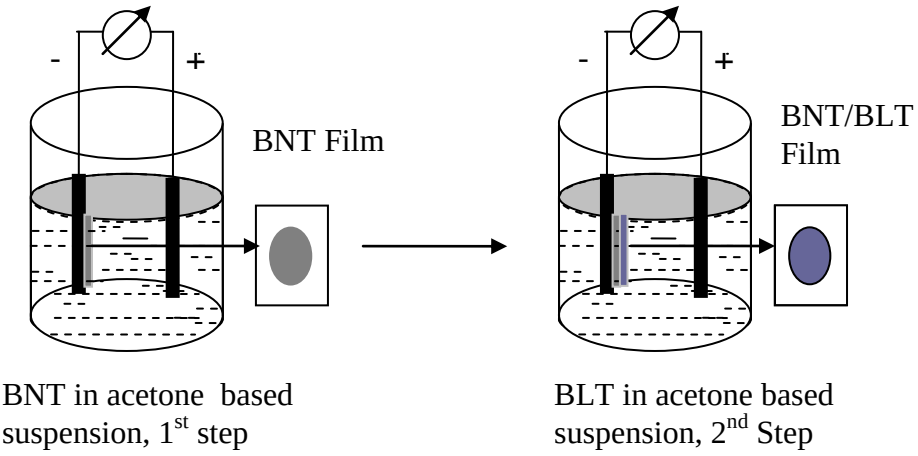

Figure 4-3: Schematic diagram of BNT/BLT thick film composite preparation.

The geometrical density of green films was calculated by calculating the volume of the deposited film and measuring the weight of deposited film. The density is given by

$$\delta = M / V \qquad (4\text{-}1)$$

where M stands for the mass of the film and V for the volume.

4.5 Drying, Compaction and Sintering

BLT, BNT and composites films were dried at room temperature for more than 24h. Drying in air was preferred over a drying in the oven to let the solvent to evaporate slowly and to minimise the possibility of creating cracks. After drying, the films were iso-statically pressed at 200 MPa for 3-5min to increase their green density.

The dried and compact films were further sintered at high temperature. To determine the sintering temperature for both systems dilatometric analysis of BLT and BNT pressed pellets (5x5x7 mm) were conducted in a computer assisted vertical dilatometer (Linseis, mod. 4 L70-2000).

The thickness of the green and sintered films was measured by a micrometer and the film thickness error was calculated by taking the average of the first deposition thickness carried out at four different times in four fresh prepared suspension of BLT in acetone with triethanolamine. The calculated error associated with the film thickness is approximately ± 1.75μm

4.6 Fabrication of Ceramics

For comparison with films, BLT ceramic discs were prepared. The discs of 0.5g were uniaxially pressed at 50 MPa (Carver Laboratory Press, Fred S. Carver Inc., USA) and further isostatically pressed at 200MPa for a high and homogeneous green density. The pressed discs were sintered from 1400ºC to 1600ºC for different periods of time to assess the effect of the microstructure on the properties like permittivity, TCε_r and loss tangent. Density of sintered discs was measured by Archimedes principle in diethyl phthalate (Fluke, 80080 with density of 1.118g/cm^3). For dielectric measurements metal-insulator-metal geometry was used and top and bottom gold electrodes were deposited by thermal evaporation on the tops of the ceramic disk.

4.7 Sample Characterization

Structure and Microstructure

The phase assemblage of the sintered BLT films and ceramics and BNT/BLT composite films was analysed by XRD.

The microstructure evolution was followed by Scanning Electron Microscopy (SEM). For that cross-sections and surface morphologies of BLT, BNT, BNT/BLT and

BLT/BNT films were analyzed by a Hitachi S-4100 SEM coupled with energy dispersive spectroscopy (EDS). Film specimens were mounted on aluminium stubs using carbon glue. Carbon paint was applied to the specimen to provide a conductive path, and to avoid charging of the sample inside the microscope. These samples were investigated using an operation voltage of 25 kV.

To view the cross section of films, a sandwich structure was constructed. The flexible films were supported by gluing a rigid alumina slide on both sides of the films. The supported film was fixed in to the epoxy resin for polishing. Films cross sections and fractured surfaces of the ceramic samples were polished by 1200 grade emery paper followed by a fine polishing in which sub sequential low grade diamond pastes (from 15 μm, 6 μm, 3 μm, 1 μm and 0.25 μm) were used. After the polishing an acid mixture of 5% HF + 45% HCl in 50% of water was used to chemically etch the polished films cross sections and to contrast the grain boundaries. Finally, the as-etched samples were cleaned by ultrasonication in acetone. The polished ceramic samples were thermally etched at temperatures 100 ºC below the corresponding sintering temperature for 10 min. In case of films the surfaces were analysed without any treatment.

Dielectric Characterization

In this work, the electrical measurements at RF frequency were conducted via a metal-insulator-metal (MIM) configuration using Au as the top electrode for both films and ceramics. For the case of films, Au top circular electrodes were sputtered using a shadow mask of 0.6 mm diameter. Films of BNT, BLT and composites with top electrodes were post-annealed at 200 ºC for 30 min to improve the interface between the metal and the films. In BLT ceramics, top and bottom Au electrodes of 5.5 mm diameter were sputtered.

The complex permittivity at RF frequency was measured as a function of temperature and frequency in capacitive cells as illustrated in Figure 4-4. The electrical properties were evaluated using an impedance bridge (HP 4284A, Agilent, USA) over a frequency range of 1 kHz to 1 MHz. The oscillation level of the applied voltage was set to 1.0 V. The analysed electrical properties include the relative permittivity, loss tangent,

temperature dependence of permittivity ($\Delta\varepsilon_r/\varepsilon_{r0}\Delta T$,) and relative permittivity-voltage variation (ε_r-V).

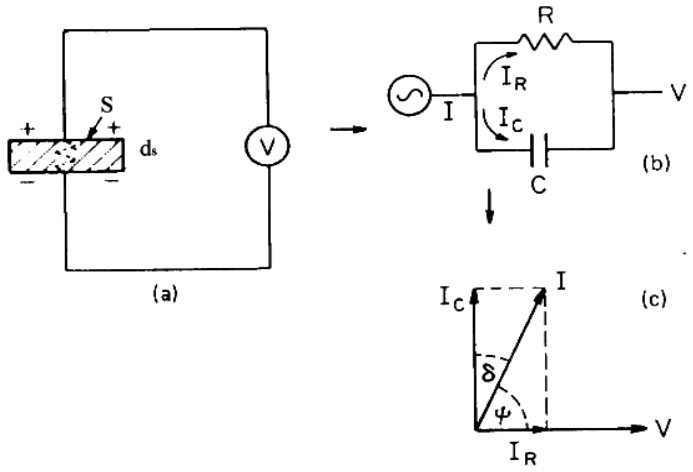

Figure 4-4: Equivalent circuit diagrams of capacitive cell (a), of charging and loss current (b), and of loss tangent for a typical dielectric (c) [1]

Error Calculation

Dielectric measurements were carried out in 5 to 6 different points along the film. The presented values of dielectric permittivity and dielectric losses correspond to the average of all the measurements and the error associate was calculated to be ± 3.9 for the dielectric permittivity and 0.0035 for the dielectric losses.

Figure 4-5 and Table 4-1 present the dielectric permittivity values and losses for BLT films sintered at 1500ºC for 1h measured at six different points.

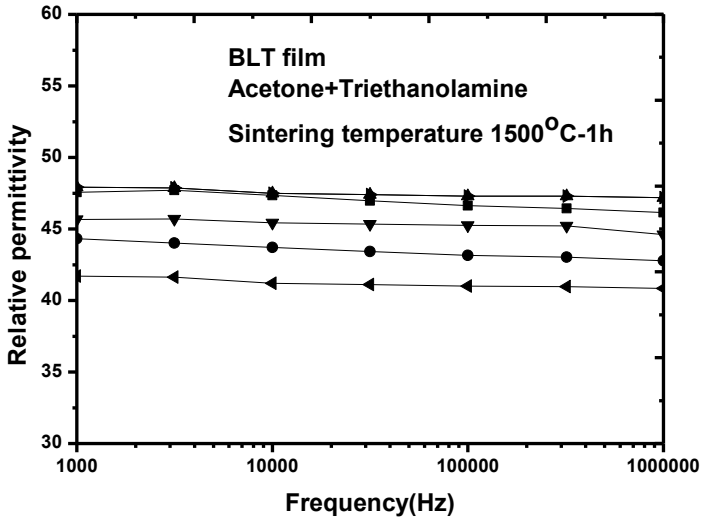

Figure 4-5: Relative permittivity as a function of frequency for BLT film sintered at 1500ºC-1h derived from acetone with triethanolamine additive.

Table 4-1: Relative permittivity at 1MHz in six points along the BLT film deposited in acetone with triethanolamine additive.

Measurement point	Permittivity at 1MhZ	Loss tangent
1	42.7	0.003
2	47.1	0.002
3	44.6	0.008
4	40.8	0.002
5	47.3	0.009
6	46.1	0.009

4.8 References

[1] Fu Zhi, "$BaNd_2Ti_5O_{14}$ Thick Films for Microelectronics Fabricated by Electrophoretic Deposition" PhD thesis, University of Aveiro(2008).

Chapter 5.
Characterization of $BaLa_4Ti_4O_{15}$ and $Ba_4Nd_{9.33}Ti_{18}O_{54}$ Powders

Abstract:
In this chapter characterization of the BLT and BNT powder is discussed. The powders are characterized in term of its phase content, thermal behaviour, particle size distribution and morphology.

5.1 Introduction:

As discussed in the Chapter 6 of the thesis a key aspect of EPD is the stability of the suspension and charge state of the particles. This behaviour is intimately related with the morphology of the powder particles, what justifies the need of a complete characterization of the powders. In the meantime, as pointed in Chapter 5 the phase formation process in BNT and BLT systems is a complex process. In order to guarantee that $BaLa_4Ti_4O_{15}$ (1:2:4) (BLT) and $Ba_4Nd_{9.33}Ti_{18}O_{54}$ (1:1:4) (BNT) powders have been synthesised the structural and phase assembly characterization is necessary.

Results and Discussion

5.2 DTA and TG

The mixed precursors of BLT and BNT were analysed by DTA and TG to obtain information on the approximated calcination temperature and Figure 5-1 represents the DTA and TG curves of both powders.

Three main peaks are observed in the DTA curve of BNT and two main plateaus in the TG curve. The first endothermic peak near to 100^{o}C corresponds to the dehydration of the starting reagents and is accompanied by the corresponding losses in the TG curve, until around 300ºC. A second quite diffuse exothermic peak ranging from 400 to almost 800^{o}C corresponds to decomposition of carbon dioxide from $BaCO_3$ and is accompanied by a marked decrease in the weight losses between 700 and 850ºC. A third peak exothermic

peak can be denoted between 900^{o}C and 1000^{o}C for which no weight loss is recorded and corresponds to the phase completeness of BNT phase formation.

Four main peaks are observed in the DTA curve of BLT and three main plateaus in the TG curve. The first endothermic peak near to 100^{o}C corresponds to the dehydration of the starting reagents and is accompanied by the corresponding losses in the TG curve. A second quite endothermic peak ranging from 390ºC which corresponds to the dehydration of $La(OH)_3$ to form LaO_3 and $La_2O_2(CO_3)$ which accompanied by the loss followed by a small weight gain in the TG curve. The third peak of around 1000^{o}C corresponds to decomposition of carbon dioxide and is accompanied by a marked decrease in the weight losses between 900 and 1050ºC. A small exothermic peak can be denoted between 1050^{o}C and 1100^{o}C for which no weight loss is recorded and corresponds to the phase completeness of BLT phase formation

From the DTA / TG analysis the reaction between the starting precursors is completed before 1150°C for both the systems, so to ensure the synthesis of monophasic powders calcination temperatures from 1200^{o}C to 1300^{o}C were selected with a heating and cooling rate of 2^{o}C/min and holding time of 3h-4h at the target temperature.

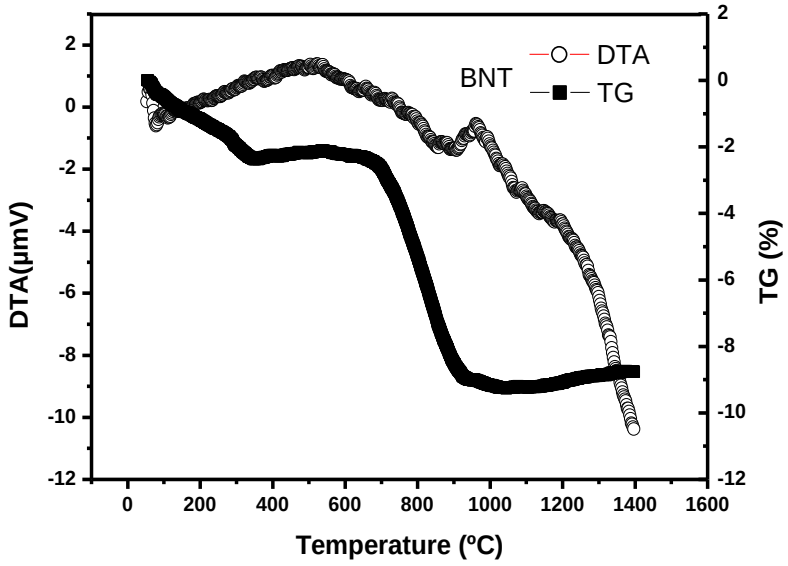

(a)

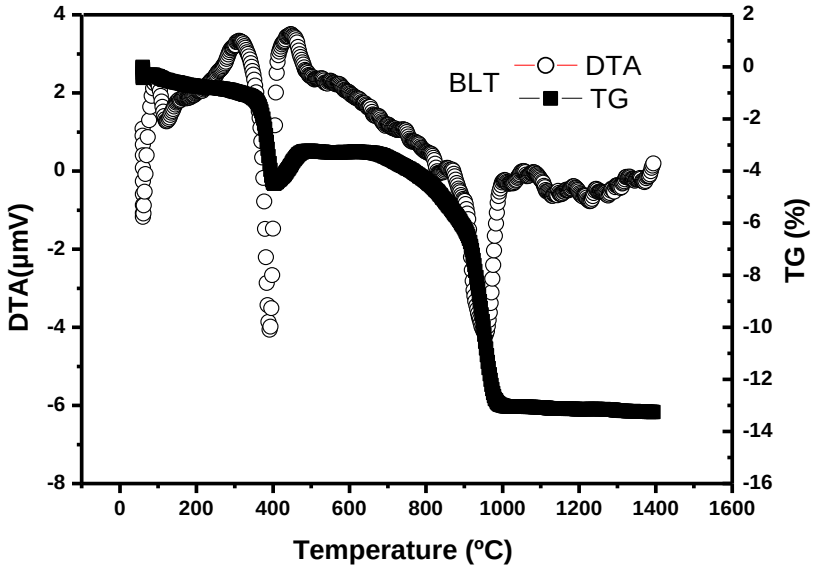

(b)

Figure 5-1: a) DTA/TG of BNT b) DTA/TG of BLT.

5.3 X-Ray Diffraction

The phase purity of the powders was confirmed by the X-ray diffraction represented in Figure- 5-2 (a) for BNT and (b) BLT powders. In this work BNT monophasic powders were obtained at 1200^{o}C/3h and monophasic BLT achieved at 1300^{o}C/3h. The effect of the calcination temperature on the phase formation of BLT is represented in Figure 5-2(c). The XRD plot shows the presence of $BaTiO_3$, $La_2Ti_2O_7$ and La_2TiO_5 phases at 1200^{o}C with the increase of calcination temperature all the phases reacted to form $BaLa_4Ti_4O_{15}$, the peaks corresponding to pure phase BLT can be seen from the XRD taken above 1200^{o}C but the other phases are also present until 1275^{o}C (Figure 5-2 (c)). Monophasic BLT powders were obtained at 1300ºC. The obtained results for the formation of BLT are corroborated by the results reported by Ohsato *et al.* [1] for BLT powders prepared by molten salt synthesis. The systematic reaction of the various phases to produce pure BLT is given in Table 5-1.

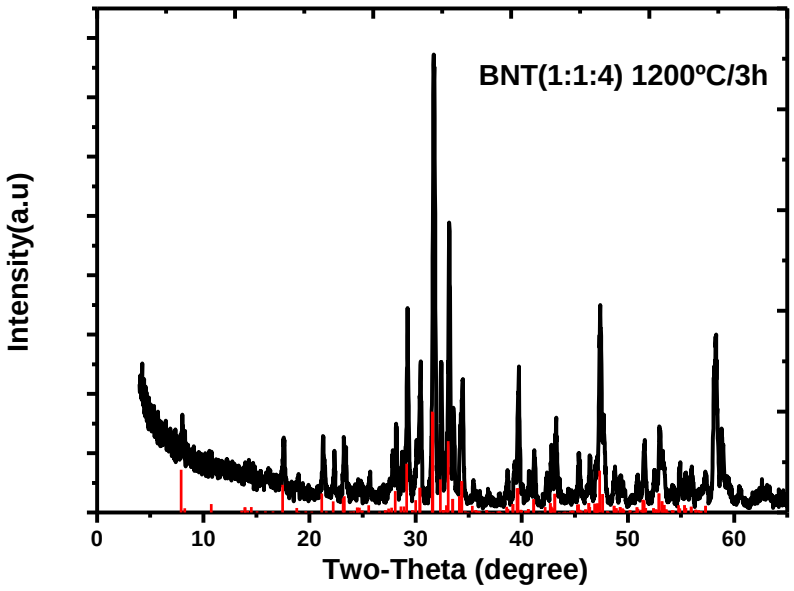
BNT(1:1:4) 1200ºC/3h
Intensity(a.u)
0
10
20
30
40
50
60
Two-Theta (degree)

(a)

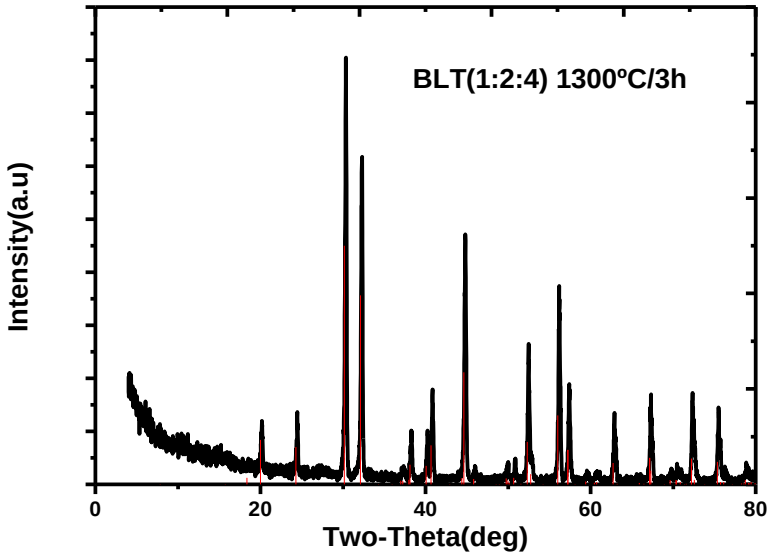
BLT(1:2:4) 1300ºC/3h
Intensity(a.u)
0
20
40
60
80
Two-Theta(deg)

(b)

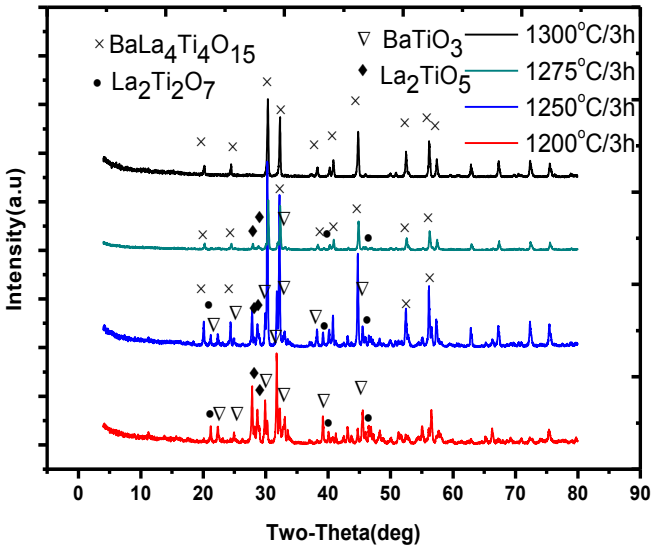

(c)

Figure 5-2: XRD of (a) BNT pure phase 1200ºC/3h (b) BLT pure phase at 1300ºC/3h (c) BLT shows the decomposition of secondary phase with increase temperature.

Table 5-1: Formation process of $BaLa_4Ti_4O_{15}$ [1].

$La_2O_3 + 2TiO_2 \rightarrow La_2Ti_2O_7$	(1)
$La_2O_3 + TiO_2 \rightarrow La_2TiO_5$	(2)
$BaCO_3 + TiO_2 \rightarrow BaTiO_3 + CO_2$	(3)
$BaTiO_3 + La_2Ti_2O_7 + La_2TiO_5 \rightarrow BaLa_4Ti_4O_{15}$	(4)

5.4 Particle Size Distribution and Morphology of Powder

Particle size distribution plays an important role in the stability of the suspension and on the green density of the films.

The particle size distribution is depicted in Figure 5-3 for BNT and BLT and both powders are characterised by a bimodal distribution. The powders are smaller than 5 micron with the highest volume percentage of particles is around 2.5 micron with a fraction of small particles below 1 micron. In comparison BLT powders possess a slight

higher volume percentage of bigger particles than BNT powders. In agreement, the specific surface area (SSA) of milled BLT and BNT powders determined by BET was 2.423 m^2/g and 4.996 m^2/g, respectively. The morphology of the particles is depicted in the SEM micrographs of Figure 5-4; clearly BLT particles are bigger than the BNT ones and exhibit a more or less platelet like shape when compared with the rod like morphology of BNT.

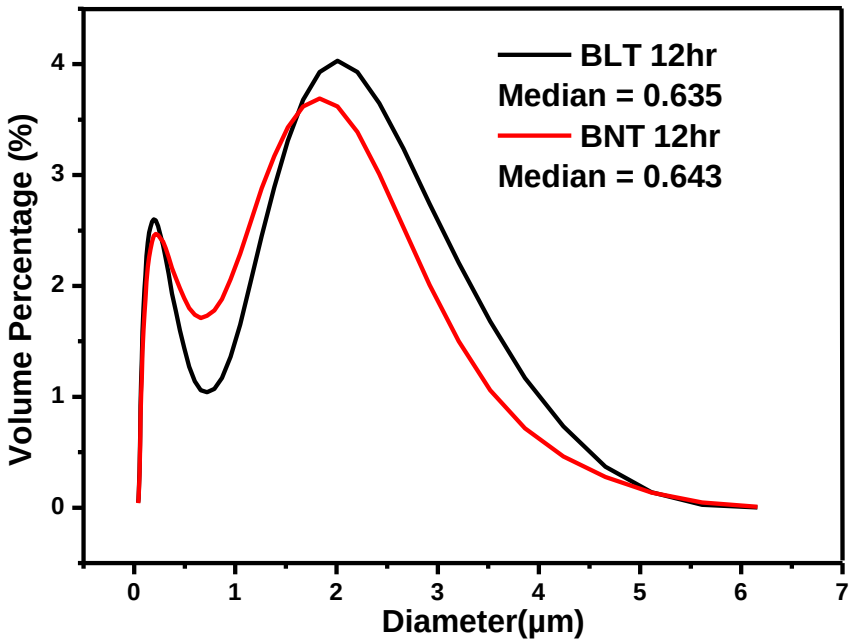

Figure 5-3: Particle size versus volume percentage for BNT and BLT powders.

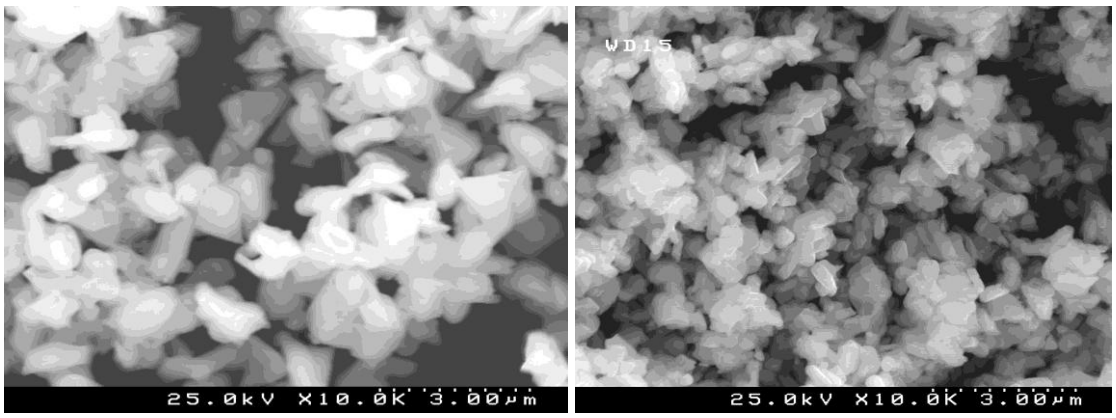

(a) (b)

Figure 5-4: SEM micrographs of the powder particles of a) BLT b) BNT

5.5 Dilatometeric Measurement

Dilatometry analysis of BNT and BLT powders is illustrated in Figure 5-5 which depicts the change in the length ($\Delta l/l_0$ x 100%, l_0 stands for the initial length and Δl for the variation of the length) with the temperature. For both compositions after the initial expansion, shrinkage starts at around 1250ºC and 1100ºC and finished at 1500^{o}C and 1400^{o}C respectively for BLT and BNT powders. This is a clear indication of the different sintering behaviour of BNT and BLT that will be reflected in the densification of the corresponding ceramics and films, in particular the composite films.

For BLT ceramics and BLT films the sintering temperatures were selected from 1400ºC to 1600ºC with heating rate of 2ºC/min to study the effect of processing. BNT films were sintered at 1450ºC/1h. In case of BNT-BLT composites in-between temperatures from 1450-1550 were selected for sintering.

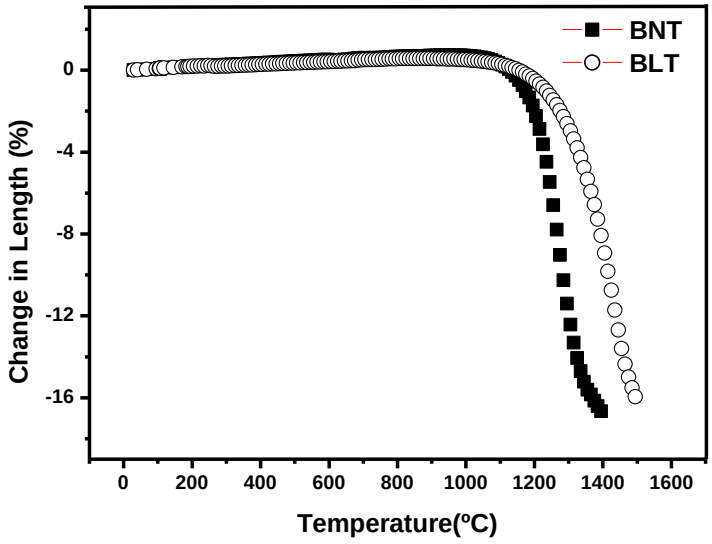

Figure 5-5: Dilatometeric curve of BLT and BNT powders.

5.6 Reference

[1]. Y Fukami , K Wada, K Kakimoto, H Ohsato., Journal of the European Ceramic Society 26 (2006) 2055–2058.

Chapter 6.
Fabrication of $BaLa_4Ti_4O_{15}$ and $Ba_{6-3x}Nd_{8+2x}Ti_{18}O_{54}$ (x=2/3) Thick Films by Electrophoretic Deposition

Abstract:

In this chapter, a comprehensively discussion on the fabrication of BLT and BNT films by EPD is presented. Suspensions based on water, ethanol, and acetone were employed and analyzed for the electrophoretic deposition (EPD) of BLT and BNT powders. The effect of suspension additives on film's deposition is studied. It is observed that ethanol with HNO_3 and acetone with triethanolamine are suitable suspension media for the deposition of BLT thick films, while in case of BNT, optimised deposited films, are achieved when acetone with triethanolamine is used. .The suspension stability behaviour is studied by means of the particle size distribution, UV transmittance and zeta potential. The deposition parameters like voltage and time and a post deposition isostatic press step are analysed in order to control the final thickness and green density of the films.

6.1 Introduction

As described in Chapter 2, the fabrication of thick films with optimised properties depends on factors, such as stability, zeta potential, viscosity and dielectric constant of the suspension and applied voltage and deposition time (*inter alia*), it is important to study this parameter.

In a previous work of the present group the fabrication by EPD of BNT(1:1:5) thick films was reported [1]. It was observed that in terms of films quality (Figure 6-1) the optimised properties were achieved for acidic media in acetone containing iodine with dielectric properties superior than BNT ceramics. It was than proved the applicability of EPD for the fabrication of functional thick films, what was viewed as the step forward for the miniaturisation of the microwave devices.

However the fabrication of BLT thick films by EPD has not yet been reported. It is then very opportune and scientifically and technically interesting to prove the adequacy of

the use of EPD to fabricate low loss BLT thick films and to compare their properties with those of BNT thick films on metal foils.

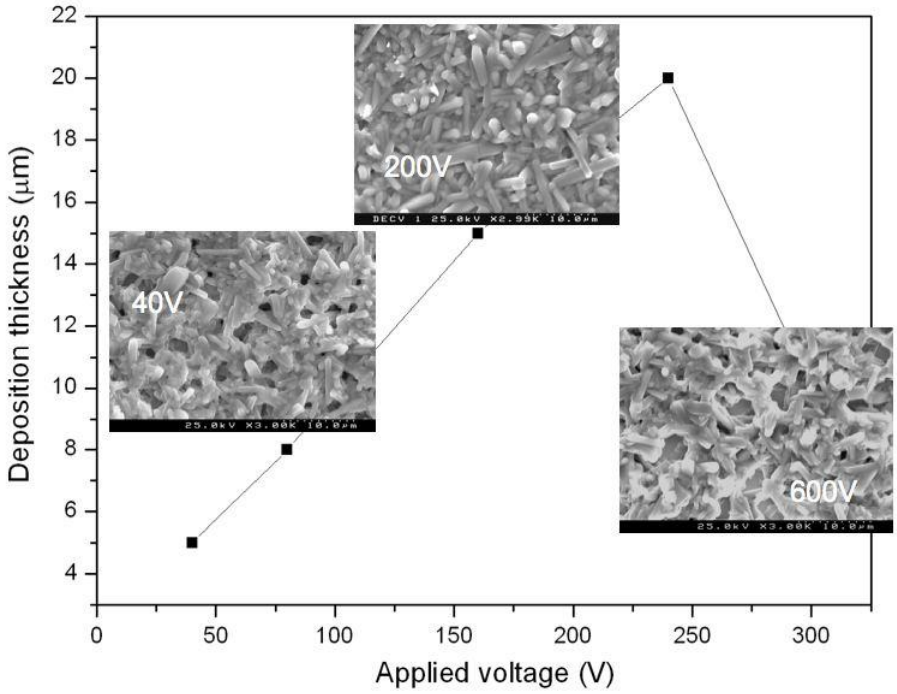

Figure 6-1: Deposited thickness of BNT films as a function of applied voltage in acetone with iodine [1]

6.2 Experiments

BLT and BNT powders were used to prepare the suspensions for EPD. The fabrication, morphology and characterization of the powders were discussed in detail in the experimental Chapters 4 and 5.

BLT and BNT (1:1:4) powder suspensions were prepared in acetone, ethanol and water. And additives such as nitric acid and triethanolamine were used to vary the pH of the suspension from acidic to basic and to vary the particle charges. The stability of each of these suspensions was inspected by UV transmittance spectroscopy and particle size analysis. For all the suspension media the suspensions prepared for transmittance spectroscopy had a similar concentration, which is an important requisite for a comparative analysis. The films were deposited under constant time and constant voltage.

6.3 The Role of Suspension Media in the Deposition of BLT and BNT Thick Films

Some physical properties (like viscosity, dielectric constant) of the suspension media used in this work (acetone, ethanol and water) are indicated in Table 6-1, together with the macroscopic observation regarding the deposition. It was observed that with the application of voltage, BLT and BNT particles move to negative electrode for organic based medium where as for water based suspension no movement was observed.

Power *et al.* [2] stated that for solvents with low dielectric constant the dissociative charging mode is insufficient and as a consequence no deposition occurs; however in the presence of high dielectric constant solvents the ionic concentration increases in the suspension, reduces the size of the double layer region and consequently the stability, therefore non aqueous media with medium dielectric constant such as acetone and ethanol, are in general effective for EPD.

Under the current EPD experiments the solid loading is quite low so the viscosity cannot be used as a parameter to evaluate the dispersion state [4-5].

Table 6-1: Physical properties of the suspension media used in the preparation of BNT and BLT suspensions for EPD.

Suspension media with additives(HNO_3 and Triethanolamine)	Dielectric constant	Viscosity (cP)=10^{-3} N s m^{-2}	EPD deposition BLT/ BNT
Acetone	20.7	0.306	Very Good / Very good
Ethanol	24.3	1.22	Good / No deposition
Water	80	0.89	No deposition / No deposition

The pH of water based suspensions and operational pH of the organic-based suspensions were measured by means of a pH meter. The operational pH of the BLT and BNT suspension in ethanol and acetone was controlled by additions of diluted nitric acid (1:10) and triethanolamine (>99.8%, Merck). The pH values for BNT and BLT suspension

media are indicated in Table 6-2, the pH value for pure acetone and ethanol is 7.97 and 7.09 respectively.

Table 6-2: The pH values for BNT and BLT in organic media with and without additives.

System	Suspension media	Additive	pH
BLT	Ethanol	-------	6.51
BLT	Ethanol	dil. HNO_3(2-3 Drops)	2.30
BLT	Acetone	-------	7.74
BLT	Acetone	Triethanolamine (1ml)	8.50
BNT	Acetone	--------	8.20
BNT	Acetone	Triethanolamine(1ml)	8.90

The variation of pH was conducted to enhance the concentration of positive and negative charged ions in the suspension to achieve high zeta potential values, required for an optimised deposition.

As an example, the zeta potential curve of BLT powders in ethanol is illustrated in Figure 6-2. The zeta potential for pH values 2-3 is near to 58mV, which means a high mobility of the particles in suspension and may result in a good deposition. As the pH increases the zeta potential decreases and the isoelectric point is attained for pH values of 8.7

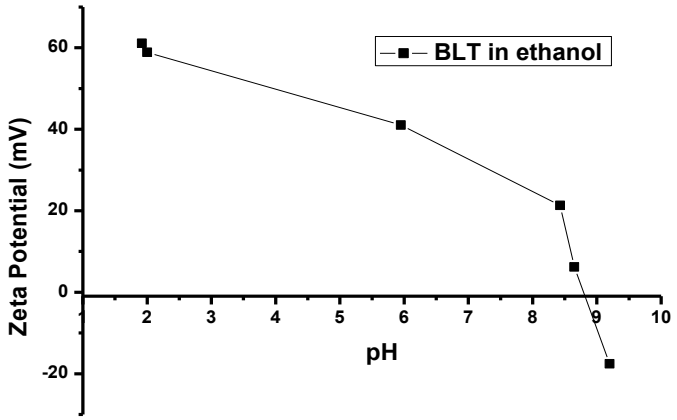

Figure 6-2: Zeta potential versus pH for BLT suspension in ethanol.

A good deposition was observed for BLT in ethanol based suspensions with pH value near to 2 as can be seen from the optical image of films morphology depicted in Figure 6-3. For BNT in acidic media no deposition was observed.

Figure 6-3: Surface morphology of BLT films deposited in ethanol suspension media with HNO_3, under 100V for 1min

In acetone based suspensions no deposition was observed for acidic media but for the basic media with pH 8-8.9 very good deposition was observed for both BLT and BNT systems, as can be seen in optical image depicted in Figures 6-4 and 6-5.

To study the electrophoretic deposition of BLT and BNT particles with basic pH, triethanolamine as an additive was used in acetone based suspensions. The choice of acetone over ethanol was made based on their pH values; pure acetone shows pH of 7.97 and with the addition of BNT particles the pH values increase for the BNT near to 8.2. In case of ethanol media, with the addition of BLT particles the pH of the suspension shifts towards lower value 6.51 (acidic), so by taking pH behaviour in account acetone was preferred over ethanol for basic deposition.

The zeta potential for BNT and BLT in pure acetone is 16.6mV and 15mV respectively. To enhance the surface charge on the particles triethanolamine was added to BNT and BLT suspension which further increase the suspension pH to 8.90 and 8.50 respectively (Table 6-2).

For the basic suspensions, i.e. acetone with triethanolamine, the deposition occurred at the negative electrode. In order to understand the mechanism behind the charge

process of BNT and BLT particles under these basic conditions zeta potential curves should be acquired, but due to experimental limitations of the equipment available at the University of Aveiro, these curves could only be obtained in water. However similar good anodic depositions were reported in the work of Widegren *et al.* [7] for the deposition of Al_2O and TiO_2 particles in ethanol based suspension with triethanolamine.

Figure 6-4: Surface morphology of BLT films deposited in acetone suspension media with triethanolamine, under 60V for 1 min.

Figure 6-5: Surface morphology of BNT films deposited in acetone suspension media with triethanolamine, under 60V for 1min.

It is worthwhile to note here that no deposition was observed in the case of water, pure ethanol and pure acetone based suspensions. The reasons behind these occurrences cannot be easily evaluated because of the complexity of EPD and are still a matter of debate.

However the following analysis can contribute to explain some of these observations.

6.4 Suspension Stability

The particle size distribution in different media (water, ethanol and acetone) is depicted in Figure 6-6 for the BLT system. As expected BLT particles show dissimilar dispersion characteristics in the different suspension media. The stability analysis was performed in water as well, so that it can be used as a reference. A bimodal distribution was observed for all the suspension media under study with and without additives. However the volume percentage of particles varied for each media. A lower percentage of particles in the range of 2 to 6µm and a higher percentage of particles in the range below 1µm were observed in organic media when compared with the water based one. This clearly indicates that the tendency for particle agglomeration in water is higher than in organic media, supporting the better stability of BLT powders in organic suspensions. The addition of additives in acetone and ethanol further increase the volume percentage of smaller size particles as expected, which assures a good EPD.

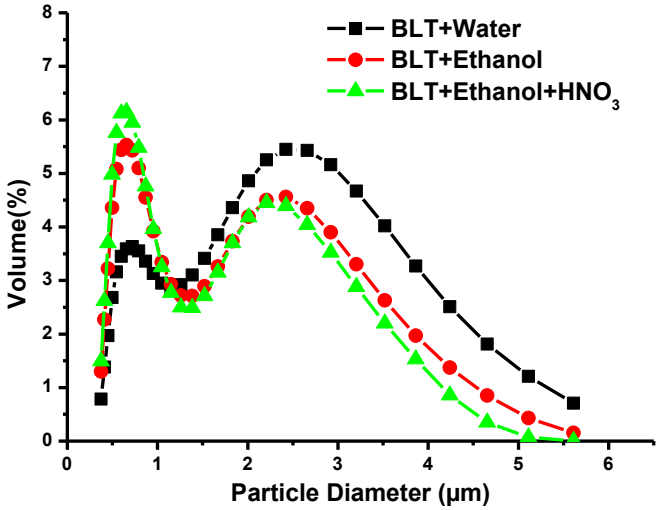

(a)

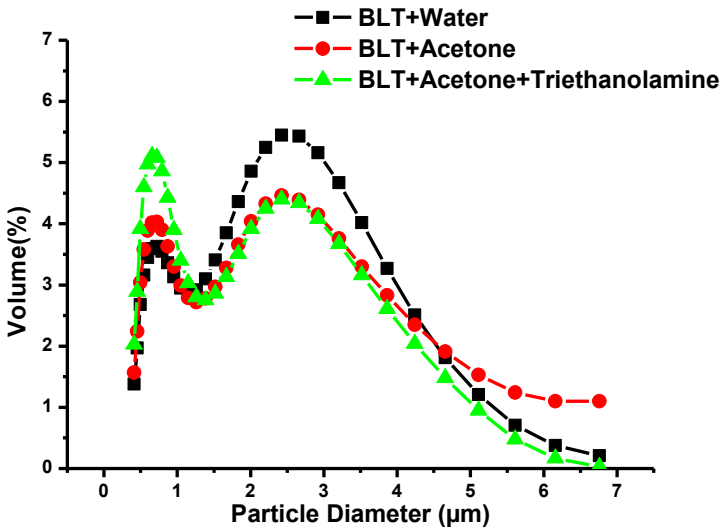

(b)

Figure 6-6: Volume percentage of particles versus particle diameter for BLT a) in ethanol and b) acetone media with and without additives.

For BNT suspensions, considerable changes can be distinguished for the case of organic suspension media acetone as compared to water presented in Figure 6-7. Similarly to BLT, BNT suspensions exhibit a bimodal distribution in all the suspension media. However in water the volume percentage of particles in the range between 2 and 6.5μm is higher and lower for the submicron range when compared with the other suspension media; a narrower distribution was indeed observed for the acetone based suspension, where the highest volume percentage of particles are smaller than 0.6μm. The addition of triethanolamine to acetone did not provoke a marked effect on the particle size distribution, just a minor increase in the volume percentage of the small size particles.

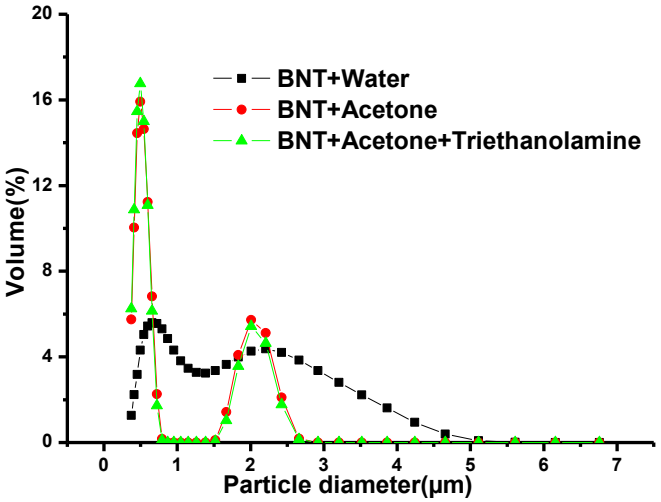

Figure 6-7: Volume percentage of particles versus particle diameter for BNT in acetone media with and without additives.

To prepare a well dispersed BLT and BNT suspension for EPD and to obtain a dense coating, a fine particle size suspension is required and BLT suspensions in ethanol and acetone and BNT suspension in acetone with additives present indeed relatively good results then in ethanol.

The stability of the suspensions with time was further studied by UV transmittance. The transmission results in acetone, ethanol and water suspension with and without additives for both systems are plotted in Figure 6-8 (a) and (b).

As high the transmission value is, as less stable the suspension will be. For BLT ethanol based suspensions, the transmittance percentage was 28% for the case of water, 23% in ethanol and 22 % in ethanol with HNO_3 addition. The waiting time was of 1 minute before every measurement. The lower transmission observed in the case of ethanol based suspension indicates a better dispersion of the particles in suspension and corroborates the results of the particle size distribution, presented above. The transmittance percentage increases with time for all the suspensions which is related with the sedimentation of the suspended particles as the time passes. However, this increase is less visible for the case of the water based suspension due to the fact that, under the same experimental conditions,

the amount of the coarse particles in suspension is very few in the water based suspensions, because they settled almost immediately, i.e. in the first seconds of settling.

For BLT in acetone based suspensions, the transmittance decreases from 20 % to 12% with the addition of triethanolamine which indicates a very good dispersion degree of the suspension as compared to the suspension without additives, as previously observed for the other additives, what ensures a good stability for the BLT suspension in acetone with triethanolamine. These observations validate the results obtained from the particle size distribution in which the volume percentage of small sized particles slightly increases with the addition of triethanolamine.

The transmittance results demonstrate that in ethanol and acetone based suspensions of BLT, some particles settle down after 7-10 min which might not be a matter of concern as deposition is carried out immediately after stirring and in the first few minutes of the settling of the suspension.

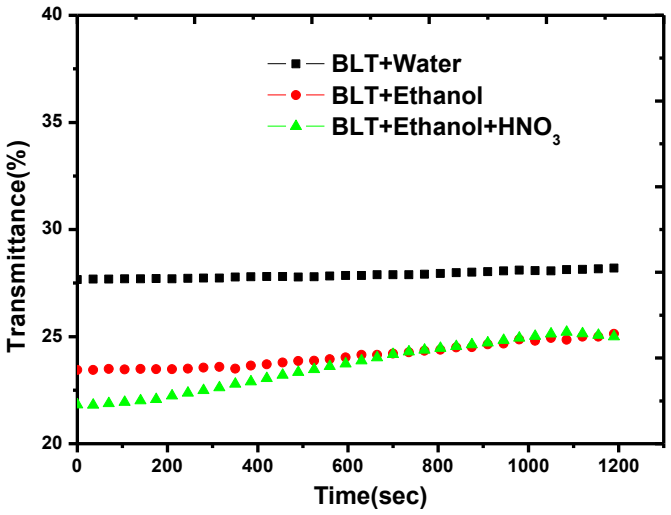

(a)

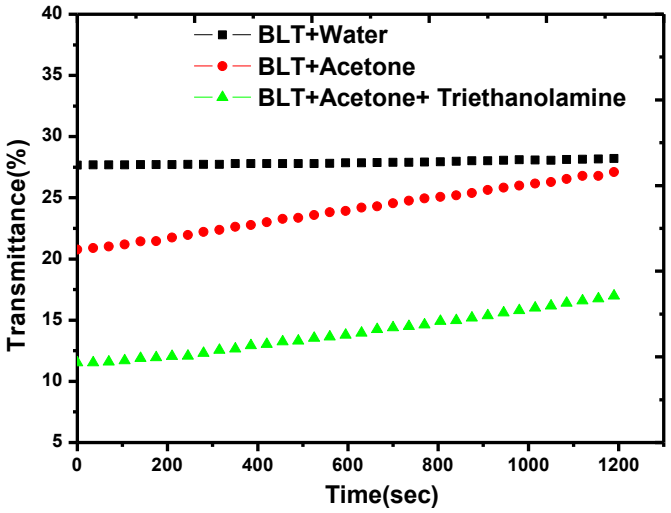

(b)

Figure 6-8: UV transmittance versus time for BLT suspensions in a) ethanol b) acetone with and without additives.

The stability behaviour of BNT suspensions in different suspension media is depicted in Figures 6-9. As observed for BLT, BNT water based suspension presents the highest transmittance values, indicating the less stable suspension when compared with equivalent suspensions in acetone and ethanol. Indeed, the transmittance percentage of BNT drops from 27% in water to 11% in acetone and acetone with additives. In suspensions with additives the particles stay stable for longer periods of time as compared to the ones without additives, ensuring better suspension stability for the EPD. The very small differences in the transmittance percentage between BNT acetone based suspensions with and without additives are in good agreement with the particle size distribution results (Figure 6-7) in which the volume percentage of the particles distributed in both media is almost equal.

The above presented results of particle size analysis and UV transmittance gave a clear idea about the stability of the organic based suspensions and about their appropriateness to be used in the flowing steps of the film deposition.

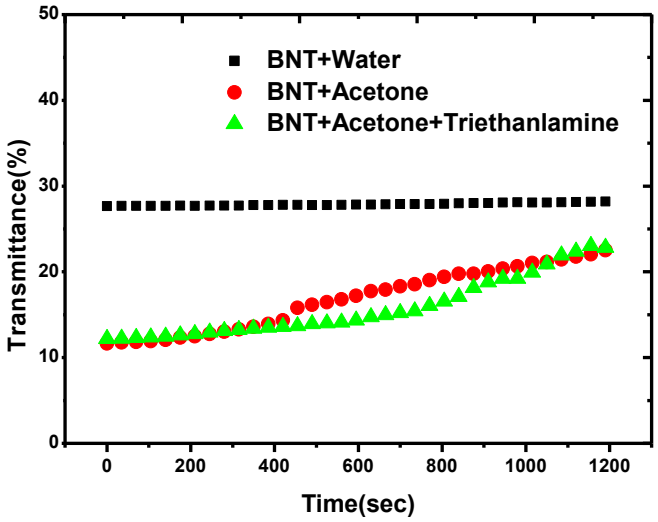

Figure 6-9: UV transmittance versus time for BNT suspensions in acetone with and without additives.

6.5 The Role of the Deposition Parameters on the EPD of BLT and BNT Thick Films

As well documented in the introduction there are several processing variables that affect the properties and quality of the deposited films. The knowledge of the effect of these variables is crucial to control the kinetics and the deposition process and the final characteristics of the films. For that, BLT and BNT films were deposited under varied deposition conditions, namely voltage and time.

The effect of the deposition voltage and time for BLT in ethanol with HNO_3 additions is presented in Figure 6-10, in which the variation of the film thickness is plotted against the time for a fixed deposition voltage and plotted against the voltage, for a fixed deposition time.

For constant voltage with time the film thickness increases linearly until 60µm and then starts to deviate from linearity for longer deposition times. The observed deviation is due to the decrease in the electric field between the electrodes because of deposited layer of particles on the substrate or to the change in the charge concentration of the suspension as the deposition goes on [5]. For constant time and varying deposition voltage the thickness of film increased more or less linearly for the voltage range from 60 to120V and

deviates from this linear behaviour for higher voltages. It is well known that with the increase of the deposition voltage the particles will be animated of high velocities and will travel very fast towards the counter charged electrode deteriorating the packing of the particles on the substrate and limiting the film thickness increase and the deposition of a closed packed structure. In addition the increased voltage may cause turbulence in the suspension, which results in non uniform surface and bulk films [6]. It was even observed that at high voltage the films tend to peeled off from the substrate.

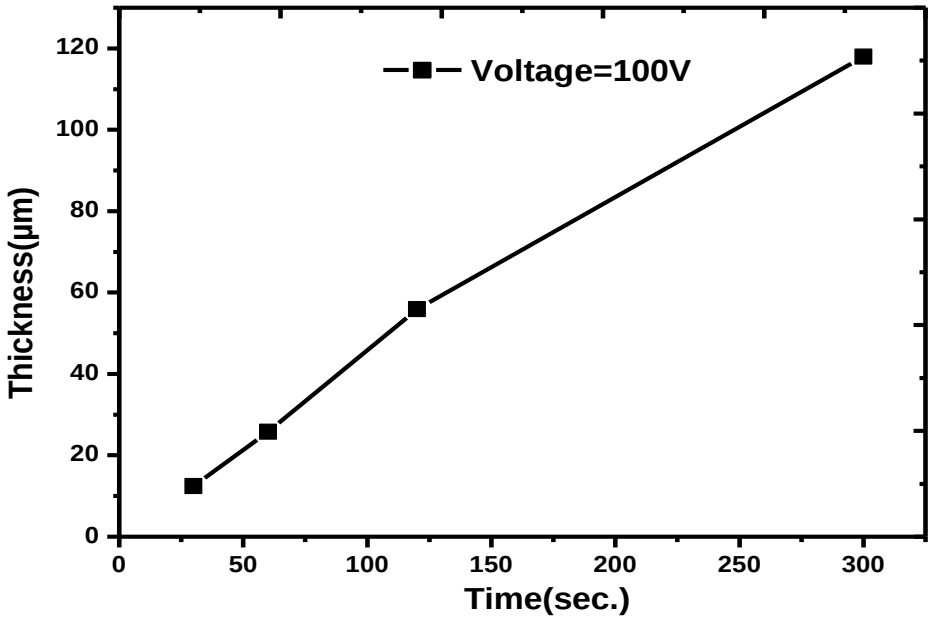

(a)

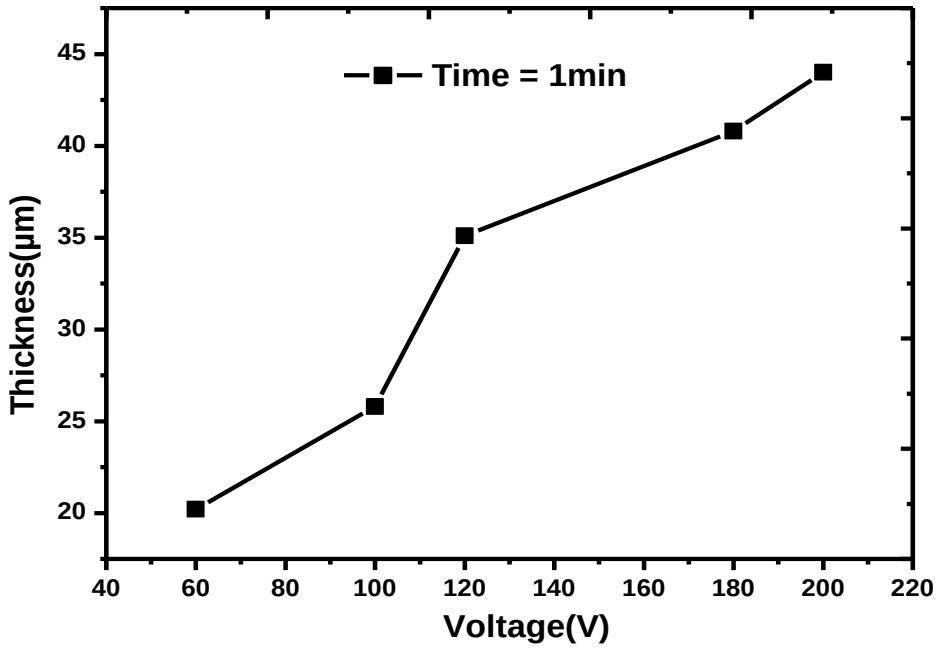

(b)

Figure 6-10: Deposited thickness of BLT films in ethanol with diluted nitric acid as a function of (a) constant voltage (b) constant time.

The topography of films deposited in ethanol was not uniform and especially for high film thickness as shown in Figure 6-3. The geometrical density of green films deposited in ethanol suspension was in between 26% to 32% of theoretical density.

The effect of the deposition voltage and deposition time on the properties of BLT films was carried out in basic media, as well.

Figure 6-11 represents the variation of BLT film thickness as a function of voltage and time for acetone with triethanolamine suspension media. As previously observed the thickness of the films deposited under constant voltage (60 V) for varied deposition times and under fixed deposition time (1 min) for varied deposition voltages, increases for initial deposition time and voltage and then the rate of thickness decreases as the deposition time or deposition voltage increases. Under 60V the maximum thickness achieved under the present conditions was about 55μm for 120sec and for longer deposition times the films peeled off from the substrate.

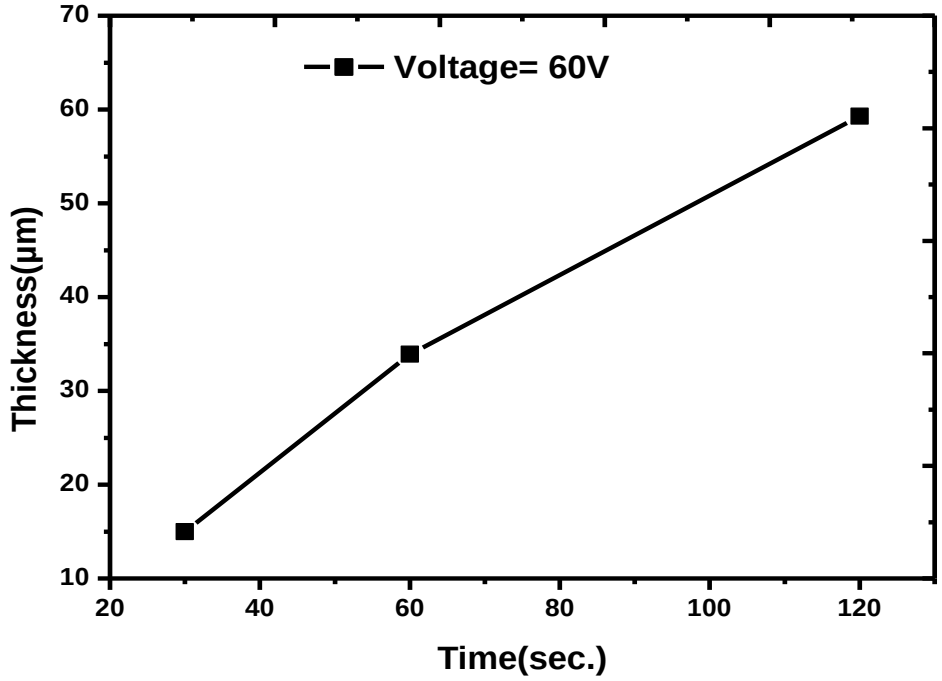

(a)

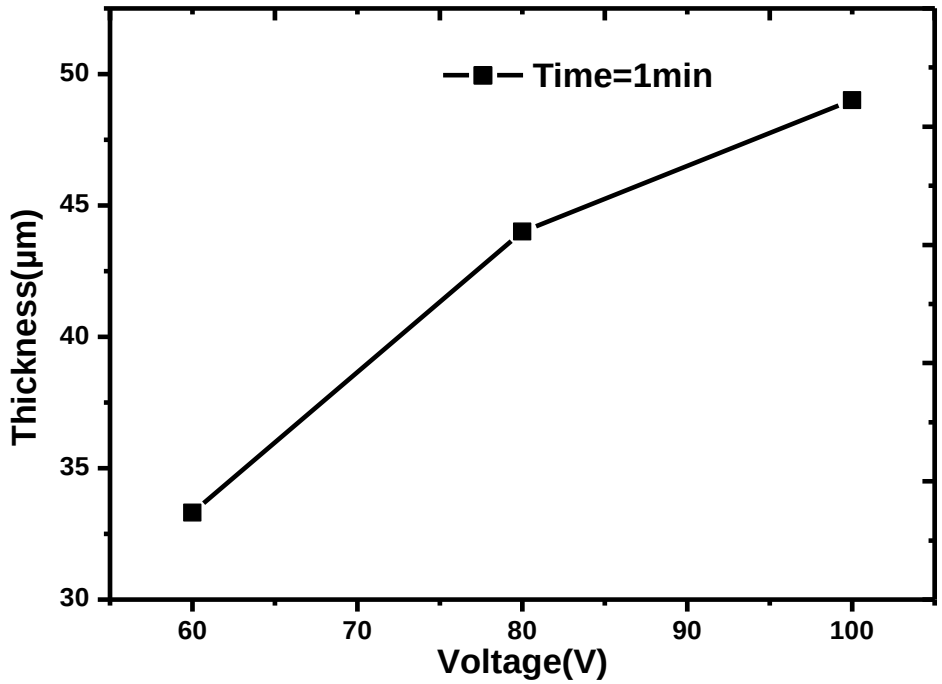

(b)

Figure 6-11: Deposited thickness of BLT films in acetone with triethanolamine as a function of (a) constant voltage (b) and constant time

This non linear behaviour is further supported by the results depicted for BLT in Figure 6-12, in which the variation of the suspension electric current is measured during the deposition and the deposit weight is plotted against the deposition time. For both variables the variation is asymptotical, indicating a decrease of the rate of the variation. The decrease of the rate of the deposit weight with time can be explained, on one hand by the decrease in the particle velocity with time related with the decrease of the current in the suspension media as the deposition time passes, on the other hand as a result of the deposited mass on the electrode which acts as a shield for the incoming particles [5]. The current was dropped from 7.9mA to 7.5mA with time because of the insulating layer created by deposited particles on the substrate.

BLT films derived from acetone with triethanolamine and presented in Figure 6-4 exhibit more uniform surface topography than BLT films derived from ethanol with nitric acid suspension media. The geometrical density of green films deposited from acetone with triethanolamine was in the range of 42% to 48% of theoretical density, considerably higher than the density of the BLT films prepared from the ethanol based suspension by approximately 10%.

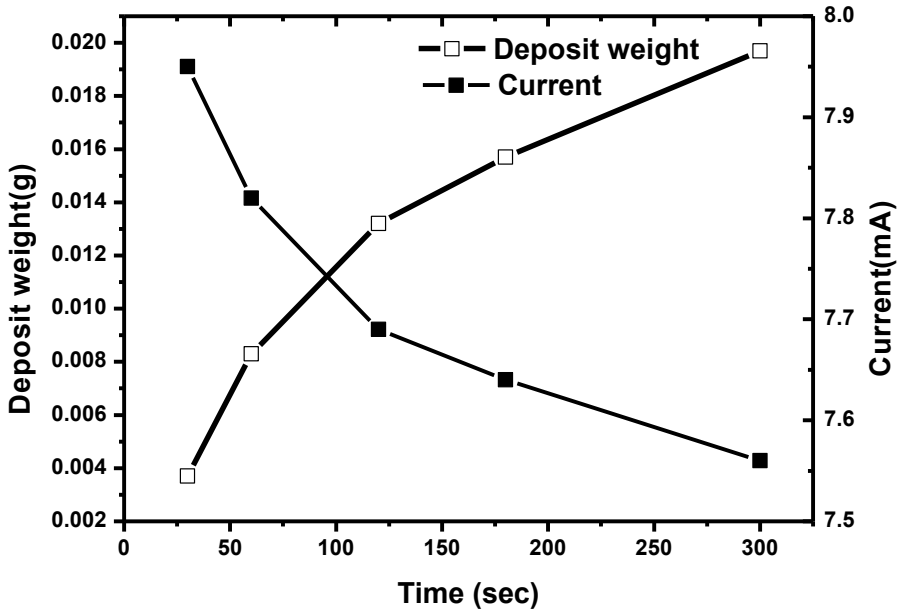

Figure 6-12: Deposited weight and suspension current as a function of time for BLT in acetone with triethanolamine.

As mentioned before the fabrication of BNT films was thoroughly studied in previous works of this group [1] and in this thesis the preparation of BNT thick films was carried out only as a mean to achieve optimised fabrication of BNT / BLT and BLT / BNT thick composite films. BNT deposition was carried out in acetone with the addition of triethanolamine and under high pH values. Very uniform deposits were formed at the negative electrode in a similar way to the BLT system under basic conditions.

The deposition parameters like, voltage, current and time were analysed to control the films properties. In Figure 6-13 film thickness is plotted as a function of time and applied voltage for constant applied voltage and time respectively. A similar variation to the previously described BLT behaviour is observed. This nonlinearity in the thickness variation was also reported for other systems like ZnO by Wang *et al*. [6].

The deposited weight and suspension electric current as a function of the deposition time are depicted in Figure 6-14. With the increase of deposition weight the current decreases which is due to the deposition of the powder insulating layer on the substrate.

The geometrical green density of the films was in between 46-50 % of theoretical density. The optical microstructure of the BNT films illustrated in Figure 6-5, evidences a very good surface morphology.

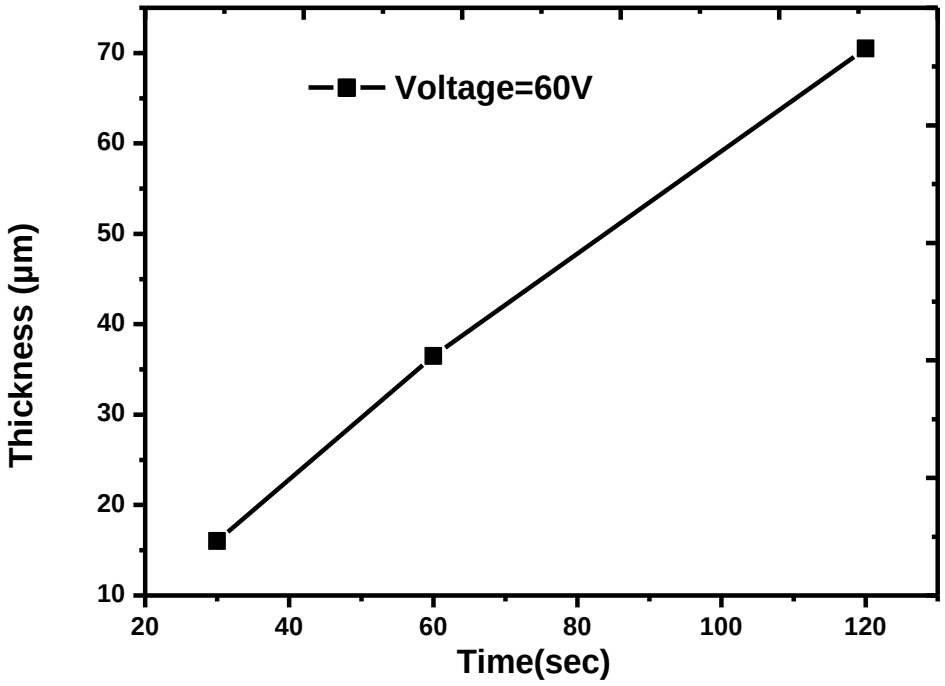

(a)

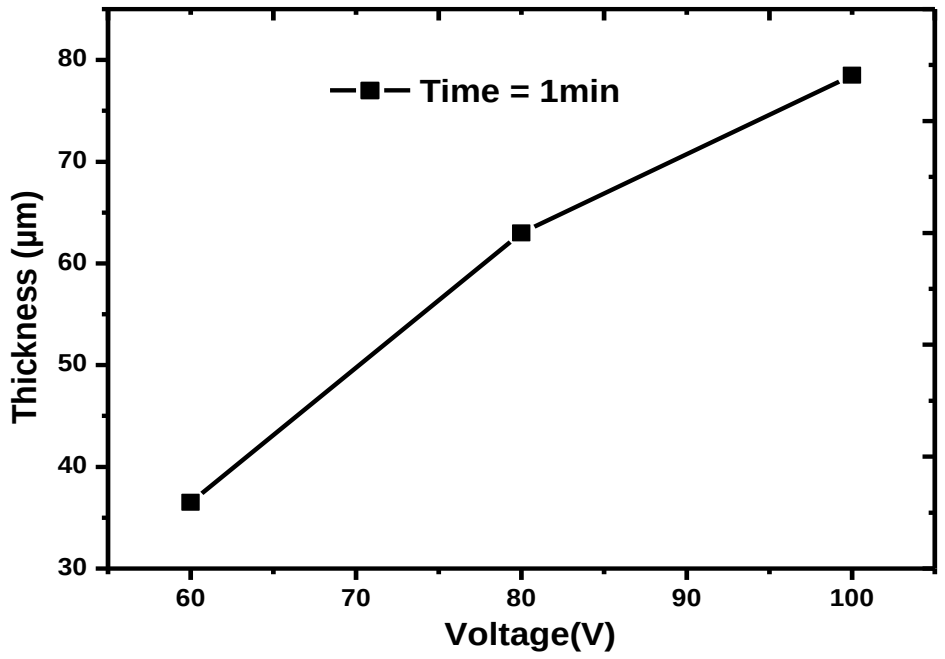

(b)

Figure 6-13: Deposited thickness of BNT films in acetone with triethanolamine as a function of (a) constant voltage (b) and constant time.

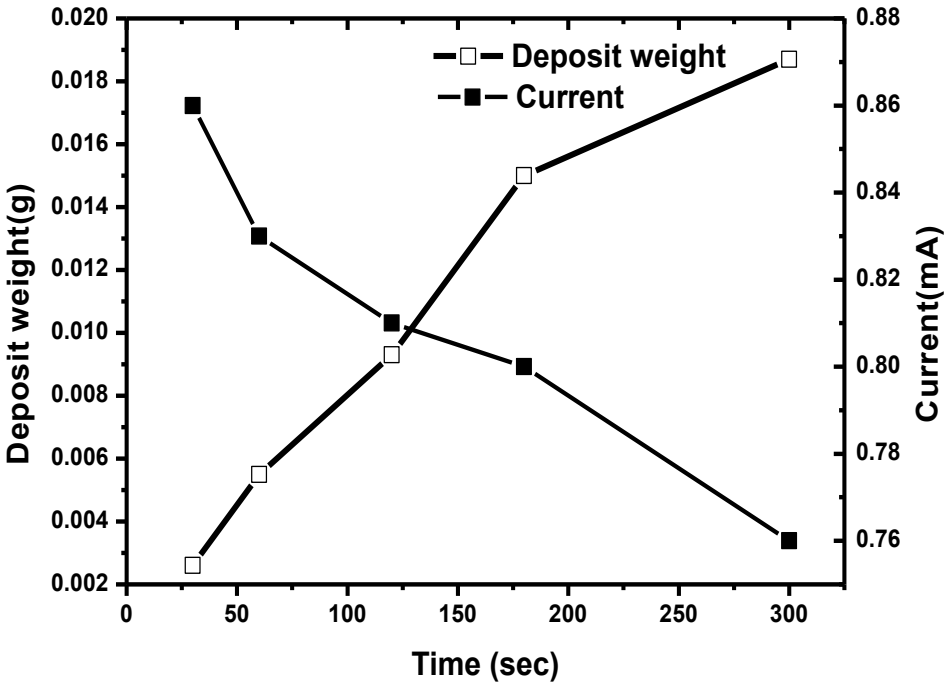

Figure 6-14: Deposited weight and suspension current as a function of time for BNT in acetone suspension with triethanolamine.

It is very important to have uniform topography and crack free surfaces to guarantee optimised film's properties. It was observed that with the increase of the green film thickness the surface become more inhomogeneous and after sintering some cracks were formed as shown in Figure 6-15. For thickness lower than 50µm the surfaces of the films were uniform and crack free after and before sintering. The cause of cracking in the case of higher thickness film may be due to development of stresses during the constrained sintering process, to the increased non uniformity of the green microstructure of the films as the film thickness increases and also to drying step that is more difficult in the thick than in the thin films.

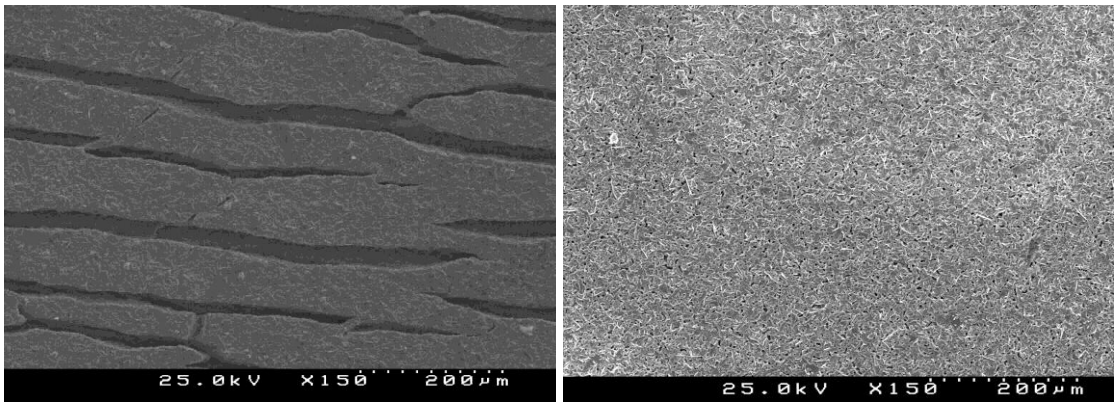

(a) (b)

Figure 6-15: SEM micrograph of BLT film, top view with thickness a) >50µm b) <50µm

6.6 Post Deposition Treatment

In generally, EPD process produces a porous layer of compacted powder and in order to enhance the density of the films, a post-deposition cold isostatic pressing (CIP) step was employed.

Although alternative approaches to enhance the sintered density of the films can be used, that include increasing the sintering temperature or introducing liquid phase sintering aids, these are not so attractive for the present studies. Due to the thermal expansion mismatch between the films and the substrate increasing the sintering temperatures will invariably lead to the formation of cracks and for case of sintering aids the dielectric losses can easily increase.

Figure 6-16 illustrates the SEM micrographs of BLT and BNT films sintered at 1450º/6h and 1450ºC/1h without and with CIP treatment at 200 MPa, respectively. The lower porosity of the CIP films is clearly seen when compared to the non CIP films. The dielectric properties of the corresponding films are depicted in Figure 6-17; the permittivity decreases and losses increases by factor of 5 to 10 for both BLT and BNT films prepared without CIP step. The CIP step is proved to be very effective in terms of green densification and, as a consequence, in terms of final dielectric response.

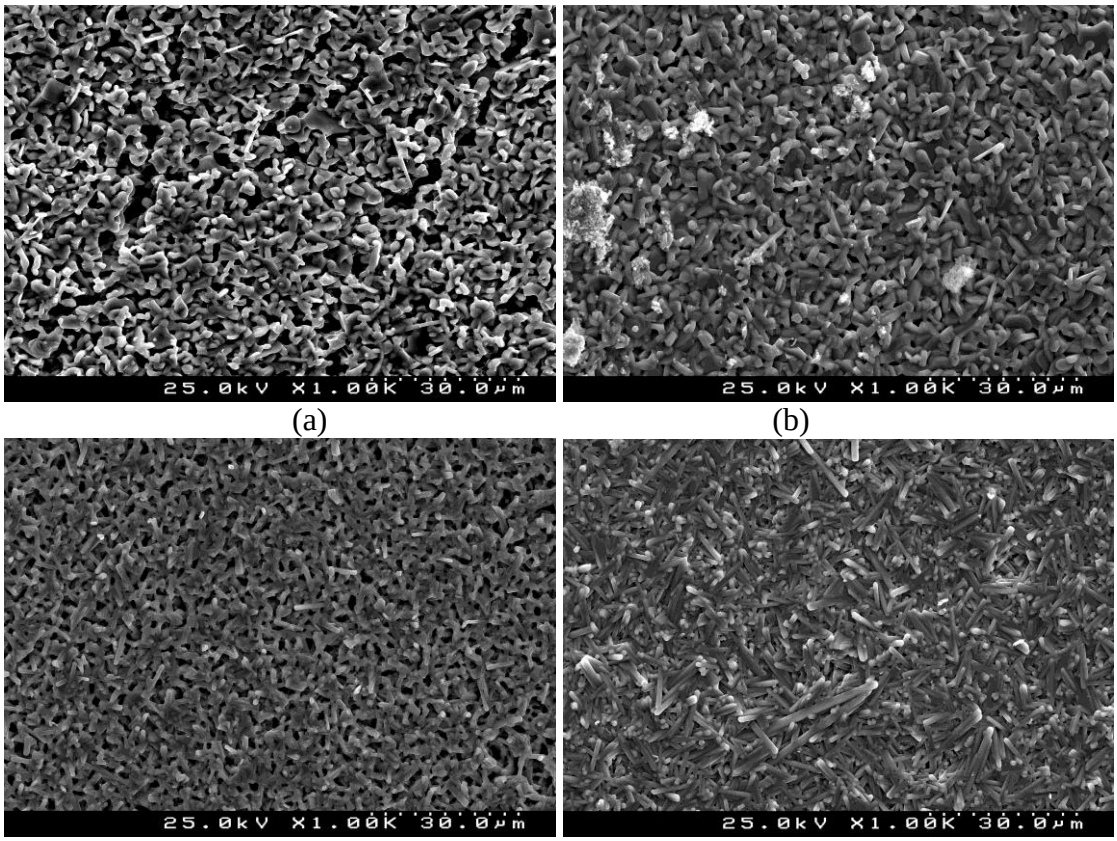

(a) (b)

(c) (d)

Figure 6-16: SEM micrograph of BLT(a,b) and BNT(c,d) sintered at 1450ºC/6h and 1450ºC/1h resp. a-c) without CIP and b-d) with CIP.

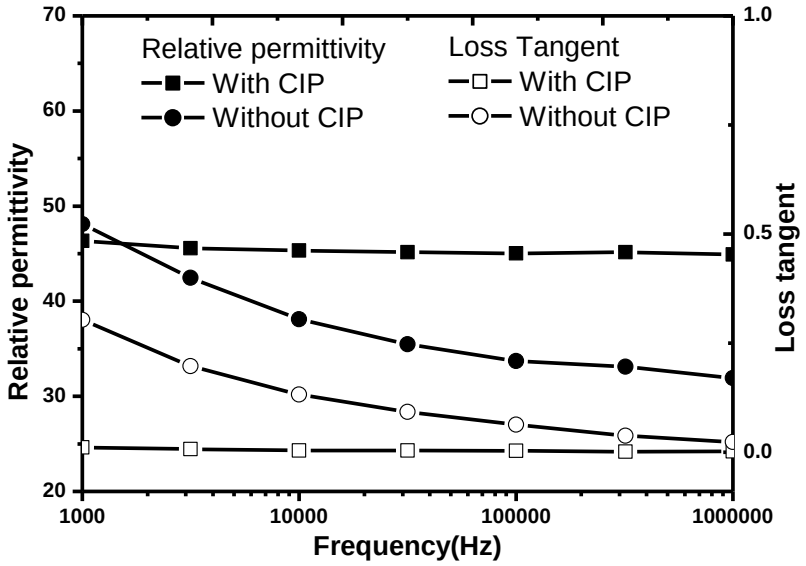

(a)

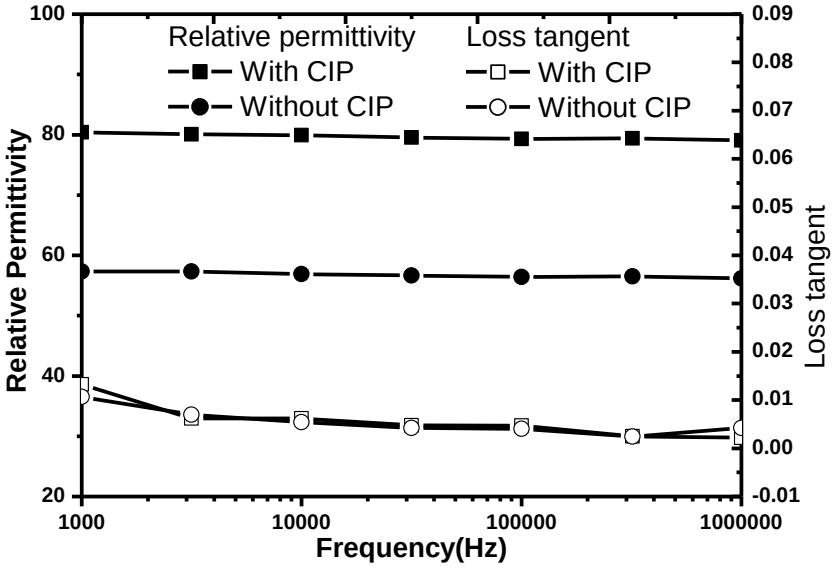

(b)

Figure 6-17: Relative permittivity and losses as a function of frequency in a) BLT b) BNT films respectively.

6.7 Conclusion

BLT and BNT thick films were successfully deposited on the platinum substrates by EPD.

Because the mechanism of EPD involves charged particles in a suspension being deposited onto an electrode under the influence of an applied electric field two groups of parameters determine the characteristics of this process: (i) those related to the suspension, and (ii) those related to the process including the physical parameters such as the electrical nature of the electrodes, the electrical conditions (voltage/intensity relationship, deposition time, etc.).

In this chapter the role of suspension media and of deposition parameters (such as voltage and time) was assessed in the deposition of BLT and BNT thick films.

It was verified that BLT thick films can be successfully deposited either in acidic and basic media of ethanol and acetone, respectively. However BNT, films were only obtained in basic suspension media of acetone with triethanolamine. Diluted nitric acid and

triethanolamine were used to vary the pH of the suspension and proved to be very useful in controlling the stability of the suspension and the quality of the deposit.

Low pH ethanol with nitric acid suspensions and high pH acetone with thriethanolamine suspensions are quite stable and allow a good dispersion of the powders particles, as indicated by the particle size distribution and UV transmittance studies.

For both systems the relation between the processing parameters (deposition voltage and time) and physical characteristics of green films was established. Under the present conditions films with thickness up to 80μm can be fabricated for both the systems with application of constant voltage and varying the deposition time, being the films with thickness up to 50μm characterised by very uniform morphologies.

With CIP, the films are denser and exhibit approximately 20% higher permittivity than films without CIP; this proves that CIP is an essential step to ensure thick films good properties.

6.8 References

[1] Fu Zhi, "$BaNd_2Ti_5O_{14}$ Thick Films for Microelectronics Fabricated by Electrophoretic Deposition" PhD thesis, University of Aveiro (2008).

[2] R W Powers., J Electrochem Soc 1975;122,482–6.

[3] B Ferrari, R Moreno, Mater Lett. 1996;28,353–5.

[4] B Ferrari, R Moreno, Journal of European Ceram Soc., 1997,17, 549–56

[5] P Sarkar,D De, H Rho, J Mater Sci 2004,39:819–23.

[6] Y C Wang, I Chi Leu, M H Hon, J American Society, 2004, 87 (1), 84-88.

[7] J Widegren, B Lennart, Journal of the European Ceramic Society 20 (2000) 659-665.

[8] I Besra, M Liu, Progress in Material Science 52 (2007) 1-61.

Chapter 7.
Microstructure and Dielectric Characterization of $BaLa_4Ti_4O_{15}$ Ceramics and Films

Abstract:

In this chapter, the microstructure and the dielectric response of BLT and BNT thick films are presented and the relationship between processing, microstructure and dielectric response established. Since BLT thick films are prepared for the first time in this work, BLT ceramics are fabricated as well and their dielectric properties compared. For equivalent sintering temperature it is observed that the grain growth in films is more anisotropic because of the film's constrained sintering. As a consequence, the dielectric permittivity is higher in films (by 11 %) when compared with ceramics where grains are more randomly distributed, at this sintering temperature. The losses measured for BLT ceramics and films, in this work are more or less 0.002 at 1MHz frequency.

The microstructure and electrical properties of BNT films were not addressed in this work because it had been previously a research topic in the group [8].

7.1 Introduction

It is well known that the processing steps of the material will affect its final microstructure and, as a consequence, the final dielectric properties. The establishment of the relationships between the processing, microstructure and properties is crucial for the understanding and control of the material response and for its application and commercialization, as well.

In addition in view of the fact that BLT thick films have not yet been reported in the literature and generally the properties of films are inferior to the properties of the

equivalent bulk ceramics, the dielectric response of BLT thick films and BLT ceramics is analysed and compared.

Despite the technological interest of BLT ceramics with a ε_r of 44, $TC\varepsilon_r$ near zero and Qf above 44,000 [5], systematic studies on the processing of BLT ceramics are still not thoroughly described in the literature. The dielectric properties of BLT systems have been reported by several groups as mentioned in Chapter 1, and the discussions have been mainly focused on the tunning of t_f without degrading the ε_r and Qf of the material. Colla *et al* [2] and Reaney *et al.* [3] have shown that t_f varies strongly in accordance with the proximity of room temperature due to phase transitions that involve tilting or rotation of ´O´ octahedral unit of the structure this studies were conducted on $SrTiO_3$ and $LaAlO_3$ solid solution. In $Ca_5Nb_2TiO_{12}$ and related compounds the variation of $TC\varepsilon_r$ with sintering temperature was observed by Bendershy *et al.* [4]. The explanation for the variation of $TC\varepsilon_r$ is associated with the disordering of the crystal, which was studied by HRTEM.

Results and Discussion

7.2 Microstructure Characterization of Ceramics

Figure 7-1 presents the SEM micrographs of the sintered ceramics. BLT ceramics sintered between 1400 and 1600 ºC present quite dense microstructures and are characterised by anisotropic grains. The density of the ceramics increases until 1500 ºC and then decreases for the samples sintered at higher temperatures and it is related with the presence of porosity, which can be seen in the SEM micrographs (Figure 7-1); corresponding density is given in Table 7-1. The grain anisotropy increases with the increase of the sintering temperature as corroborated by the calculated aspect ratio of the grains that varies from 3 to 24 with the sintering temperature. For the sintering temperatures up to 1500ºC the longest grain dimension varies between 5 to 20 µm and it increases drastically with the sintering temperature to 52µm. Concomitantly the density of the sample decreases for the highest sintering temperatures because of this abnormal anisotropic grain growth which results in the entrapment of some pores inside the grains. The anisotropic behaviour of BLT (1:1:4) ceramics was also observed by Fukami *et al* [7] and Reaney *et al* [5].

Table 7-1: Physical parameters of BLT ceramic sintered at different temperatures.

Sintering Temperature(°C)	Relative density	Maximum Aspect ratio of Grain	Maximum Size of the grain in longer axis (μm)
1400°C-6h	93%	3	5
1450°C-6h	94%	5	6
1500°C-6h	96%	10	15 -20
1550°C-2h	95%	22	52
1600°C-2h	95%	24	52

Figure 7-2 presents the EDS spectra of BLT ceramics sintered at 1450°C/6h that confirms the ceramic composition and indicates that no extra phases are present. Chemical elemental mapping was performed on these ceramics and it was observed that some specific grains are rich in Ba and Ti and deficient in La, as shown in Figure 7-3. To have a clear picture about this distribution back scattered electron spectroscopy was performed and in some regions a few grains have a slightly different light contrast (Figure 7-4), what seems to corroborate the observations of the elemental mapping. Due to the XRD detection limits (~ 3% volume) this compositional variation was not observed by XRD and it was not possible, with the available resources to identify the stoichiometry of this BLT phase. Similar findings were reported by Okawa *et al* [6] for this composition.

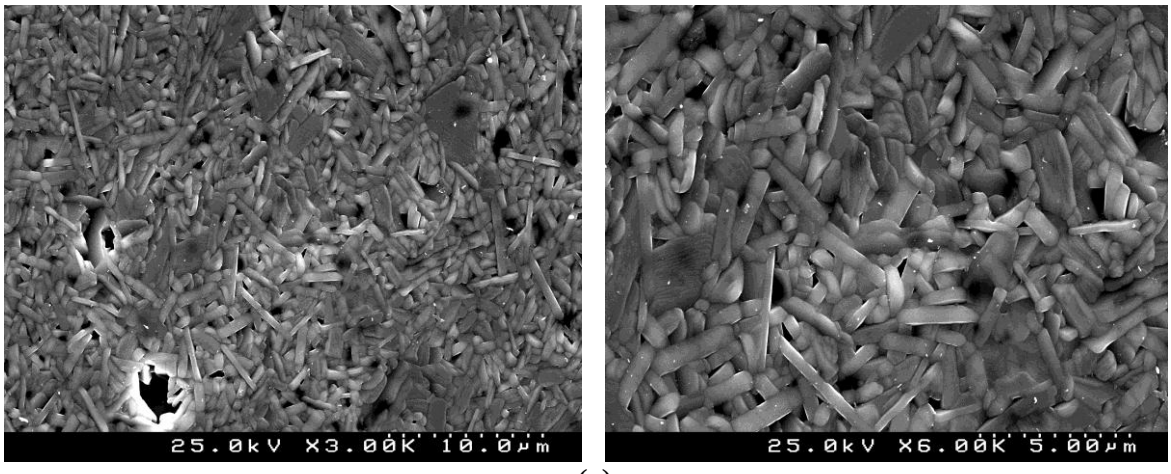

(a)

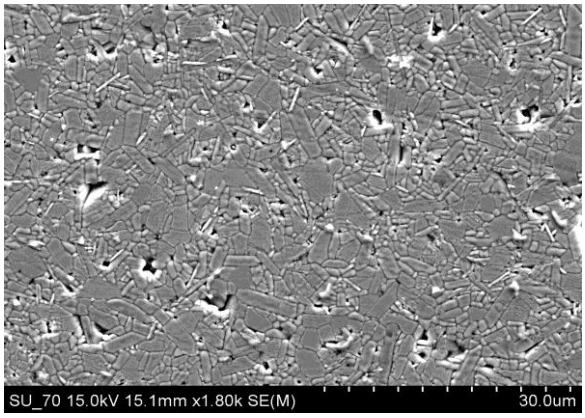
SU_70 15.0kV 15.1mm x1.80k SE(M)
30.0um

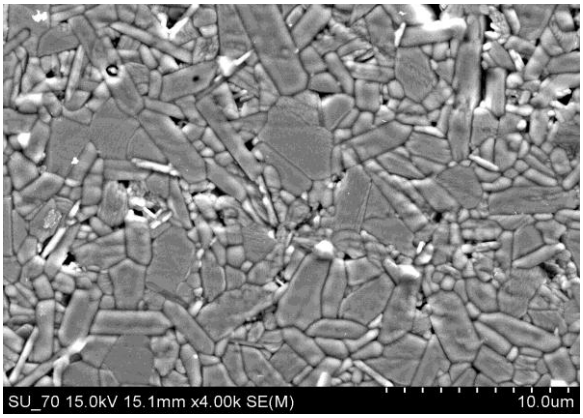
SU_70 15.0kV 15.1mm x4.00k SE(M)
10.0um

(b)

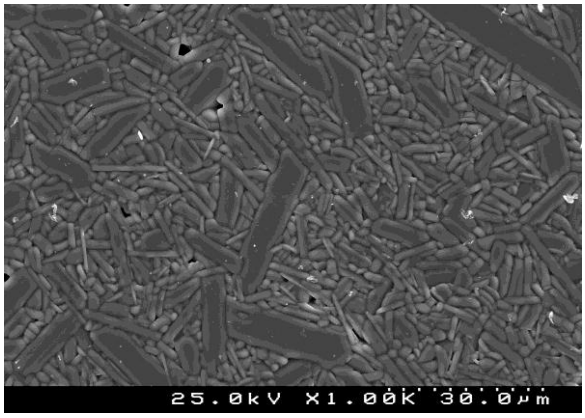
25.0kV X1.00K 30.0µm

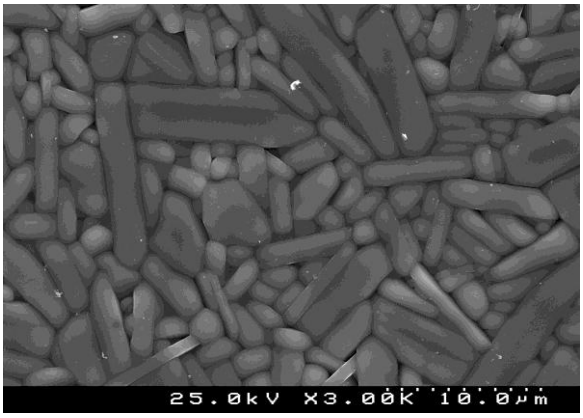
25.0kV X3.00K 10.0µm

(c)

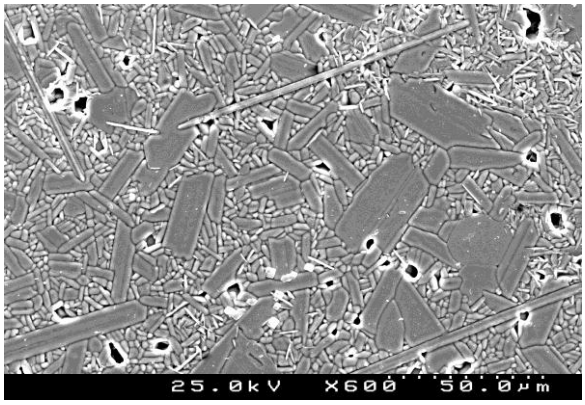
25.0kV X600 50.0µm

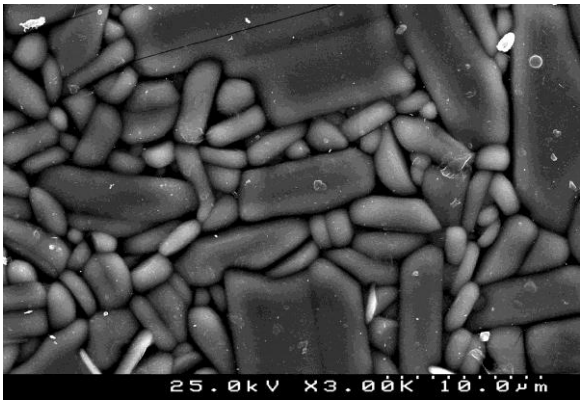
25.0kV X3.00K 10.0µm

(d)

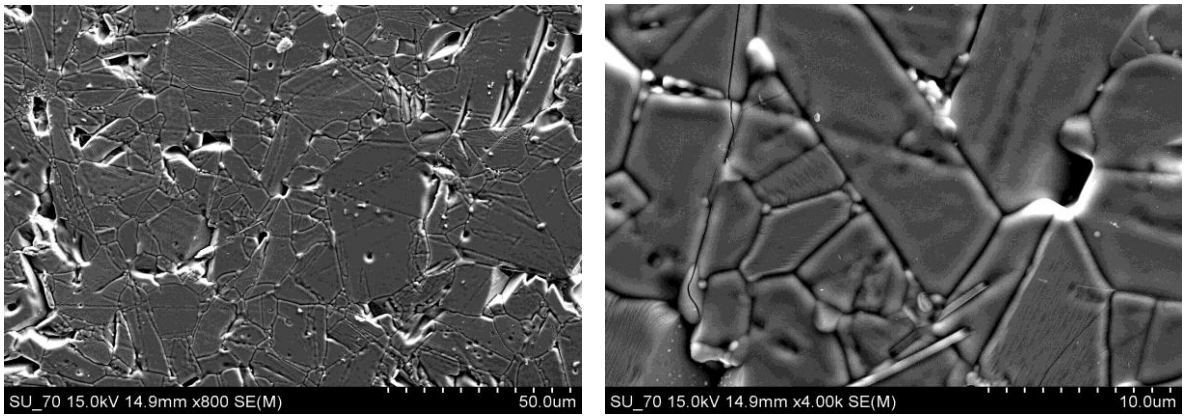

(e)

Figure 7-1: SEM micrographs of BLT ceramics sintered at different temperatures a) 1400ºC/6h, b) 1450ºC/6h c) 1500ºC/6h d) 1550ºC/2h e) 1600ºC/2h.

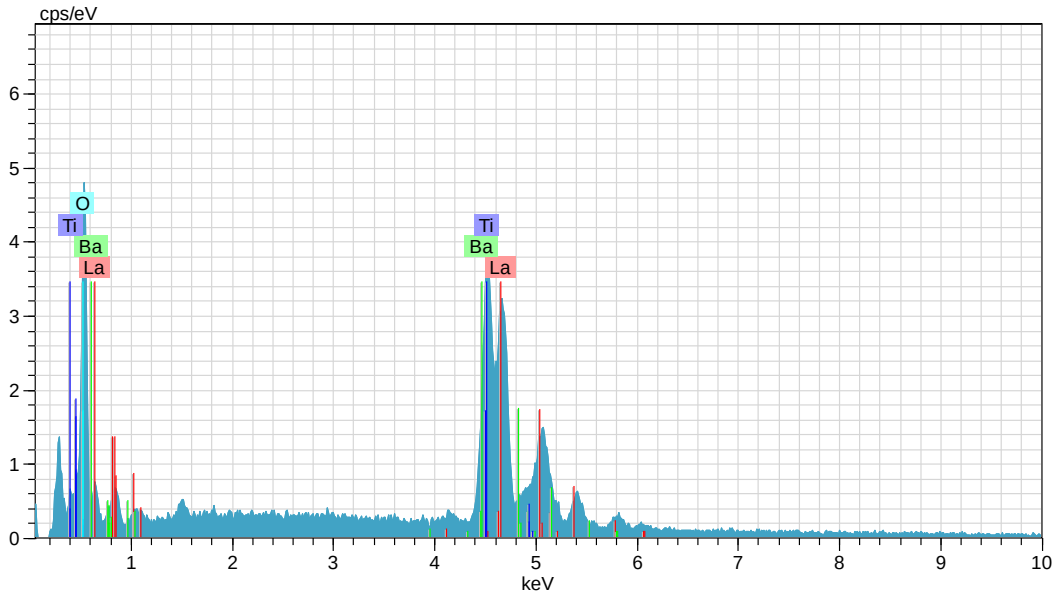

Figure 7-2: EDS spectra of BLT ceramics sintered at 1450ºC/6h.

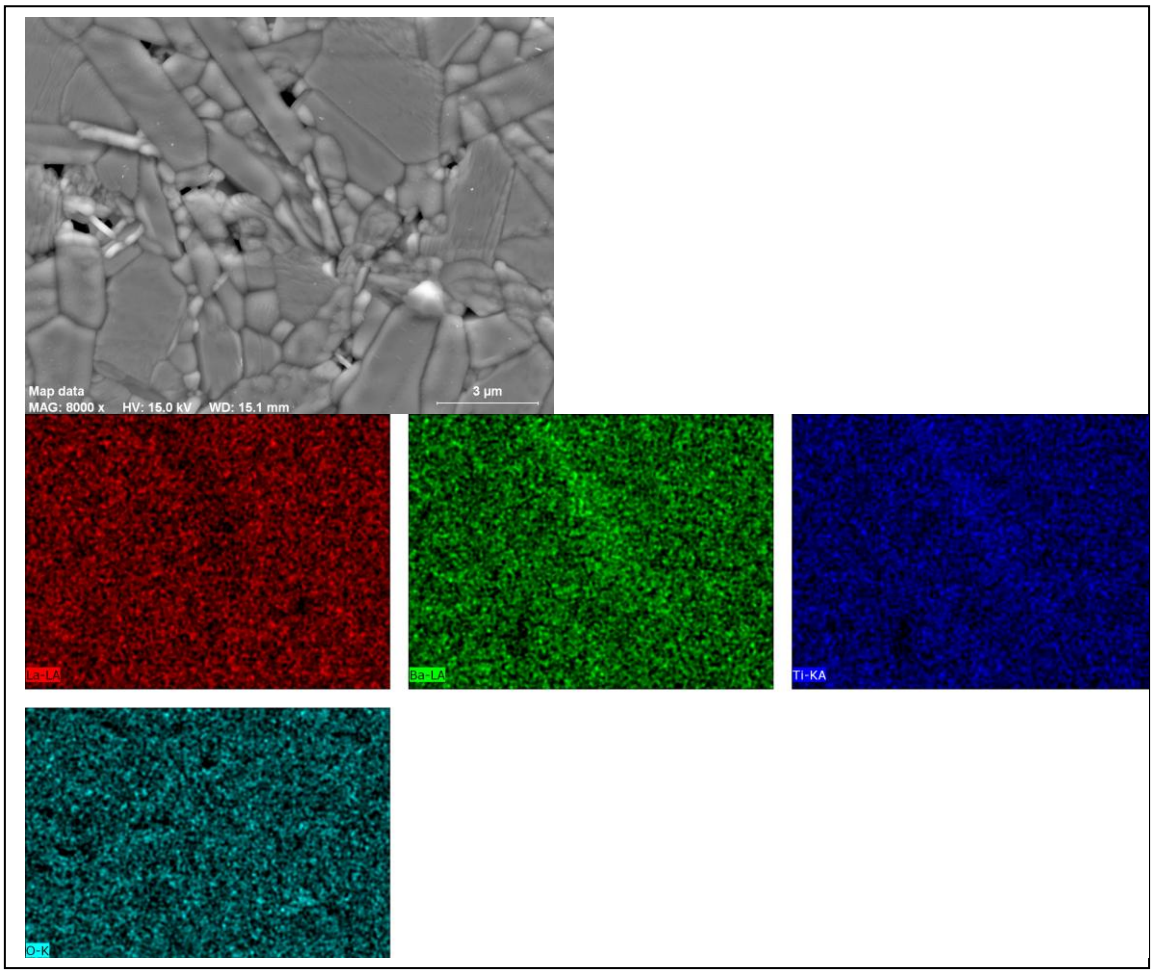

Figure 7-3: EDS mapping of BLT ceramics sintered at 1450ºC/6h

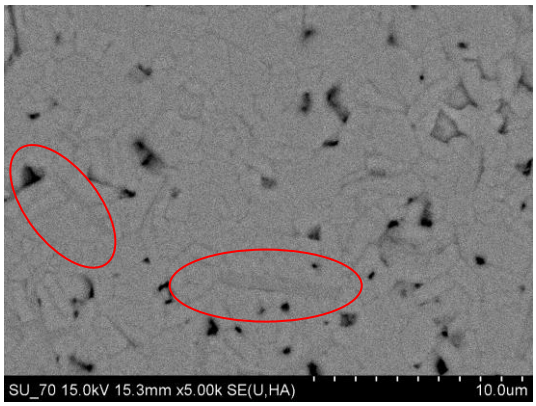

Figure 7-4: Back Scattered SEM micrograph of BLT ceramic at 1450ºC/6h (secondary phase encircle in red).

Electrical Characterization of BLT Ceramics

Figure 7-5 (a) and (b) represents the dielectric permittivity and losses as a function of frequency and temperature for BLT sintered ceramics. With the increase of the sintering temperature the dielectric permittivity increased until the sintering temperature of 1500 ºC; for further augment of the sintering temperature the abnormal grain growth occurs resulting in lower density (Table 7-1 and Figures 7-5(a)) and as a consequence in lower dielectric permittivity.

The relative dielectric permittivity previously reported [3-12] ranges from 44 to 49.1 in GHz frequency. In this work the maximum permittivity of BLT ceramic was 51 at 1MHz frequency for ceramic sintered at 1500ºC/6h with a relative density of 96%. The reason of high relative permittivity may be related with the size of the grains and their distribution. For ceramics sintered at 1500º C the grain sizes varies from 2 to 20μm in the longest axis of grain and has higher density compared to ceramics sintered at higher and lower temperatures.

The losses were measured at 1 MHz and varied between 0.009 and 0.001. The comparison with the literature reports is difficult since the reported values correspond to the MW range.

The permittivity of the BLT ceramics varies almost linearly with temperature as shown in Figure 7-5(b), which is good from the application point of view.

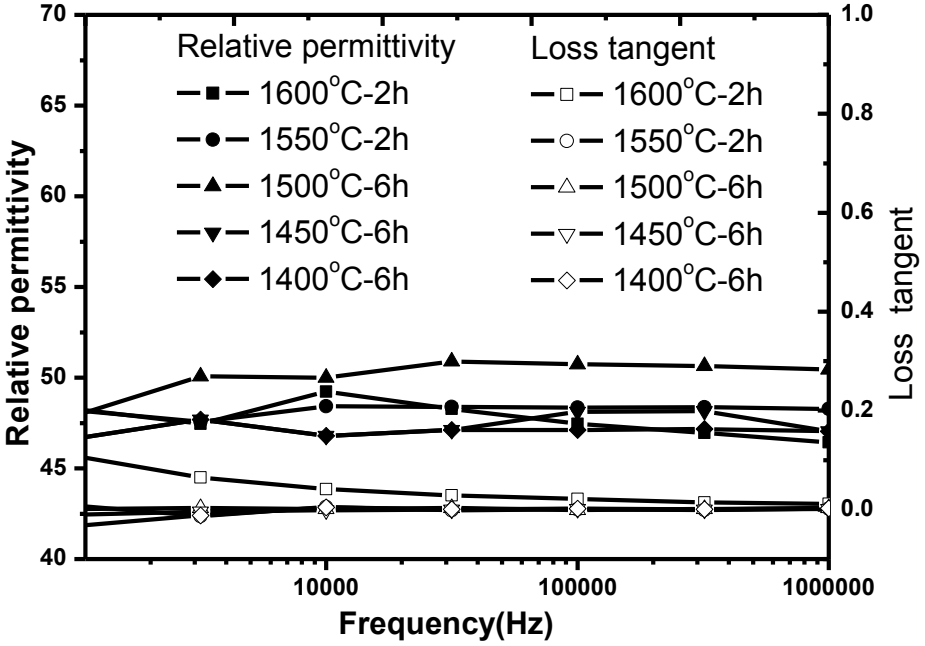

(a)

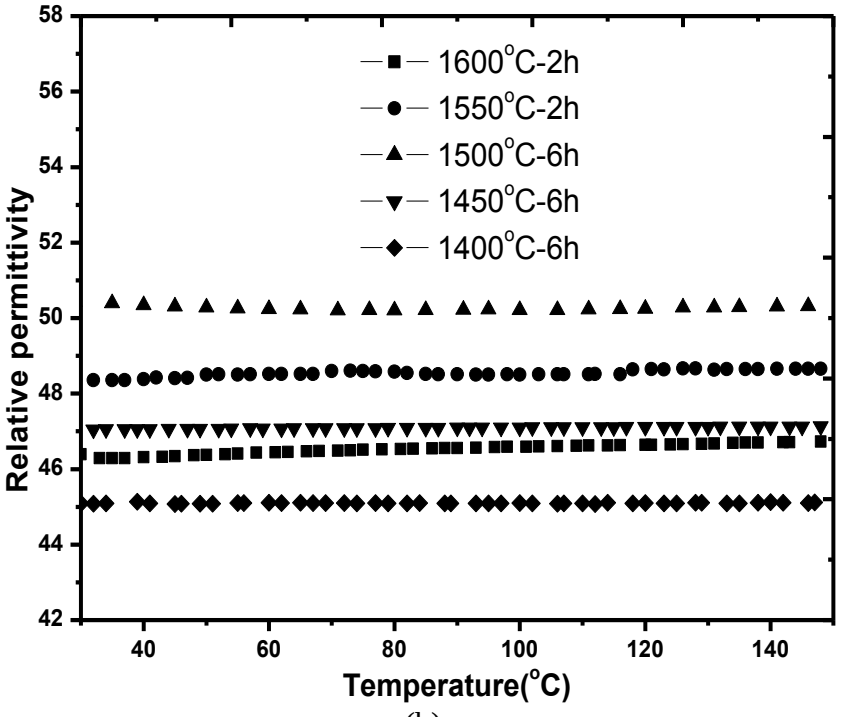

(b)

Figure 7-5: Dielectric properties of sintered BLT ceramics: a) relative permittivity and losses as a function of frequency and b) relative permittivity as a function of temperature.

The observed behaviour of the temperature coefficient of the relative permittivity ($TC\varepsilon_r$) as a function of processing temperature is highly unusual and according to the authors knowledge was not reported in the literature until now. There is a double-crossing of zero $TC\varepsilon_r$ with the processing temperature as depicted in Figure 7-6. The temperature dependence of the relative permittivity ($TC\varepsilon_r$) changes from a positive ($TC\varepsilon_r$ of 15.3ppm/ºC for the sample sintered at 1400ºC) to a negative value ($TC\varepsilon_r$ about -38ppm/ºC for the sample sintered at 1500ºC) and again changes to a positive one with the increase of the sintering temperature.

A similar observation was reported by Cava *et al.* [4] for the system $Ca_5Nd_2TiO_{12}$ (Figure7-7). The reason for the variation of $TC\varepsilon_r$ was suggested to be related with the ordering of cations in the B sites which was studied by HTEM. Cava found that the degree of B sites cation ordering is higher in ceramics sintered at intermediate temperatures as when compared with ceramics sintered at low and high temperature where $TC\varepsilon_r$ have high positive values.

It is worth to mention, that this finding might be very useful for the tailoring the $TC\varepsilon_r$ to near zero of BLT ceramics. However further studies of the microstructure and crystallographic nature of BLT ceramics, that are out of the aim of this thesis, are needed to understand these observations.

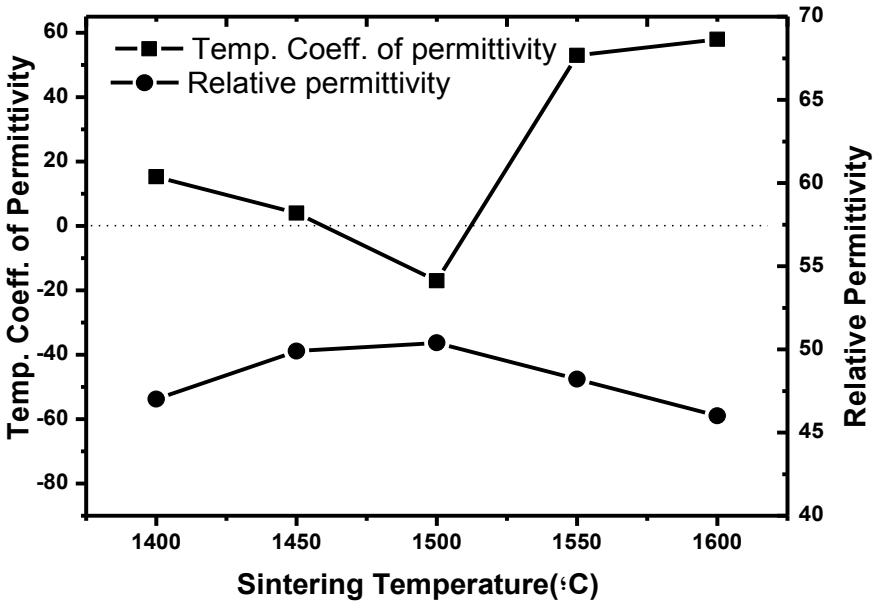

Figure 7-6: TCε_r and relative permittivity as a function of sintering temperature for BLT ceramics at 1MHz and temperature for permittivity was measured from 30ºC to 120ºC.

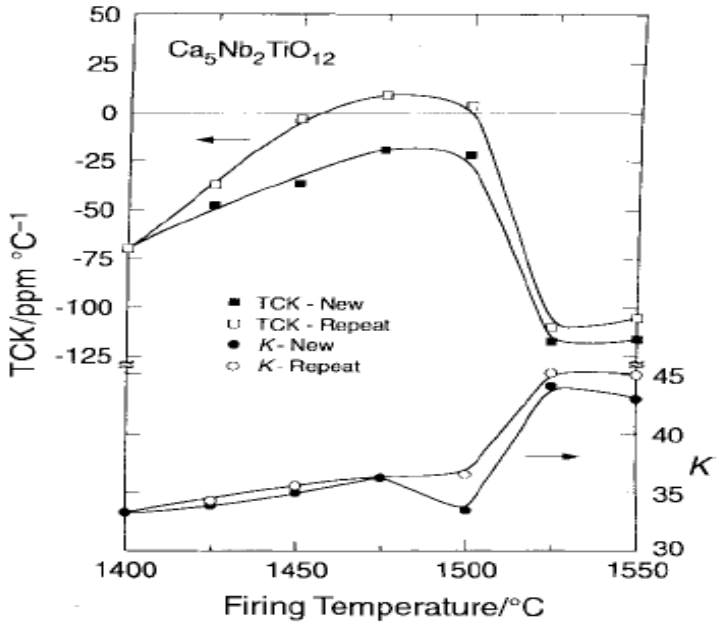

Figure 7-7: TCε_r or TCK and relative permittivity as a function of sintering temperature for $Ca_5Nd_2TiO_{12}$ and for $Ca_5Ta_2TiO_{12}$ [4].

7.3 Microstructure Characterization of BLT Films

The SEM micrographs of 10µm thick BLT films deposited in acetone based suspensions and iso statically pressed are illustrated in Figure 7-8.

Films were sintered at 1400ºC to 1600ºC and as the sintering temperature increases films become denser, which can be seen from the SEM micrograph, the grain size along the longest axis increases from 2 to 30µm with the sintering temperature (presented in Table 7-2).

Table 7-2: Maximum grain size along the longest axis and corresponding sintering temperature for BLT films.

Sintering Temperature	**1400ºC**	**1450ºC**	**1500ºC**	**1550ºC**	**1600ºC**
Max. size of grain along the longest axis (µm)	**3**	**4**	**15**	**20**	**30**

Figure 7-9 illustrates the cross sections of BLT films sintered at1450ºC/1h, showing that the bounding between the substrate and the film is quite good. The EDS was performed on these films to inspect the presence of secondary elements (Figure 7-10) and no extra elements besides BLT composition were detected.

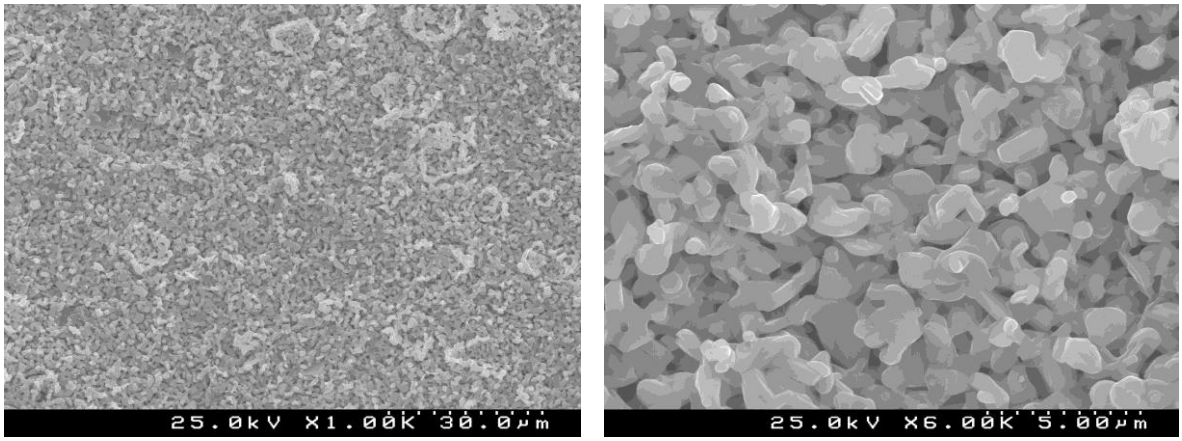

(a)

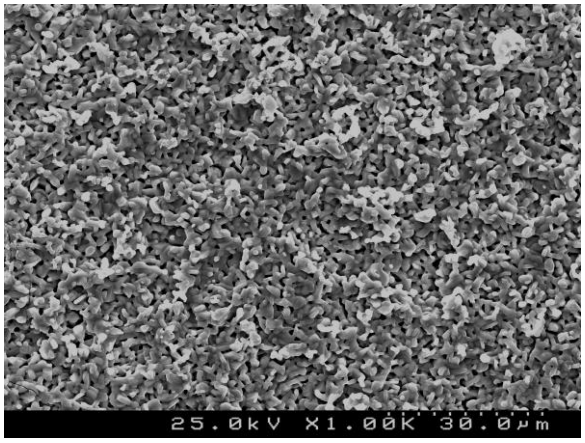
25.0kV X1.00K 30.0µm

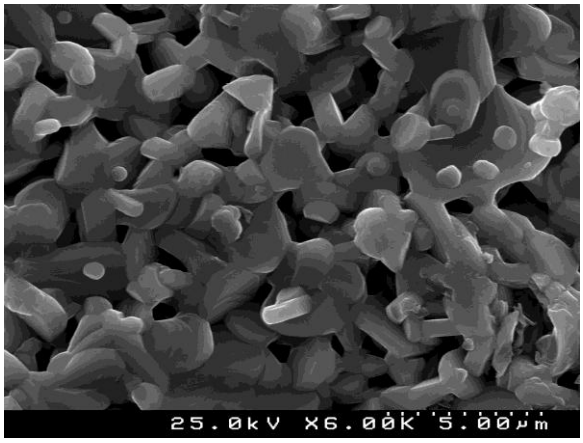
25.0kV X6.00K 5.00µm

(b)

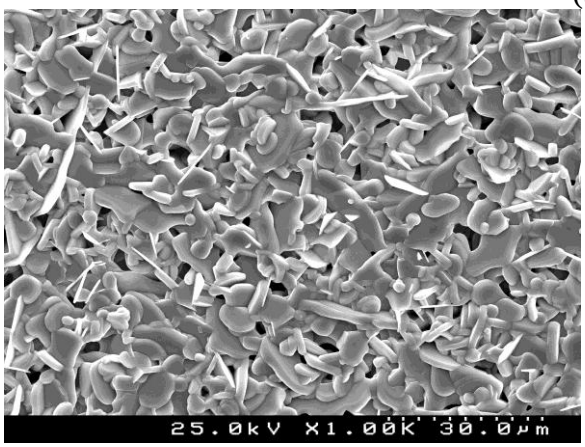
25.0kV X1.00K 30.0µm

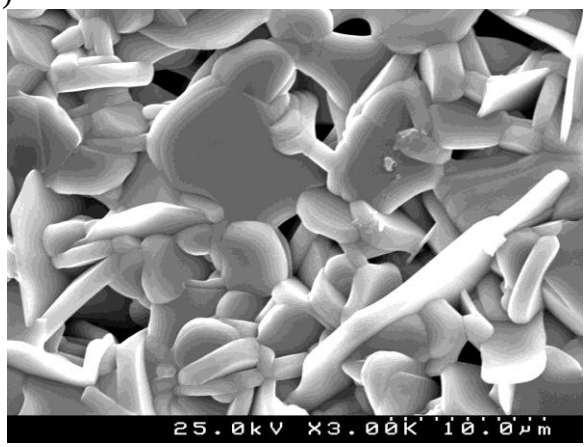
25.0kV X3.00K 10.0µm

(c)

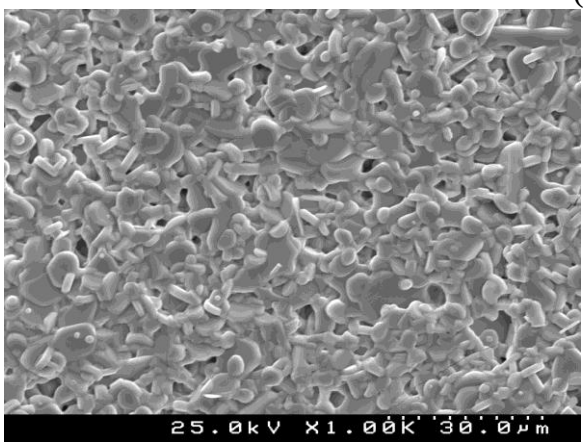
25.0kV X1.00K 30.0µm

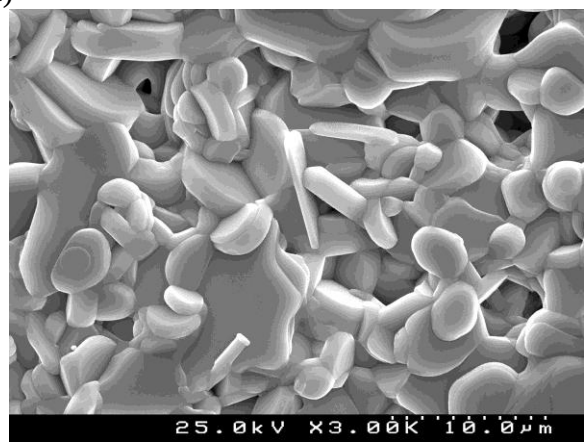
25.0kV X3.00K 10.0µm

(d)

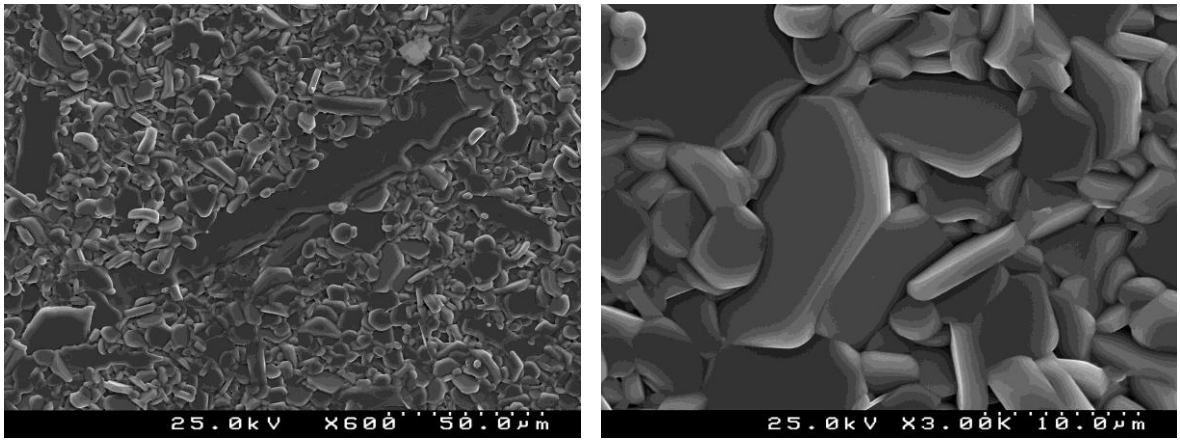

(e)

Figure 7-8: SEM micrographs of BLT films derived from acetone suspension with triethanolamine and sintered at a) 1400ºC/1h b) 1450ºC/1h c) 1500ºC/1h d) 1550ºC/1h e) 1600ºC/1h.

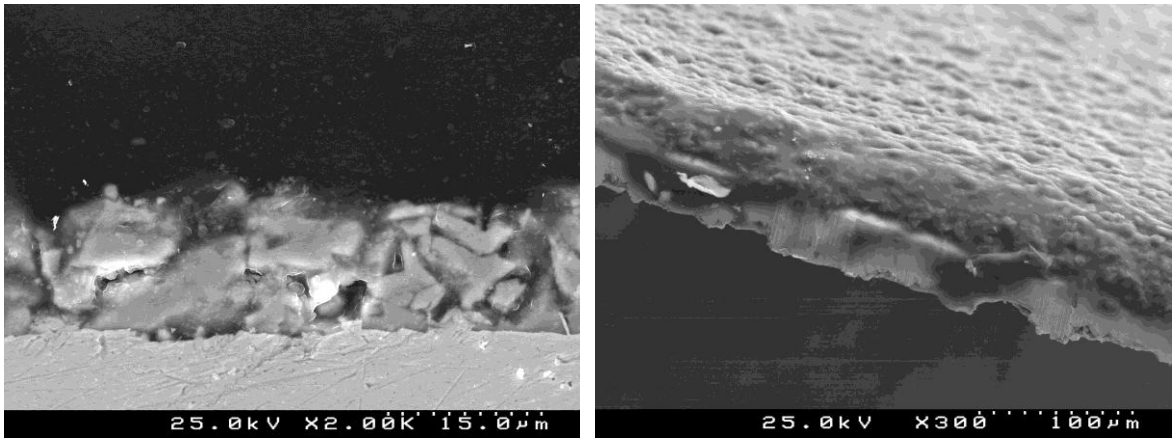

Figure 7-9: SEM micrographs of cross sections of BLT film sintered at 1450ºC/1h and derived from acetone suspension with triethanolamine.

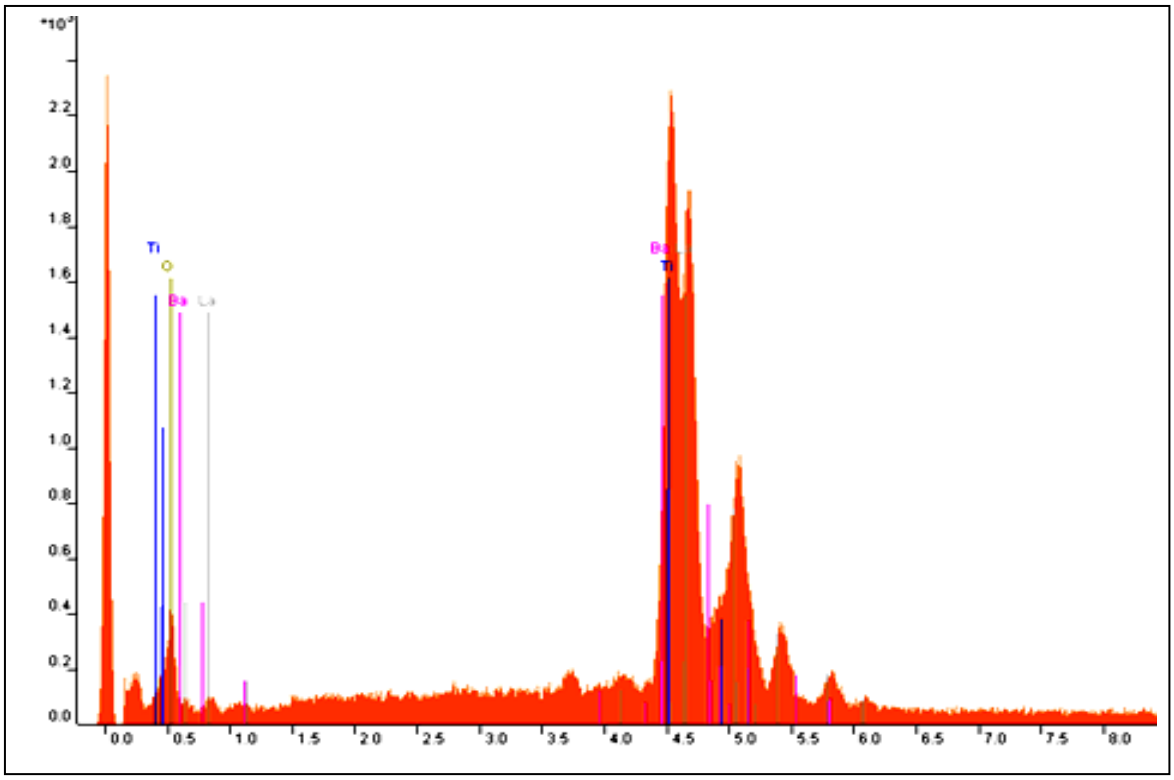

Figure 7-10: EDS of BLT film sintered at 1450ºC/1h derived from acetone suspension with triethanolamine.

Electrical Characterization of BLT Films

The variation of the relative permittivity and losses as a function of frequency and temperature for BLT films sintered at 1400ºC to 1600ºC for 1hour are depicted in Figure 7-11. With the increase of the sintering temperature there is a decrease in the porosity (Figure 7-8), an increase in the dielectric permittivity and the losses approached to zero. The maximum permittivity of about 57.5 was achieved for films sintered at 1600ºC/1h and with loss tangent lower than 0.002 at 1 MHz frequency. The permittivity doesn't vary much with increasing temperature from 30 to 100ºC (Figure 7-11(b)), that is an essential characteristic in microwave applications in terms of frequency selectivity. The poor properties of films sintered at lower temperature are due to the higher porosity as compared to the films sintered at high temperatures.

The calculated $TC\varepsilon_r$ are summarised in Table 7-3. $TC\varepsilon_r$ remains positive and approaches to zero as the sintering temperature of the film increases; $TC\varepsilon_r$ varies from +103ppm/ºC to +30ppm/ºC for BLT films sintered from

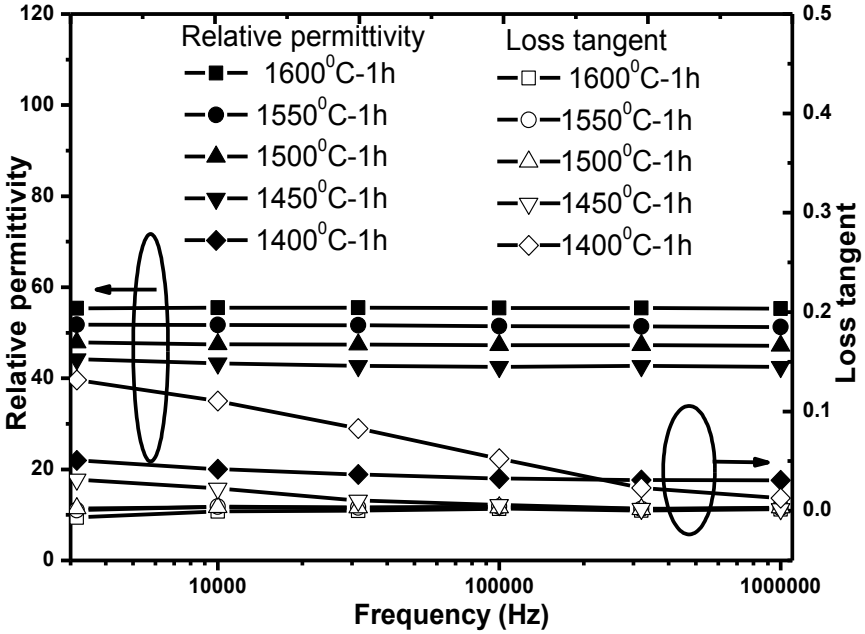

(a)

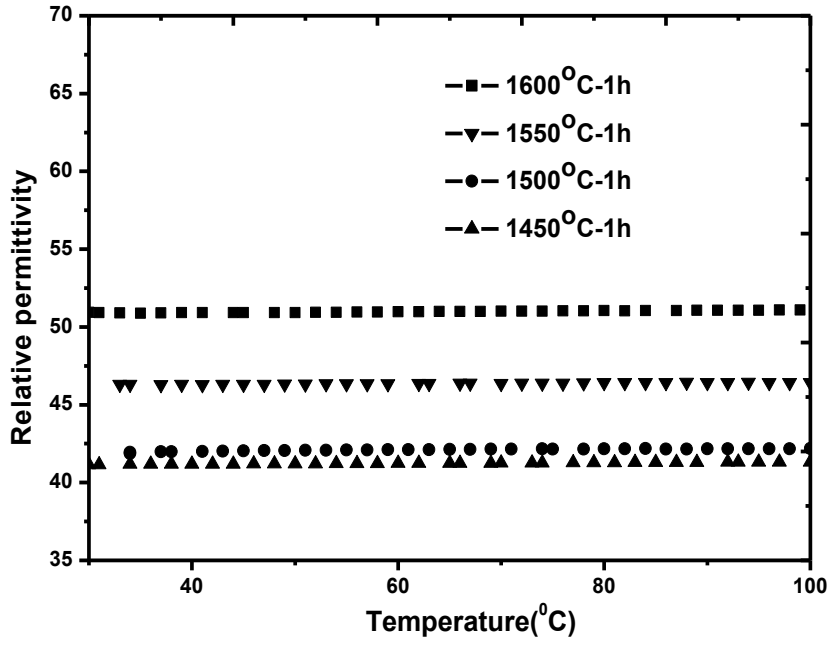

(b)

Figure 7-11: Dielectric properties of sintered BLT films: a) relative permittivity and losses as a function of the frequency and b) relative permittivity as a function of the temperature.

1450ºC to 1600ºC. This behaviour might be related with details of the microstructure or modifications of the degree of ordering as suggested by [4]. Indeed, it was reported that $TC\varepsilon_r$ of BNT thick films approaches to zero with the increase of the sintering temperature or aspect ratio of the film [11].

The dielectric permittivity and loss tangent of different thick BLT films and ceramics sintered at 1450ºC for 6h represented in Figure 7-12 as a function of frequency. It can be seen that, with the increase of the film thickness, from 13 to 30 µm the dielectric properties approach to wards those of the ceramics. In fact, in thick films the contribution of the film bulk to the dielectric response is higher than in a thin film, diluting the contribution of any interfacial layer between the film and the substrate, usually deleterious to the film dielectric response. On the other hand, as the bulk thickness of the film increases the effect of the constrained sintering becomes diluted as well, and the grain growth and grain orientation in this case becomes more similar to the bulk microstructure.

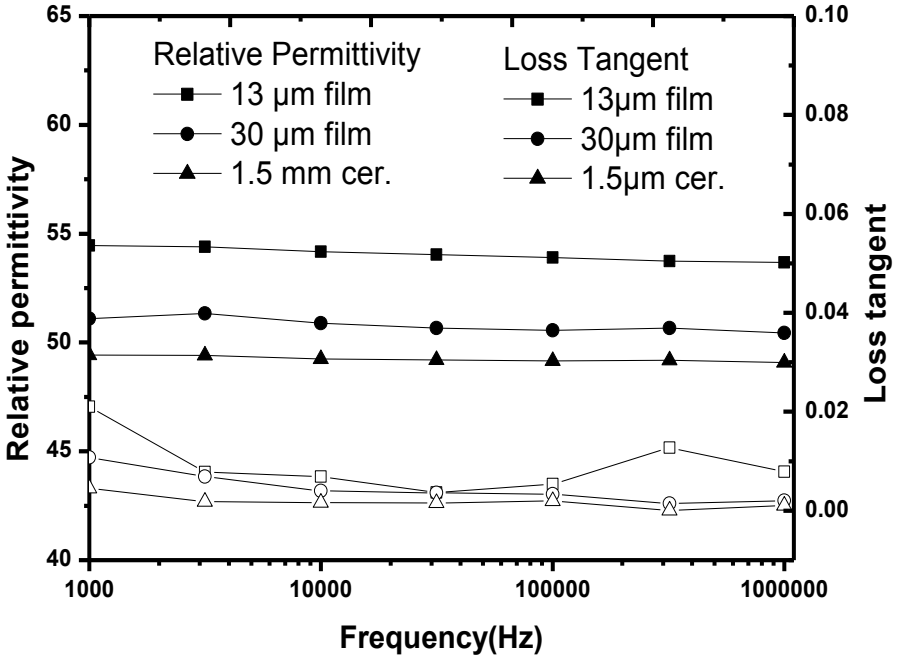

Figure 7-12: Relative permittivity and losses as a function of frequency for 13µm, 30µm thick BLT films and 1.5 mm thick ceramic.

7.4 BLT Films and Ceramics Comparison

Table 7-3 summarises the properties of BLT films and ceramics prepared under the current work. In general the dielectric response of BLT films doesn't differ too much from the ones of BLT ceramics, in terms of dielectric permittivity and dielectric losses. However the main differences reside in the temperature coefficient of the dielectric permittivity.

At low sintering temperature the permittivity of ceramics is higher than the equivalent films what might be due to the high degree of porosity of the films. On the other hand films sintered at 1550 and 1600ºC present higher dielectric permittivity what might be related with the anisotropy of the microstructure and with the change in grain size.

Reaney *et al.* [5] reported the dependence of the electrical response on the anisotropy of the microstructure of BLT ceramics. The dielectric permittivity is higher by 20 % when measured in perpendicular direction of pressing than in parallel direction of pressing. Similar findings were observed for BNT films with needle shape like morphology by Fu Zhi *et al*. [8] and attributed to the constrained sintering which promotes to elongated growth of the grains. Similar behaviour in terms of dielectric response and microstructure was also observed for other compounds such as $Bi_4Ti_3O_{12}$ [9], $PbBi_4Ti_4O_{15}$ and $Pb_2Bi_4Ti_5O_{18}$ [10].

Concerning $TC\varepsilon_r$ the variation between films and ceramics and its dependence on the sintering temperature is appreciable. As well reported in the literature $TC\varepsilon_r$ depends on many aspects, namely on tolerance factor [3], ordering of B sites cations with change in the sintering temperature [4] and aspect ratio of the grain size [11] what might affect in a similar way the $TC\varepsilon_r$ of thick films. However, for the case of films, on top of that one needs to consider the changes induced by the constrained sintering, either the residual porosity or the altered degree of the microstructure anisotropy when compared with equivalent ceramics. The analysis of the variation of $TC\varepsilon_r$ in films becomes more difficult and in order to distinguish between the possible contributions to this variation systematic

studies are necessary, that were out of the objective of this master thesis and are currently under investigation.

Noteworthy here, is the observation that the variation of $TC\varepsilon_r$ in films is very dependent on the processing conditions and the full understand of this variation in order to tailor the final properties of the films is essential for the complete exploitation of the possible commercial applications for thick films of MW materials.

Table 7-3: Dielectric characteristics of BLT films and ceramics.

Sintering Temperature (ºC)	Permittivity at 1MHz (Ceramics)	Permittivity at 1MHz (Films)	Loss tangent at 1MHz (Ceramics)	Loss tangent at 1MHz (Films)	$TC\varepsilon_r$ (30-100)ºC (Ceramics) (ppm/ºC)	$TC\varepsilon_r$ (30-100)ºC (Films) (ppm/ºC)
1450	44	42	0.001	0.009	+4	+103
1500	51	47	0.002	0.003	-17	+58
1550	48	53	0.002	0.002	+44	+58
1600	46	58	0.001	0.002	+62	+30

7.5 Conclusion

BLT thick films and ceramics possess typical microstructures in which anisotropic grain growth took place with the increasing sintering temperature. In general BLT thick films are less dense than equivalent ceramics.

The dielectric permittivity, dielectric losses and temperature coefficient of the permittivity of 10µm thick BLT films sintered at 1600ºC are 58, 0.002 and +30ppm/ºC at 1MHz, respectively. A maximum relative permittivity of 51, loss tangent of 0.002 and $TC\varepsilon_r$ of -17ppm/ºC at 1MHz were obtained for BLT ceramics sintered at 1500ºC.

In comparison with BLT ceramics the dielectric response is quite similar in terms of dielectric permittivity and dielectric losses, being the small differences attributed to the density and to the constrained sintering that takes place in thick films. With the increase of thickness the dielectric behaviour of BLT films approach to the one of equivalent ceramics.

However, appreciable differences were observed in terms of $TC\varepsilon_r$ and its dependence on the sintering temperature. $TC\varepsilon_r$ of BLT films sintered between 1450ºC and 1600ºC decrease from 103ppm/ºC to 30ppm/ºC, while for the case of ceramics it first decreases with the sintering temperature and then increases. These results are particularly relevant because they clearly show the dependence of $TC\varepsilon_r$ on the processing parameters and the differences between bulk ceramics and thick films. The effect of the processing on $TC\varepsilon_r$ variation is complex and many variables seem to play a role, including the anisotropy growth of the grains and ionic disorder. Because of that the reasons behind this difference are not clear at the moment. This understanding is fundamental and will open opportunities to developed materials with tailored responses.

7.6 References

[1] Takashi Okawa, Katsumas Kiucchi, Hiraoki Okoki Okabe and Hitoshi Ohsato, Ferroelectrics, 2002, Vol 272, 345-250.

[2] E Colla, I M. Reaney and N Setter, J. Appl. Phys., (1993) 74 [5] 3414-3425.

[3] I M. Reaney, E L Colla and N Setter, Jap. J. Appl. Phys. (1994) 33 [7] (1) 3984-3990.

[4] L A Bendershy,J J Krajewski, R J Cava, Journal of the European Cer. Soc. 21 (2001), 2653-2658.

[5] H Zheng, D I Woodwand, L Gillie and I M Reaney, J. Phy. Condens Matter 18(2006) 7051-7063.

[6] Takashi Okawai, Katsumasa K, Hiroki O and Hitoshi Ohsato, Jpn. J. Appl. Phys. Vol. 40 (2001) pp. 5779–5782 Part 1, No. 9B, September 2001

[7] Y Fukami, K Wada, K Kakimoto, H Ohsato, Journal of the European Ceramic Society 26 (2006) 2055–2058.

[8] Fu Zhi, "$BaNd_2Ti_5O_{14}$ Thick Films for Microelectronics Fabricated by Electrophoretic Deposition" PhD thesis, University of Aveiro(2008).

[9] T.Takenaka and K Sakata 1980 Japan. J. Appl. Phys. 19 31–9.

[10] M Miyayama and I.S.Yi,2000 *Ceram.* Int. 26 529–33.

[11] Zhi Fu, Paula M Vilarinho, Aiying Wu and Angus I. Kingon Adv. Funct. Mater. 2009, 19, 1-11.

[12] Isuhak Naseemabeevi Jawahar, Narayana Iyer Santha, and Mailadil Thomas Sebastian, Pezholil Mohanan. J. Mater. Res., Dec 2002 Vol. 17, No. 12, 2084-89.

Chapter 8.
Characterization of $BaLa_4Ti_4O_{15}$ and $Ba_4Nd_{9.33}Ti_{18}O_{54}$ Composite Thick Films by Electrophoretic Deposition

Abstract:

In this chapter, the fabrication of composite thick films of BNT/BLT and BLT/BNT by electrophoretic deposition is described. The composite thick films are characterized by SEM and EDS to study the uniformity of the deposition and composition respectively. Dielectric response is assessed at 1 MHz.

8.1 Introduction

As mentioned before, there is a gap in terms of dielectrics between high permittivity (low Qf) and low permittivity (high Qf) materials suitable for specific microwave applications (Figure 3-1). Currently no commercial material with near zero τ_f, high Qf and permittivity between 45-80 is available [1].

One of the approaches that is being considered to tailor the dielectric response of MW ceramics and namely to obtain t_f near zero is to conjugate in the same material end members compositions with opposite sign of t_f. Ceramic composites of near zero t_f have been prepared in the systems of $CaTiO_3$-$NdAlO_3$ and $ZrTiO_4$-$ZnNd_2O_6$ by solid state reaction [2-3]. Zheng *et al.* [1] successfully prepared composites of $BaLa_4Ti_4O_{15}$ and $Ba_4Nd_{9.33}Ti_{18}O_{54}$ by solid state reaction and reported t_f ~ -20ppm/ºC, Qf 10,000GHz and permittivity of ~ 61, for the xBNT-(1-x)BLT ($0 \leq x \leq 0.75$) composite. To achieve high density and to decrease the processing costs of this composite materials the same group used a glass composition (B_2O_3-Bi_2O_3-ZnO-SiO_2 (BBZS) as a sintering aid and successfully decrease the sintering temperature by 350ºC from 1500ºC [4].

As a bulk material the most stringent properties needed to be used as MW resonator and filters, are Qf >40,000 GHz and t_f near zero. For antenna core technology, the less stringent requirement for Qf and t_f due to metallisation dominates the dielectric loss broadening the resonant frequency. The vast array of different antenna frequencies requires materials with $20 < \varepsilon_r < 80$. In addition, the use of such materials in handsets will ultimately

necessitate low cost raw materials and low processing costs as production volumes increases and profit margin reduces.

As per author´s knowledge no work has been reported about the fabrication of thick composite film for functional electroceramics by electrophoretic deposition technique so, the attempt was made to fabricate functional electoceramic composite thick film of BNT-BLT with EPD. However, this technique has been used to prepare nano composites, polymer-polymer composite and glass/polymer composites for other applications like mechanical, medical, *inter alia* [5-6].

By keeping this in view, attempts to fabricate composite thick films of BNT/BLT and BLT/BNT by EPD were undertaken in this work, to prove the concept that EPD is a viable, low cost and versatile technique to design and engineer thick composite films for miniaturised dielectric MW / High frequency applications.

8.2 Experimental

BLT-BNT composite films were fabricated in acetone based suspension with triethanolamine and the details of fabrication are given in Chapter 4.

In BNT/BLT composite the first layer of BNT was carried out at 60V for 30 second, followed by the layer of BLT carried out at 100V for 60 second. In a similar way BLT/BNT composite thick films were fabricated by carried out each layer of BNT and BLT at 60V for 30 second.

The deposition behaviour for individual BNT and BLT films with time and constant voltage was depicted in Chapter 6, also illustrated in Figure 8-1 for convenience; the deposited thickness corresponds to the green film.

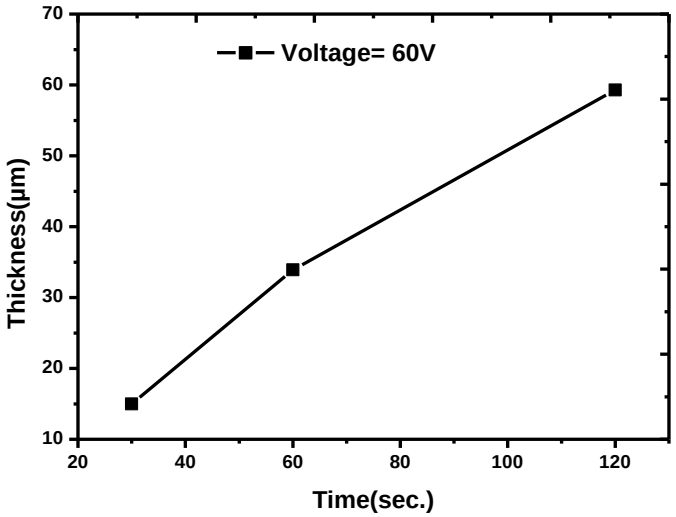

(a)

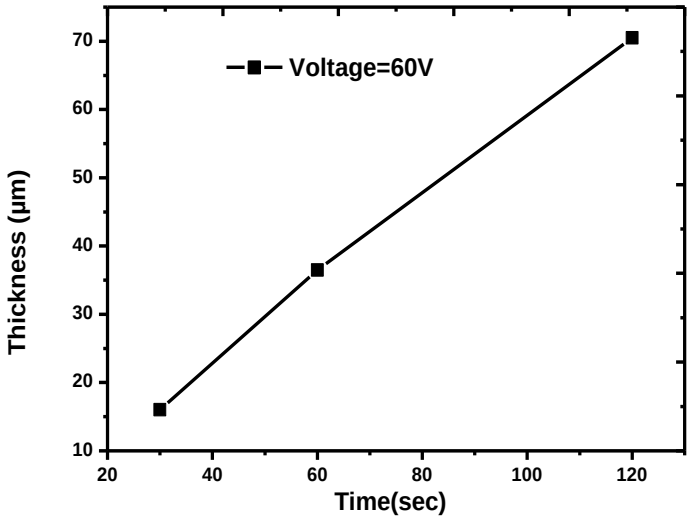

(b)

Figure 8-1: Deposited thickness versus time in acetone based suspension with triethanolamine for a) BLT b) BNT.

Results and Discussion

8.3 Microstructure of BNT/BLT and BLT/BNT Composite Thick Films

To examine the layered structure of BNT-BLT composite thick films cross sections were prepared. The preparation of cross section was a complicated task due to the flexible

nature of the used substrate and required precise chemical etching reagents for good grain boundary contrast.

Figure 8-2(b) depicts the cross-section microstructure of BNT/BLT composite films with a total thickness of 30µm sintered at 1500ºC/6h. As clearly seen from the images composite film is quite dense and very homogeneous, with no abrupt interface between the two layers and the substrate, since no gaps are visible. Top view of the film shows the platelet like shape of BLT with very good densification (Figure 8-2(a)). EDS analysis was performed on the composite thick films to check the chemical homogeneity of the composite and the results are presented in Figure 8-3.

According to the deposition parameters for BNT and BLT, the BNT layer deposited at 60V for 30 second should have the thickness of 17µm and the top layer of BLT deposited at 100V for 60 second should be near to 46 µm so, the total thickness of green composite film should be approximately 63µm. If one deduces around 16% of shrinkage during the sintering, then the film should be near 50 µm, but the total thickness obtained in BNT/BLT composite thick film is 30µm after sintered.

In the previous studies, it was observed that the thickness does not increase linearly through out the deposition thickness because of the decrease in electric field with time. This could be the case for BNT/BLT composite thick film in which the second deposition should be performed for longer time and at high voltage, when compared with the deposition of individual layers.

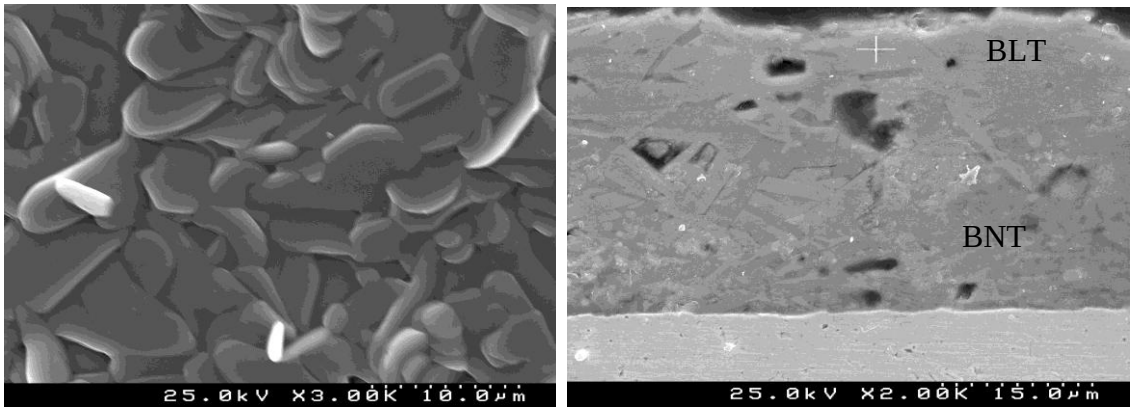

(a) (b)

Figure 8-2: SEM micrographs of BNT/BLT thick film composite sintered at 1500ºC/6h a) top view of film b) cross section view.

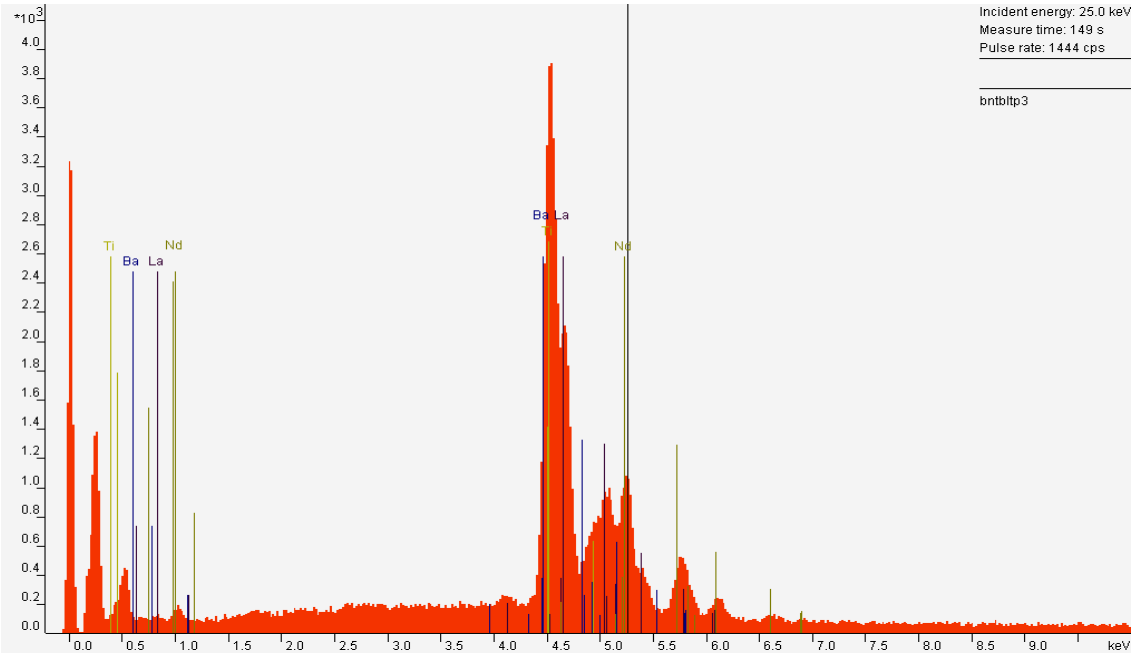

Figure 8-3: EDS of BNT/BLT thick film composite.

Figure 8-4(b) depicts the cross-section microstructure of BLT/BNT composite films with a total thickness of 24µm sintered at 1500ºC/1h. The cross section image reflect that composite film is dense and very homogeneous, with no abrupt interface between the two layers and the substrate, since no gaps are visible. It is difficult to distinguish the BLT and BNT layer as no visual contrast can be seen between the layers. In the top view of the SEM image one can see the presence of BNT rod like grains with some amount of porosity (Figure 8-4 (a)) and EDS spectra (Figure 8-5) confirm the presence of all the elements of BLT and BNT excluding any possibility of secondary element in the composite thick film.

According to the deposition parameter depicted in Figure 8-1, the first layer of BLT should be 15µm thick, deposited at 60V for 30 second, followed by the second layer of BNT 17µm thick, carried out at 60V for 30 second. So, the predicted thickness for the green film according to the deposition parameter should be 32 µm and if one deduces the shrinkage by 16% one will get the value of thickness for sintered film of 26 µm which is quite close to what it was achieved for this BLT/BNT composite layer structure (24 µm).

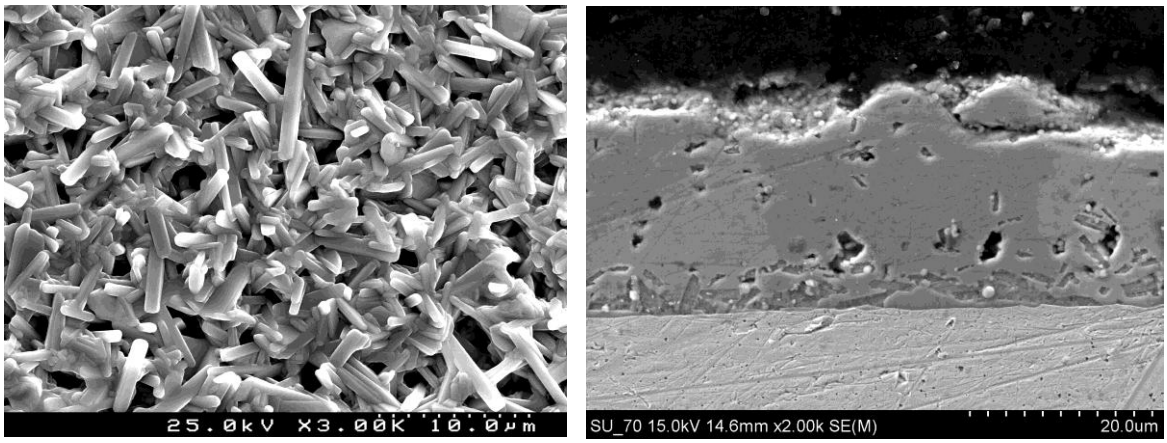

(a) (b)

Figure 8-4: SEM micrographs of BLT/BNT thick film composite sintered at 1500ºC/1h a) top view of film b) cross section view.

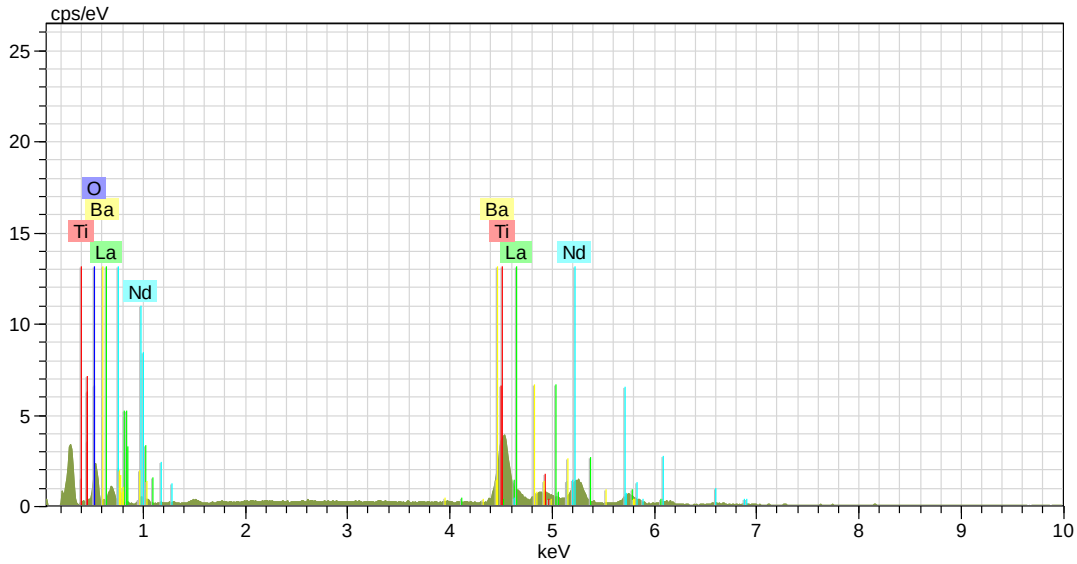

Figure 8-5: EDS spectra of BLT/BNT thick film composite.

8.4 Electrical Properties of BNT/BLT and BLT/BNT Composite Thick Films

The measurements were performed at different points of the films and the represented results correspond to maximum and minimum values obtained in these films. Figure 8-6(a) depicts the relative permittivity and losses plotted as a function of the frequency and temperature for BNT/BLT composite films. The maximum relative permittivity obtained in the composite film was of ~72 and the minimum of ~60 with losses of about 0.002. The relative permittivity as a function of temperature is presented in Figure 8-6 (b). Relative permittivity does not vary much with the temperature and the TCε_r of -16ppm^{o}C for BNT/BLT composite films.

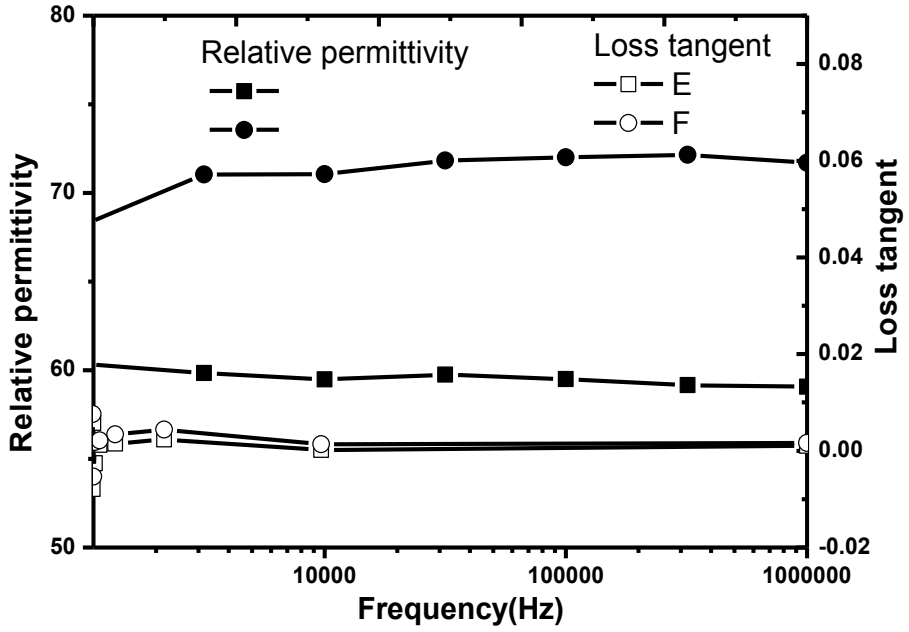

(a)

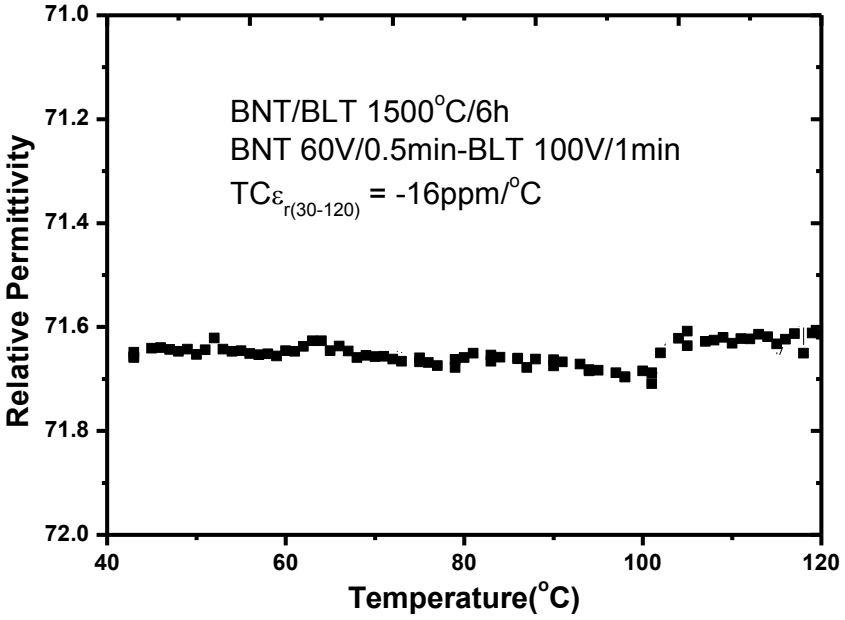

(b)

Figure 8-6: Dielectric properties of BNT/BLT 30µm thick film composite (a) relative permittivity and losses versus frequency and (b) relative permittivity versus temperature.

24µm thick BLT/BNT composite films presents a relative permittivity between 64 - 59 with loss tangent of 0.009 (Figure-8-7). The $TC\varepsilon_r$ of the material is +113ppm/ºC which is opposite in sign and quite higher when compared with the value obtained for BNT/BLT composites. In this case, no contrast was viewed in the cross-section although, top view of the BLT/BNT composite film shows the BNT rod like grains on the top of the composite film with higher amount of porosity which might be the reason of higher losses and lower permittivity as compare to BNT/BLT composite films.

Table 8.1 present the summary of the deposition parameters and properties of BNT-BLT composite thick films.

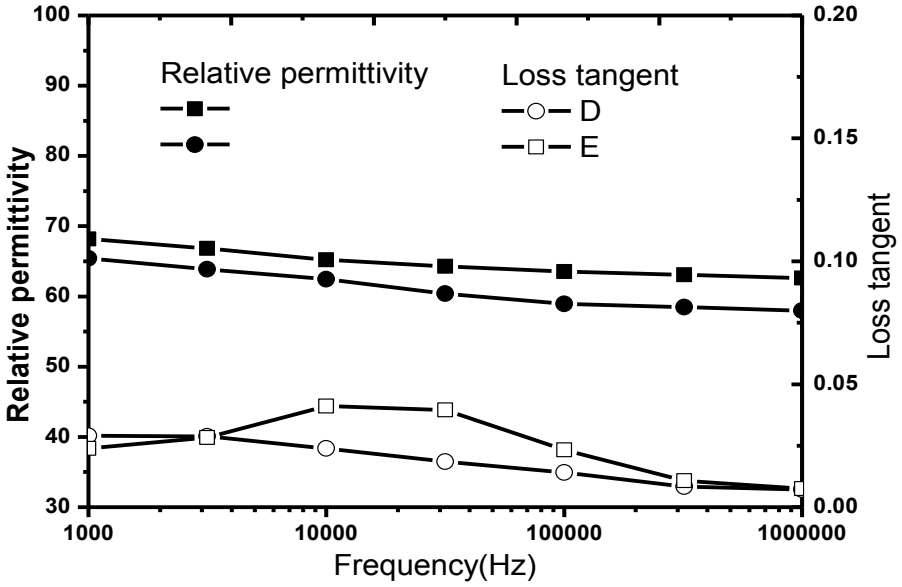

(a)

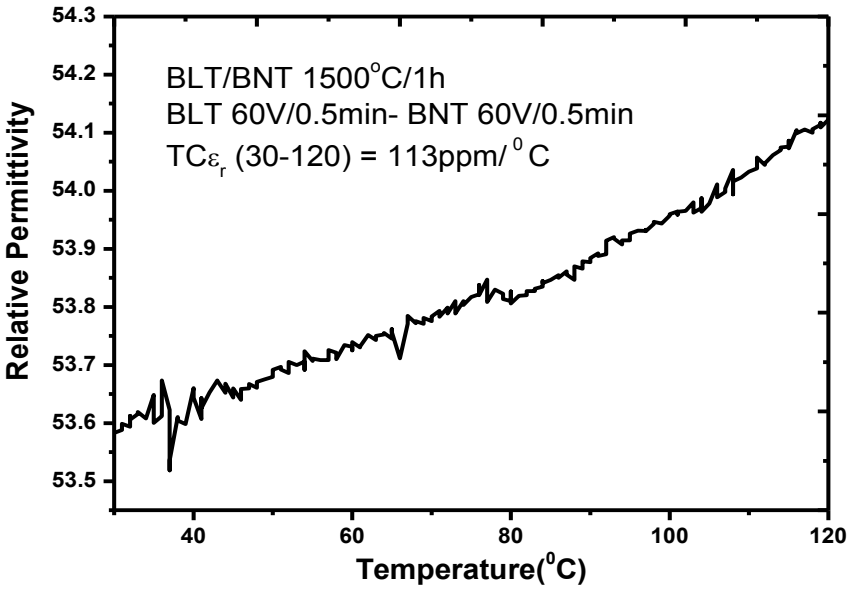

(b)

Figure 8-7: Dielectric properties of BLT/BNT 24µm thick films composite: (a) relative permittivity and losses versus frequency and (b) relative permittivity versus temperature.

Table 8-1: Parameters of deposition and electrical properties of thick films composites of BNT-BLT.

Composite System/Sintering Temperature	Time of deposition of layer	Thickness of film (μm)	Permittivity(1MHz)	Loss Tangent (δ)	Temperature Coefficient with Permittivity (ppm/ºC)
BNT/BLT 1500ºC-6h	60V-30 sec. 100V-60sec.	30	~71	0.002	-16
BLT/BNT 1500ºC-1h	60V-30 sec. 60V-30sec.	24	~63	0.005	+113

8.5 Conclusion

By applying a very simple technological approach that doesn't rely on additional modifications or the use of additives and modifiers, it has been proved that layered composites thick films of BNT–BLT system can be fabricated by EPD.

It was also observed that there are some limitations in this process when one needs to control the thickness of the composite film. In the process used in this work for the fabrication of composites, the first layer acts as an barrier for the second layer which affects the deposition of the second layer and the overall thickness of the composite film. Further studies on the composite deposition parameters are needed in order to optimise for example the thickness control.

It is shown that the gap in terms of materials with $45<\varepsilon_r<80$ can be filled with composite thick films of BNT-BLT fabricated by EPD. The properties obtained for these composite thick films are ε_r ~60-70, $TC\varepsilon_r$ ~-16ppm/ºC and loss tan(δ) ~0.002 which are quite close to the composite ceramics reported before [1]. This constitutes an important result since together with the ability to decrease the size, contributing to the miniaturization of the device size, composite thick layered structures can be used to tailor the materials properties.

To further improve the composite properties an optimum control on the deposition parameters or the use of intermediate drying and pressing steps or the use of additives and modifiers should be exploited. Moreover to assure low fabrication costs ways to reduce the

sintering temperature of the composite without affecting the electrical properties are also required for the composite films under study.

8.6 References

[1] Hong Zheng, I M Reaney, Japanese Journal of Applied Physics Vol. 44. no.5A, 2005, pp3087- 3090, 2005.

[2] H Zheng, G D C Csete de Gyo¨rgyfalva, R Quimby, H Bagshaw, R Ubic, I M Reaney and J. Yarwood: J. Euro. Ceram. Soc. 23 (2003) 2653.

[3] D M Iddles: Private communication.

[4] Hong Zheng , Ian M Reaney , Duncan Muir , Tim Price , David M. Iddles, Journal of the European Ceramic Society 27 (2007) 4479–4487.

[5] I Zhitomirsky, J Mater Sci (2006) 41:8186–8195.

[6] J Li, I Zhitomirsky, Journal of Material Process. Tech., Vol 209, issue 7, 3452-3459.

Chapter 9. Future Work

This work was performed in a systematic way and it was proved that the Electrophoretic deposition technique is an adequate technique for the fabrication of BLT films and BLT-BNT composites thick films on metallic substrates. However it is still necessary to continue these studies in order to optimize some parameters related with the deposition of composite thick films and some scientific questions need to be answered as well. Below is a list, that does not intend to be exhaustive, but indicates some of the most relevant aspects that need further studies.

1. Further studies are needed to optimise the deposition conditions for BNT-BLT and BLT – BNT composites, namely the exact control of the layer thickness, to increase the number of the multilayer's, among others.

2. To make thick dielectric films of practical use, it is necessary to reduce the sintering temperature in order to be make these films compatible with low cost metallic or non metallic substrates; low sintering temperature attempts are then required, that may include the study of different sintering aids.

3. The role of triethanolamine in the acetone based suspension needs to be exploited and clarified.

4. The dependence of $TC\varepsilon_r$ of BLT thick films on the film processing conditions and microstructure requires systematic studies of constrained sintering of thick films on metallic foils.